FINITE ELEMENT ANALYSIS OF FLEXIBLE PIPES: BENDING COMBINED WITH TENSILE LOAD

Cristiano Alves Pinto Mosqueira Gomes

Dissertação de Mestrado apresentada ao Programa de Pós-graduação em Engenharia Civil, COPPE, da Universidade Federal do Rio de Janeiro, como parte dos requisitos necessários à obtenção do título de Mestre em Engenharia Civil.

Orientador(es): Ney Roitman
José Renato Mendes de Sousa

Rio de Janeiro
Outubro de 2017

FINITE ELEMENT ANALYSIS OF FLEXIBLE PIPES:
BENDING COMBINED WITH TENSILE LOAD

Cristiano Alves Pinto Mosqueira Gomes

DISSERTAÇÃO SUBMETIDA AO CORPO DOCENTE DO INSTITUTO ALBERTO LUIZ COIMBRA DE PÓS-GRADUAÇÃO E PESQUISA DE ENGENHARIA (COPPE) DA UNIVERSIDADE FEDERAL DO RIO DE JANEIRO COMO PARTE DOS REQUISITOS NECESSÁRIOS PARA A OBTENÇÃO DO GRAU DE MESTRE EM CIÊNCIAS EM ENGENHARIA CIVIL.

Examinada por:

_____

Prof. Ney Roitman, D.Sc.

_____

Prof. José Renato Mendes de Sousa, D.Sc.

_____

Dr. George Carneiro Campello, D.Sc.

_____

Prof. Celso Pupo Pesce, D.Sc.

RIO DE JANEIRO, RJ - BRASIL
OUTUBRO DE 2017

Gomes, Cristiano Alves Pinto Mosqueira

Finite Element Analysis of Flexible Pipes: Bending Combined With Tensile Load / Cristiano Alves Pinto Mosqueira Gomes. – Rio de Janeiro: UFRJ/COPPE, 2017.

XV, 85 p.: il.; 29,7 cm.

Orientadores: Ney Roitman

José Renato Mendes de Sousa

Dissertação (mestrado) – UFRJ/ COPPE/ Programa de Engenharia Civil, 2017.

Referências Bibliográficas: p. 77-85.

1. Flexible pipe. 2. FEA. 3. Local analysis. 4. Bending. 5. Finite elements. I. Roitman, Ney de *et al*. II. Universidade Federal do Rio de Janeiro, COPPE, Programa de Engenharia Civil. III. Título.

Aos meus pais, Marcelino Gomes e Andréa Mosqueira.

Aos meus irmãos e avós.

À RAISSA.

AGRADECIMENTOS

A UFRJ e ao Governo Federal pelo ensino público de qualidade.

Aos Professores José Renato e Ney Roitman pelo apoio e pela valiosa e paciente orientação durante a execução de nosso trabalho.

Aos companheiros da TechnipFMC, em especial Alex Saint-Clair e Fabio Arruda pela valorização da qualificação profissional e flexibilização quando necessária.

Aos amigos da COPPE – PEC, em especial a Erika Moura (Petrobras) e Marcelo Protásio (TechnipFMC) pela amizade e companheirismo.

Aos meus avós Linnéa e Álvaro pelo amor e carinho. Ao meu avô e exemplo pelo incentivo incansável para a conclusão deste trabalho.

Aos meus irmãos e amigos: Gustavo, Bernardo e Fernanda.

Aos meus pais Marcelino Gomes e Andréa Mosqueira, que, além do amor e caráter, me proporcionaram uma educação de excelência, inestimável para a minha jornada.

Agradeço, por fim, à minha noiva, companheira e amiga, Raissa pelo amor incondicional e compreensão dos sacrifícios e privações.

Resumo da Dissertação apresentada à COPPE/UFRJ como parte dos requisitos necessários para a obtenção do grau de Mestre em Ciências (M.Sc.)

ANÁLISE DE TUBOS FLEXÍVEIS POR ELEMENTOS FINITOS: CARGA DE FLEXÃO COMBINADA COM TRAÇÃO

Cristiano Alves Pinto Mosqueira Gomes

Outubro/2017

Orientadores: Ney Roitman
José Renato Mendes de Sousa

Programa: Engenharia Civil

A robustez e versatilidade da tecnologia dos dutos flexíveis para a indústria petrolífera offshore foram decisivas para a conquista de recordes consecutivos no que se refere à lâmina d'água de explotação. Em algumas aplicações, essa tecnologia é a única disponível e adequada, mas, por outro lado, a predição do comportamento mecânico dessas estruturas quando fletidas ainda se constitui em um grande desafio para o dimensionamento, por exemplo, à fadiga.

Desse modo, essa dissertação apresenta um novo modelo de elementos finitos tridimensional e não linear para análise local de dutos flexíveis. Este modelo, além de ser capaz de representar todos os arames de tração e todas as camadas da estrutura, permite não só aplicar cargas axissimétricas, mas também momentos fletores.

A efetividade do modelo proposto é corroborada pela satisfatória concordância dos resultados numéricos com medidas experimentais obtidas através de testes nos quais uma amostra de duto flexível é submetida a cargas de tração pura e também tração combinada com flexão.

Abstract of Dissertation presented to COPPE/UFRJ as a partial fulfillment of the requirements for the degree of Master of Science (M.Sc.)

FINITE ELEMENT ANALYSIS OF FLEXIBLE PIPES:
BENDING COMBINED WITH TENSILE LOAD

Cristiano Alves Pinto Mosqueira Gomes

October/2017

Advisors: Ney Roitman
José Renato Mendes de Sousa

Department: Civil Engineering

The robustness and versatility of the flexible pipeline technology for the offshore oil industry were decisive for the achievement of consecutive records regarding the water depth. In some applications, this technology is the only available and suitable, but on the other hand, the prediction of the mechanical behavior of these structures when under bending is still a great challenge for design suitable, for example, to fatigue.

Thus, this dissertation presents a new three-dimensional and non-linear FE model for local analysis of flexible pipes. This model, in addition to being able to represent all the tension armor wires and all the layers of the structure, allows not only the application of axisymmetric loads, but also bending moments.

The effectiveness of the proposed model is corroborated by the satisfactory agreement of the numerical results with experimental measurements obtained through tests in which a flexible pipe sample is subjected to pure tension load and also combined tension with bending.

TABLE OF CONTENTS

LIST OF FIGURES

LIST OF TABLES

NOMENCLATURE

API	American Petroleum Institute
E&P	Exploration and production
FE	Finite element
FEA	Finite Element Analysis
FEM	Finite element method
Flexible pipe's annulus	Region between the pressure sheath barrier and an outer polymer barrier.
FPSO	Floating Production Storage and Offloading
HDPE	High density polyethylene
IFPEN	IFP Energies Nouvelles, former French Institute of Petroleum (*Institut Français du Pétrole*)
O&G	Oil and gas
PE	polyethylene (PE),
PA	polyamide (PA),
PVDF	polyvinylidene fluoride (PVDF),
SHM	Structural Health Monitoring
XLPE	crosslinked polyethylene

LIST OF SYMBOLS

h	Thickness
w	Width
υ	Poisson's ratio
n_t	Number of tendons
E	Elastic modulus of the material
α	Lay angle
I	Moment of inertia
A	Cross sectional area of the profile
L_p	Pitch of the tendon
I_x	Minimum principal moment of inertia
J_t	Torsional constant of the tendon
G	Transverse shear modulus of the material
K	Compacity factor
τ_{max}	Limit shear stress in the contact interface
μ	Friction coefficient
τ	Adhesion
P_c	Contact pressure between layers
κ	Curvature
κ_f	Critical Curvature
h_{shell}	Equivalent thickness of the shell
G_{shell}	Transverse shear modulus of the shell
E_{shell}	Elastic modulus of the shell
$\sigma_t(P_c, \kappa_f, \theta)$	Normal Axial Stress due to Friction
a	Average radius of the layer
M_f	Friction moment or moment of internal friction
EI_{fs}	Full-slip bending stiffness
EI_{ns}	No-slip bending stiffness

$\kappa_{contact}$	Curvature at which lateral contact occurs between adjacent tensile armor wires
r	radius of tensile armor layer
R	Bending radius
θ	Circumferential angle of flexible pipe
S	Deformed length of the helix on the torus

CHAPTER 1. INTRODUCTION

1.1 MOTIVATION

Despite occasional crises, the oil and gas (O&G) industry has demonstrated a prolonged period of significant growth, following global demand for hydrocarbon energy, as shown in Figure 1.1.

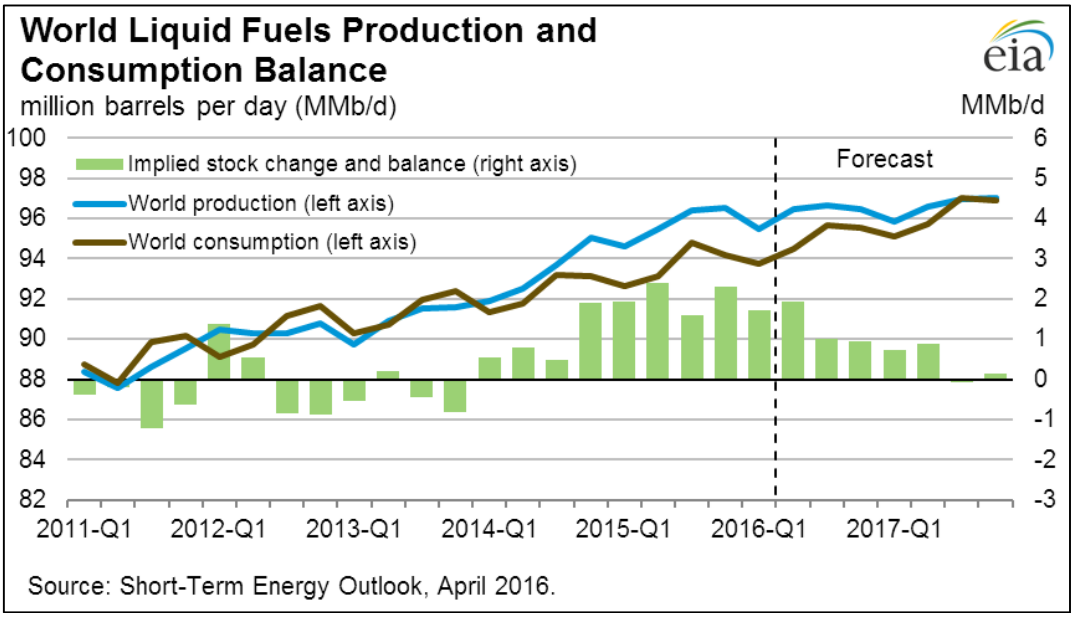

Figure 1.1. World Liquid Fuels Production and Consumption Balance (EIA - THE U.S. ENERGY INFORMATION ADMINISTRATION, 2016).

Although about 60% of O&G worldwide supply is extracted onshore, the competition between different oil sources is noteworthy. Over the last decades, offshore O&G production has increased compared to onshore production, as indicated in Figure 1.2, and this increase relies greatly in the use of FPSOs and semi-submersibles, which have also been working on ever-increasing water depths, as can be depicted in Figure 1.3 and Figure 1.4. There are several reasons for that, but, in short, the use of these floating vessels allows the development of marginal fields in remote locations, where a fixed platform would be impractical and/or

uneconomical. Besides, FPSOs can be relocated and reused, for example, in case of field depletion.

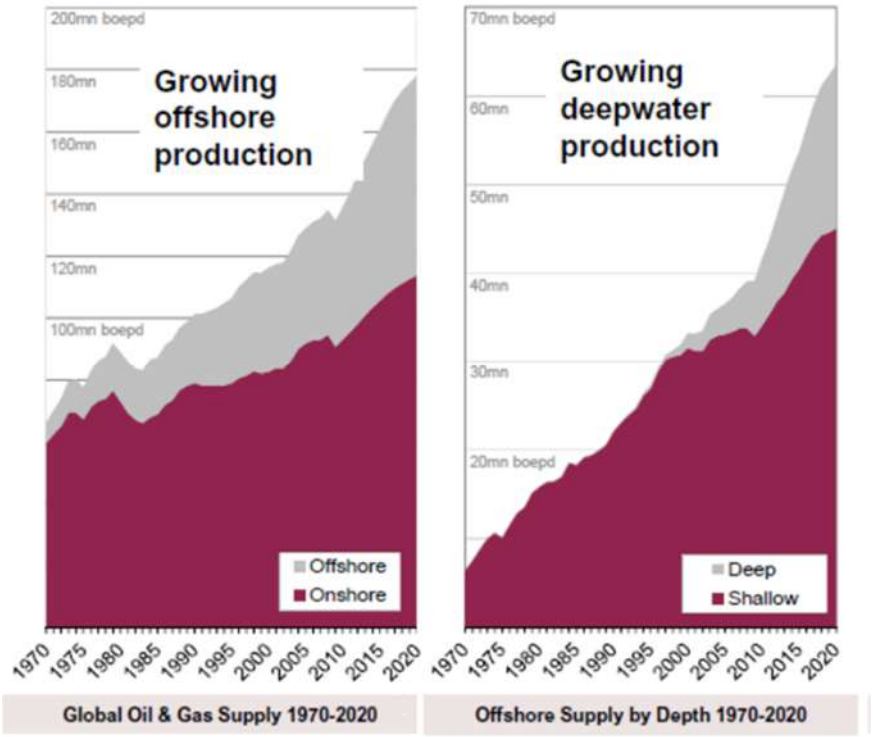

Figure 1.2. Offshore production (KOPITS, 2012).

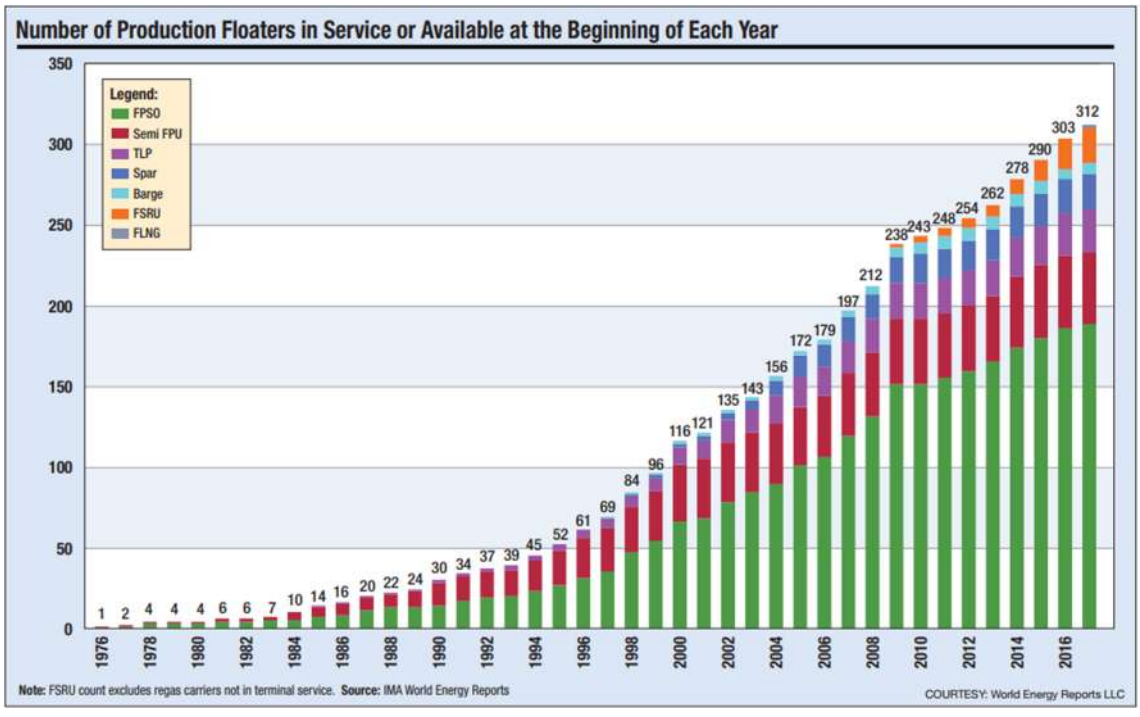

Figure 1.3. Floating Production Systems. (OFFSHORE MAGAZINE, 2016).

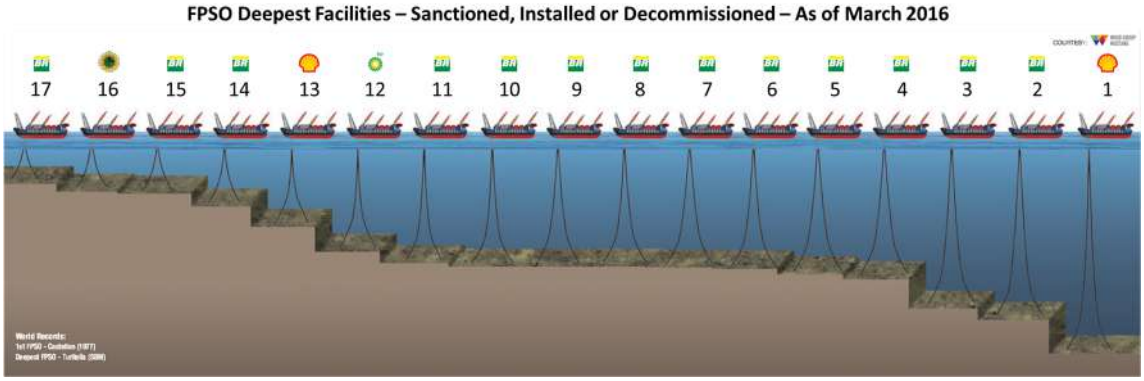

#	Name	Operator	Year	Depth
1	Turitella	Shell	2016	2896m
2	BW Pionner	Petrobras	2012	2600m
3	Dynamic Producer	Petrobras	2011	2500m
4	Cidade de Itaguaí	Petrobras	2015	2240m
5	Cidade de Mangaratiba	Petrobras	2014	2200m
6	Cidade de Angra dos Reis	Petrobras	2010	2150m
7	Cidade de Ilha Bela	Petrobras	2014	2140m
8	Cidade de Marica	Petrobras	2016	2120m
9	Cidade de São Vicente	Petrobras	2009	2120m
10	Cidade de Paraty	Petrobras	2013	2120m
11	Cidade de São Paulo	Petrobras	2013	2100m
12	PSVM	BP	2012	2000m
13	BC-10 Espírito Santo	Shell	2009	1780m
14	Piranema Spirit	Petrobras	2007	1600m
15	Capixaba	Petrobras	2010	1485m
16	Agbami	NIPCO - Nigeria	2008	1462m
17	P-54	Petrobras	2007	1400m

Figure 1.4. FPSO Deepest Facilities and Petrobras achievements (adapted from (OFFSHORE MAGAZINE, 2016)).

In this scenario, the use of unbonded flexible pipes (or, simply, flexible pipes), such as the one presented in Figure 1.5, instead of rigid (carbon steel) pipes, is often advantageous due to several reasons as their compliance with the movements imposed by the floating vessels, the ability to absorb harsh environmental loads and easiness of installation. In Brazil, these structures have been firstly used in 1977 with the early production systems designed for Enchova, Garoupa and Namorado fields (FACHINI, 2014) in water depths close to 100 m. In 2016, more than 12,000 km of flexible pipes were in operation in Brazil (MATOSO, 2016).

Figure 1.5. Flexible Pipe in operation (adapted from (SUBSEA WORLD NEWS, 2017)).

According to (AMERICAN PETROLEUM INDUSTRY, 2014), a flexible pipe is an assembly of a pipe body and end-fittings where the pipe body is composed of layered materials that form a pressure-containing conduit and allows large deflections. Normally, the pipe body is build up as a composite structure composed of metallic and polymers layers.

Despite the successful use of these structures in offshore O&G applications, offshore O&G fields are moving fast to water depths close to 3,000m (Figure 1.6) and, consequently, there is a need to not only design flexible pipes capable of resisting the loads associated with this scenario, but also to reduce the conservatism in their design. Moreover, some of the first flexible pipes installed in deep and ultra-deep waters are reaching or have already reached their limit service lives and operators wish to extend their use.

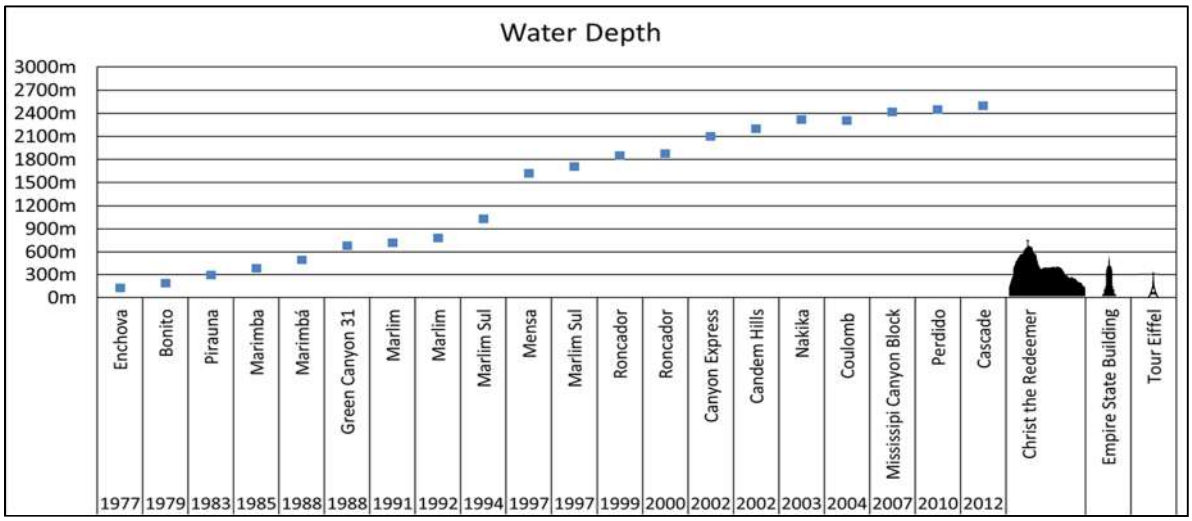

Figure 1.6. Progression with water depth.

Despite the robustness and confidence attributed to flexible pipes, the determination of their fatigue limits still deserves great attention. Among the main requirements for a reliable fatigue analysis, it could be highlighted the:

- Determination of the actual operating conditions (top tension, annulus condition, internal pressure, curvatures etc.);
- Structural analysis;

The determination of the actual operating conditions could be fulfilled by the implementation, for instance, of several SHM solutions, such as those from Figure 1.7. The term SHM, i.e., Structural Health Monitoring, refers to monitoring systems that aims to gain knowledge of the integrity of in-service structures on a continuous real-time basis.

Flexible Pipe ready for Flooding Detection System

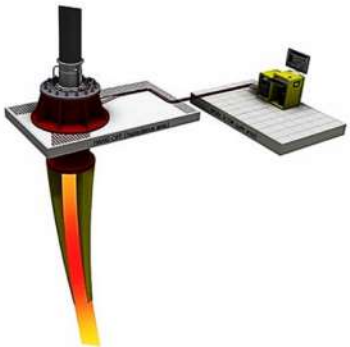

Scheme of a monitoring system for curvature

Figure 1.7. Examples of SHM solutions (adapted from (ELOSTA, *et al.*, 2017)).

The structural analysis, as pointed out by several authors such as (SOUSA, *et al.*, 2012), (LONDOÑO, *et al.*, 2014), (LIU, 2014), (XIQIA, *et al.*, 2015), (TANG, *et al.*, 2015) and (SÆVIK, *et al.*, 2017), aims to adequately predict the stresses and strains that are induced in the flexible pipe layers by operational loads. Stresses are assessed by relying on a set of different theories and assumptions, which, consequently, play a decisive role in predicting fatigue damage.

In this scenario, the response of flexible pipes to bending is a key aspect, but, despite being studied since practically the beginning of the flexible pipe industry, until today there are still open discussions on this response which directly affects the global and local mechanical analyses of flexible pipes.

Therefore, the challenge and importance of bending analysis for a robust and game-changing technology, such as flexible pipes, is noteworthy. From this, came the interest in the topic of this dissertation.

1.2 OBJECTIVE

This dissertation presents a FE model to predict the structural response of a flexible pipe subjected to pure and combined tensile and bending loads.

The model employs shell elements to represent all layers of the pipe and their interactions are ensured with contact elements. The model was constructed using ANSYS® Multiphysics package and its implicit solver. The results obtained with this model are compared to those from experimental tests performed at COPPE/UFRJ.

1.3 DESCRIPTION OF THE CHAPTERS

In this dissertation, firstly, Chapter 2 presents the flexible pipe structure and the state of the art of the local axisymmetric and bending analyses. Next, in Chapter 3, the finite element model proposed in this study is described. After that, in Chapter 4, the results from experimental tests performed at COPPE/UFRJ are presented and compared to those obtained with the FE model. The responses of the pipe to tension and bending combined with tension are studied enlightened by these results. Finally, the main conclusions of this work as well as proposals for future works are stated.

CHAPTER 2. FLEXIBLE PIPE

2.1 FLEXIBLE PIPE STRUCTURE

As described by (BRAESTRUP, *et al.*, 2009), unbonded flexible pipes are custom designed and complex multi-layered structures, built from several helically wound metallic wires or strips combined with concentric layers of polymers, textiles and fabric tapes. Figure 2.1 presents the structure of a typical unbonded flexible pipe.

Figure 2.1. Typical unbonded flexible pipe. (adapted from (LONDOÑO*, et al.*, 2014)).

The modularity is a remarkable quality in its construction. The layers of the pipe are independent, but designed to interact with one another. Each layer can be made fit-for-purpose and independently adjusted to best meet specific field requirements, which are related to the use of the pipe, such as water and gas injection lines or production and gas export lines.

As shown in Figure 2.1, the internal structure of a flexible pipe usually comprises an inner carcass, an internal plastic sheath, a pressure armor, anti-wear tapes, tensile armors and an external sheath. Other layers may be present to address other structural demands. In the following, a brief description of these main layers is presented, but more

details can be found, for instance, in API RP 17B (AMERICAN PETROLEUM INDUSTRY, 2014).

CARCASS

The carcass, the innermost layer, is designed to resist radial external loads (crushing and hydrostatic pressure), and to serve as a mechanical protection for the pressure sheath against, for instance, the erosion caused by the passage of solid fluid particles such as sand.

The layer is manufactured by cold forming a flat stainless-steel strip into an interlocking structure thus forming a corrugated profile (Figure 2.2). This strip is laid with an angle close to 90˚ with respect to the axis of the pipe.

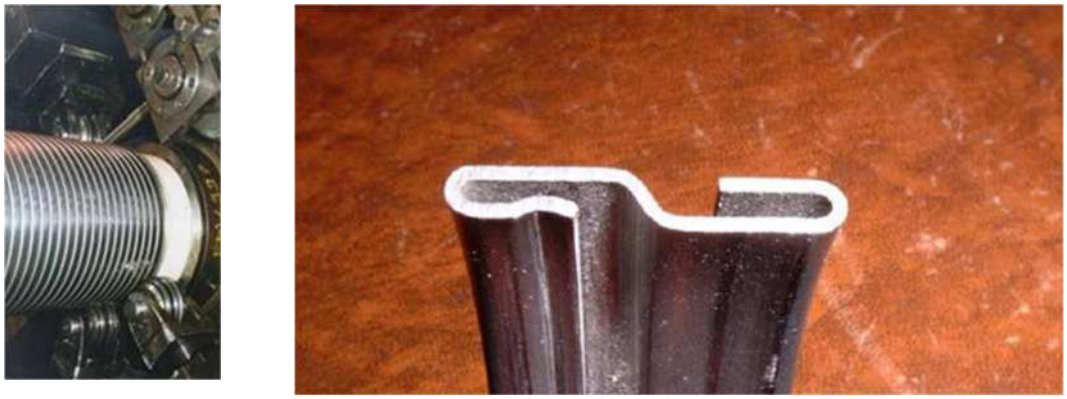

Figure 2.2. Manufacturing process of Carcass (adapted from (FACHINI, 2014))

It also should be noted that, unbonded flexible pipes can be rough-bore or smooth bore, depending on whether the carcass is present or not, respectively.

PRESSURE SHEATH

The pressure sheath is a polymeric layer that is normally extruded over the carcass. The polymer extrusion process, as shown in Figure 2.3, is continuous. In order to avoid any mechanical property loss, the extrusion temperature and sheath thickness are respected within narrow manufacturing tolerances. The main function of this layer is to seal the bore of the flexible pipe.

Figure 2.3. Manufacturing process of pressure sheath (FACHINI, 2014)

The design of the pressure sheath depends on the chemical compatibility with the bore fluids, polymer aging, loads and permeation characteristics. According to the (AMERICAN PETROLEUM INDUSTRY, 2014), this sheath is manufactured from polyamide (PA), polyvinylidene fluoride (PVDF), high density polyethylene (HDPE), polyethylene (PE), or crosslinked polyethylene (XLPE).

PRESSURE ARMOR

According to the (AMERICAN PETROLEUM INDUSTRY, 2014), the pressure armor is a structural layer with a lay angle close to 90° that resists internal and, possibly, external pressure and mechanical crushing loads. This layer structurally supports the pressure sheath, as shown in Figure 2.4, and consists of an interlocked metallic construction with typical cross-sections shown in Figure 2.5.

The design of the pressure armor depends on the loads that act on the flexible pipe and, moreover, on the annulus conditions (pH, temperature, corrosive gases). The typical material for this layer is high strength carbon steel.

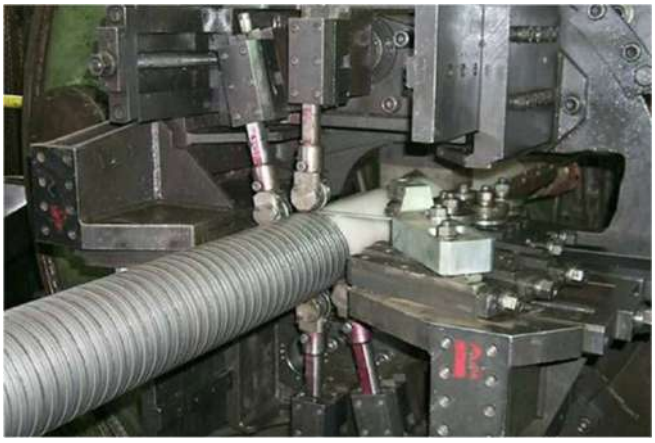

Figure 2.4. Manufacturing process of pressure armors (FACHINI, 2014)

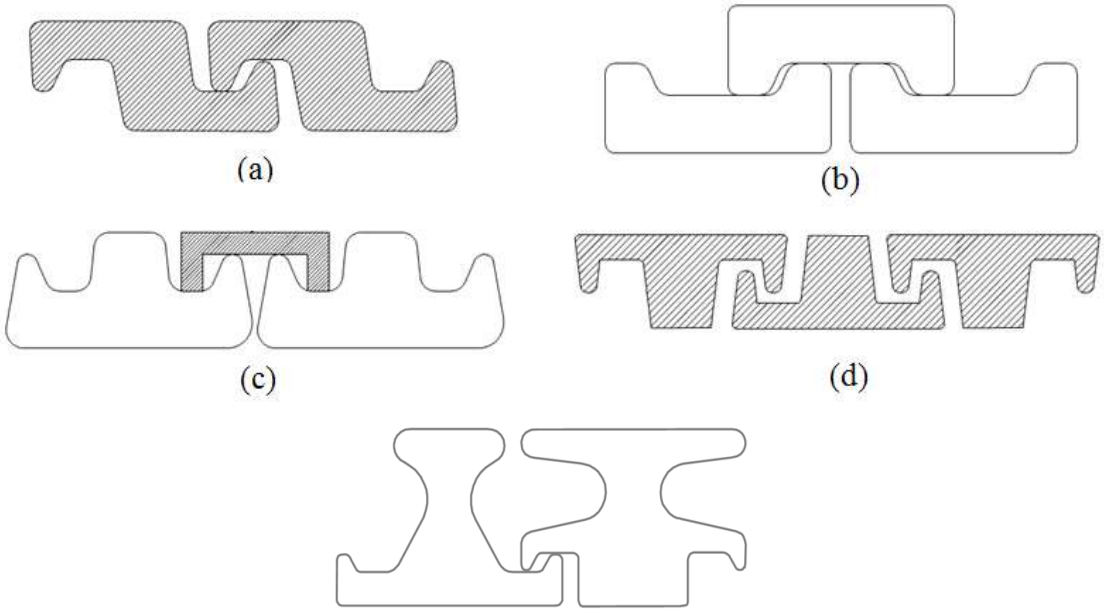

Figure 2.5. (a) Z-shape, (b) C-shape, (c) T-shape 1, (d) T-shape 2 (e) PSI (MIYAZAKI, 2015)

TENSILE ARMORS

The tensile armors are manufactured from thin high strength metallic wires laid in two or four layers and cross wound for torsional balance. The cross-section of these wires is approximately rectangular and typical lay angles vary between 20° and 55° with respect to the longitudinal axis (Figure 2.6).

Figure 2.6. Manufacturing process of tensile armors (FACHINI, 2014)

The tensile armors are designed to sustain (totally or partially) tension, internal pressure and end-cap effects.

ANTI-WEAR TAPE

If two layers of armors are in direct contact, wear or fretting may occur between them. As an example, in 20 years of operation, the tensile armor wires of a flexible riser subjected to cyclic bending loads may present a cumulative slip of about 50 km as mentioned by (FERGESTAD & LØTVEIT, 2014). Aiming at reducing this effect, anti-wear layers are employed to reduce friction between layers and improve the fatigue performance of risers designed to withstand dynamic loads.

These layers are usually positioned between the pressure armor and the inner tensile armor layer and between the tensile armor layers by either extruded thermoplastic sheath or tape wrapping. Furthermore, these layers are usually not leakproof and are usually manufactured from polyamide (PA), polyvinylidene fluoride (PVDF) or high-density polyethylene (HDPE) (AMERICAN PETROLEUM INDUSTRY, 2014).

EXTERNAL SHEATH

The external sheath is designed to keep the tensile armors in position after forming and protect the annulus of the pipe. This sheath is manufactured from a polymeric material

such as high-density polyethylene (HDPE), polyamide (PA), or thermoplastic elastomer (TPE) extruded over the tensile armor layers (AMERICAN PETROLEUM INDUSTRY, 2014).

ADDITIONAL LAYERS

There are other layers that play important roles in certain structures and applications such as high strength tapes, thermal insulation layers and intermediate (anticollapse), sacrificial sheaths and protective sheaths.

High strength tapes are used to resist the excessive radial displacement of the tensile armor wires that may lead to birdcaging failure (AMERICAN PETROLEUM INDUSTRY, 2014). Insulation layers are included to provide a further passive insulation to reduce heat loss from the bore fluids. Intermediate (anticollapse) sheaths are used to increase the pipe collapse resistance by preventing seawater pressure from acting directly on the internal pressure sheath in the event of a breach in the outer sheath or end-fitting outer sheath seal leakage. Sacrificial sheaths are located above the carcass or below the pressure armor and are used to protect the pressure sheath. Finally, a protective sheath may be placed above the outer sheath in order to have a redundancy and increase the protection from external mechanical loads.

More information about these and other layers can be found in (AMERICAN PETROLEUM INDUSTRY, 2014) and (FERGESTAD & LØTVEIT, 2014).

2.2 LOCAL ANALYSIS OF FLEXIBLE PIPES

Based on the description presented in the previous section regarding the layers of a flexible pipe, it can be depicted that the assessment of stresses, deformations and stiffnesses of this structure is a very complex goal and requires specific models.

In this context, several analytical and numerical studies and models were developed with the purpose of representing certain structural responses and, particularly, the response to tensile (or, generally, axisymmetric) and bending loads. In the next sections, some of these works are briefly presented.

TENSILE RESPONSE

Under tension load, the tensile armors tend to squeeze the inner core of the flexible pipe, inducing normal compressive stresses in the carcass and pressure armor. It is noted that the contact pressure tends to increase from the interface of the outer tensile armor with the anti-wear tape to the interface of the internal tensile armor with the innermost anti-wear tape, where the contact pressure is known as squeeze pressure. There is a coupled behavior between tension and torsion, i.e. when the flexible pipe is under tension, an axial rotation occurs, if the axial rotation of the pipe is allowed, or a reaction torque can be imposed on the flexible pipe, if the axial rotation of the pipe is restricted.

In general, the available models predict well the main characteristics of the response to tension and other axisymmetric loads, but, there are, however, some uncertainties related, for example, to the axial-torsional coupling.

The first models to predict this type of response in flexible pipes date from the early 1980's, but these first models often rely on parameters that had to be previously calibrated to obtain adequate results. However, (FERET & BOURNAZEL, 1987), by assuming that the pipe is composed of several concentric tubular and helical armor layers, formulated a set of linear equations that govern the axisymmetric response of flexible pipes. This model served as a base to several analytical models employed by the industry, such as the computational program FRAES, which is used by Petrobras to perform the local mechanical analysis of flexible pipes under axisymmetric loading (BATISTA, *et al.*, 1989).

(WITZ & TAN, 1992) presents a nonlinear analytical model for the axial-torsional behavior of flexible pipes under moderate loads. This model considers the polymeric layers as thin-walled cylinders and the response of the armors are governed by Clebsh-Kirchoff-Love's equilibrium equations. Three different structures were analyzed: a typical marine cable, a flexible riser and an umbilical cable. The results of the model agreed well with those from tensile experimental tests.

(WITZ, 1996), presented a test campaign carried out with a 2.5in flexible pipe including experimental data related to both the axial-torsional and flexural structural responses of the pipe. The load vs displacement curves predicted by several analytical models were compared to those from the experimental tests. In a general manner, all results agreed well, but the response to torsion was better estimated with the models that

considered separation between layers. Moreover, some discrepancy was observed in the axial-torsional coupling response of the pipe.

(CUSTÓDIO & VAZ, 2002) proposed an analytical formulation for the response of umbilical cables and flexible pipes subjected to monotonic loading of tension, torque, internal and external pressures, improving the available models by considering geometric, material, and contact nonlinearities.

(RAMOS, 2001) presented an analytical formulation for the structural response of flexible pipes subjected to combined loads of bending, torque, axial tension and internal and external pressures. A work related to this study is presented (RAMOS, *et al.*, 2004).

(RAMOS, *et al.*, 2008) performed a set of tests with a 2.5" flexible pipe sample under alternating axial tension with and without internal pressure. The influence of the boundary conditions on the response of the pipe was also analyzed and discussed. The results were compared to the previously proposed model of (RAMOS, *et al.*, 2004).

(RAMOS, *et al*., 2014) presented some further investigations into the behavior of the flexible pipe sample from the same full scale tests previously described in (RAMOS, *et al.*, 2008). This investigation considers repeatability and an evaluation over the axial strains in the armor wires, highlighting that although uniformity is not fully observed in practice, even considering only axisymmetric loads, analytical values can be used to predict the average of experimental strain value.

Despite their computational efficiency and reasonable agreement with experimental tests, analytical models rely on several simplifying assumptions that may interfere in some aspects of the pipe's response. These assumptions may be divided into four groups (CUSTÓDIO & VAZ, 2002):

- Regularity of initial geometry;
- Reduction to simple plane cross-section analyses.
- Negligible effects of shear and friction.
- Linearity of the response.

Available numerical models do not consider some of these assumptions, but usually demand high computational resources.

(CRUZ, 1996) developed a FE model in which the inner carcass, pressure armor and polymeric layers are modeled with three-dimensional solid elements and the tensile armors with three-dimensional beam elements. Contact between layers were addressed with three-dimensional beam or truss elements. This model was employed to analyze the

response of flexible pipes to tension and crushing loads. A preprocessor called GERFLEX was also developed to generate FE meshes to be analyzed with the commercial packages of ANSYS® (GERFLEX, 1995).

(SOUSA, 1999) employed the model proposed by (CRUZ, 1996) to study the response of flexible pipes to other axisymmetric loads and bending. The numerical responses were compared to those obtained with the analytical model of (BATISTA, *et al.*, 1989).

(SOUSA, 2005) proposed a FE model based on shells and beams finite elements and node-to-node contact elements. This model was employed to analyze the response of flexible pipes to different types of loads such as axisymmetric, bending and crushing loads. The failure mechanisms related to axial compression and excessive external pressure were also discussed. The predictions of the model were compared to experimental measurements indicating reasonable agreement. A FE mesh generator called RISERTOOLS was also developed. The FE meshes are generated to be analyzed with ANSYS® package.

(BAHTUI, *et al.*, 2008) studied the response of a five-layer flexible pipe to cyclic pure tension with a detailed nonlinear solid three-dimensional FE model developed for ABAQUS/Explicit®. The model addresses contact nonlinearities and is compared only with an analytical model, presenting good correlation, but demanding great computational cost.

(MERINO, *et al.*, 2009), (MERINO, *et al.*, 2010) and (MERINO, *et al.*, 2016) analyzed a set of tests with a 4” flexible pipe sample including pure axial tension and pure torsion and torsion combined with axial tension, respectively. Numerical analyses were conducted with the model proposed by (SOUSA, 2005) and the obtained results were compared to those from experimental tests conducted at COPPE/UFRJ. These studies evidenced the linear response of the pipe to tension and a nonlinear response to torsion, which was credited to friction between layers. Furthermore, the impact of considering the relative axial translation and rotation of the pipe’s layers along its length is pointed as the main reason for the discrepancies observed between the axial-torsional coupling coefficients calculated by the numerical model and those estimated by traditional analytical models.

(SÆVIK, 2011) proposed a model for the axisymmetric response, adopting formulations based on large displacements and small strains theory. At the end, the model

is validated using data from a test of an 8in flexible riser briefly described. Besides this, two alternative formulations are proposed for predicting bending stresses in tensile armour wires.

(SOUSA, *et al*., 2013b) studied the response of a 2.5” flexible pipe subjected to pure tension, torsion combined with tension, tension combined with internal pressure and torsion combined with tension and internal pressure. Authors used a modified version of the model proposed by (SOUSA, 2005) in which the contact between layers is ensured with surface or line to surface contact elements. The predictions of the model agreed well with the experimental measurements.

The study of (EDMANS, *et al*., 2012) presented a model based on shell elements and ABAQUS/Standard®, the implicit non-linear solver of ABAQUS®. The model was verified just for axisymmetric loads such as axial tension and internal/external pressure.

In (GONZALEZ, *et al.*, 2015), the proposed model consists, mainly, of shell elements and is evaluated under pure tension load. Only the carcass and the pressure armor were modeled with rebar elements. In this study, ABAQUS/Explicit® was employed.

BENDING ANALYSES

One of the main advantages of flexible pipes over conventional rigid steel pipes is the capacity to withstand large bending curvatures without structural damage, whilst maintaining the necessary axial and pressure robustness. Contrary to the discussed almost linear response to axisymmetric loads, flexible pipes have a hysteretic non-linear bending response. This behavior is highly governed by the relative sliding between adjacent layers, especially the tensile armor wires, which have their sliding prevented by the interlayer friction that is largely related with interlayer pressures. In short, the bending response is also related to the axisymmetric loading ((KEBADZE, 2000), (CAIRE, 2014) and (PÉRONNE, *et al*., 2015)).

Even though there are still open discussions on the response of flexible pipes to bending loads, this response has been studied since practically the beginning of the flexible pipe industry with analytical and numerical models and also experimental tests.

The hysteretic behavior, when a pipe is subjected to bending loads, is represented, approximately, by the non-linear moment vs curvature diagram presented in Figure 2.7.

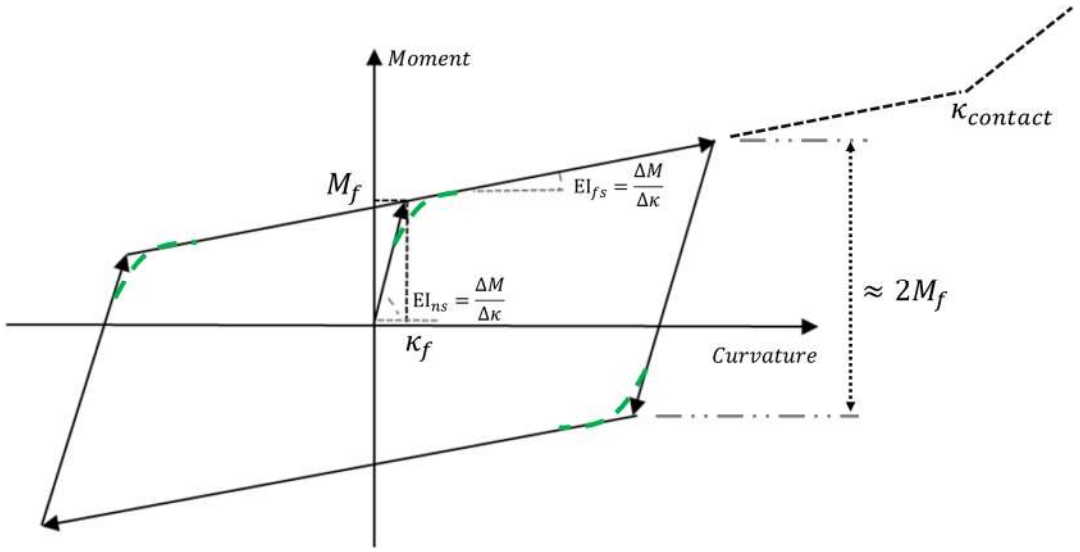

Figure 2.7. Moment x Curvature graph (adapted from (LONDOÑO, *et al.*, 2014))

The response of the pipe to bending is governed by the relative slip mechanism between the tensile armor layers (FERGESTAD & LØTVEIT, 2014). When the imposed curvature κ is small, the interlayer friction prevents the relative slippage. This leads to a linear bending moment vs curvature relationship with an initially very high tangent stiffness. This tangent stiffness is called no-slip bending stiffness, EI_{ns}.

The moment needed to overcome the friction forces, M_f , is called the friction moment or moment of internal friction. This moment depends on the contact pressure, P_c, between the pipe layers and, consequently, on the axisymmetric loads applied to the pipe such as axial tension and external and internal pressures (FERGESTAD & LØTVEIT, 2014), (LONDOÑO, *et al.*, 2014) and (LIU, 2014).

As curvature increases, interlayer friction is progressively overcome, allowing the relative movement of the armor wires. This relative movement leads to tangent stiffnesses much lower than the no-slip value. The minimum value of this stiffness is called full-slip bending stiffness, EI_{fs} (SOUSA, *et al.*, 2015), and is mainly related to the bending stiffness of the polymeric sheaths. The area within the hysteretic loop corresponds to the energy consumed by internal friction during this process (LIU, 2014).

Some recent studies, such as (SÆVIK, 2011) and (LIU, 2014), however, approximate the moment curvature relationship by a tri-linear curve and define three regimes: stick regime; stick to slip regime and full slip regime.

It is important to highlight, in Figure 2.7, that the full slip regime is achieved with twice the friction moment in case of curvature reversal. Moreover, Figure 2.7 also indicates the curvature at which lateral contact occurs between adjacent tensile armor wires, $\kappa_{contact}$. This contact causes a significant increase in the bending stiffness of the flexible pipe, besides considerably increasing the stresses in the wires. The flexible pipe is not designed to operate with such large curvatures (or small radius), which can be estimate with equations presented in (SHI, 2014) and (FERGESTAD & LØTVEIT, 2014). Moreover, a minimum bending radius (MBR) has to be established for design purposes. This radius is calculated including safety factors, as discussed in (AMERICAN PETROLEUM INDUSTRY, 2014). The minimum bending radius (MBR) is also experimentally assessed in (PESCE, *et al*., 2011).

All analytical models and, in a certain extent some numerical models, assume that the tensile armor wires slide over a torus following known paths, which are usually geodesics or loxodromics of the torus. The geodesic is the curve that links two points in the torus by following the shortest distance between them, while the loxodromic is the curve that links two points of the torus always making an equal angle with each of its meridians, i.e. cross section of the torus. Figure 2.8 exemplifies theses curves.

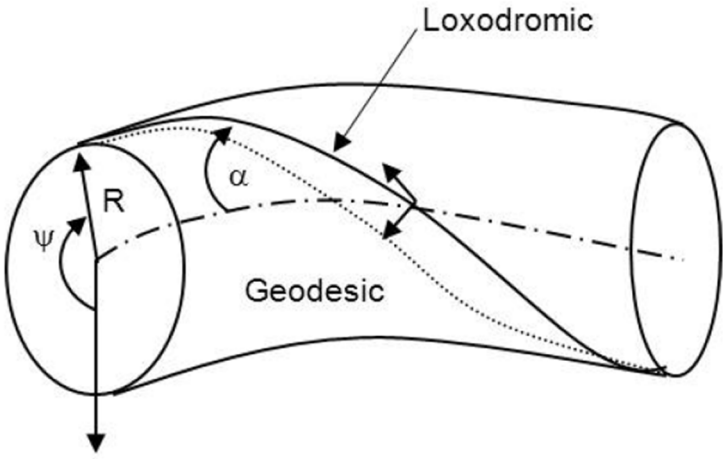

Figure 2.8. Loxodromic and Geodesic curves (FERGESTAD & LØTVEIT, 2014).

The geodesic or loxodromic hypothesis is an open issue in the analysis of flexible pipes to bending loads and the response will actually be confined between those two curves.

(FERET & BOURNAZEL, 1987) observed the bending hysteretic loop in a flexible pipe and considered that the tensile armors move and behave elastically tending to rearrange following geodesic lines. (FERET & MOMPLOT, 1991) updated the model of (FERET & BOURNAZEL, 1987) by proposing a different equation to calculate the normal curvature changes in the tensile armor wires, but also assuming the geodesic hypothesis.

(BERGE, *et al*., 1992) indicated that the geodesic hypothesis does not provide adequate results for the stress state in the tensile armor wires. The authors proposed, therefore, that the deformed configuration of these wires follows loxodromic curves. New equations to calculate the bending stiffnesses and internal friction moments in flexible pipes are proposed as well as equations to calculate the stress components in these wires.

(ESTRIER, 1992) unites the theories presented by (FERET & MOMPLOT, 1991) and (BERGE, *et al*., 1992) by assuming that before the slippage the wires follow a loxodromic curve and after the slippage follow a geodesic curve. Equations to estimate the stresses in the wires of the flexible pipe are deduced and employed in the fatigue analysis of a flexible pipe.

(KEBADZE & KRAINCANIC, 2000) presented an analytical model describing the variation of the bending stiffness of an armor layer as a function of curvature, friction coefficient and interlayer pressures from the non-slip to the full-slip bending regime. Several assumptions were adopted, such as: armor wires sliding only along their own axes (loxodromic hypothesis), negligible contact pressure induced by bending itself, bending conditions far from the terminations, equal static and dynamic friction coefficients, no lateral contact between wires and negligible bending and torsional stiffness of individual armor wires.

(RAMOS JR. & PESCE, 2002) presented an analytical model to represent the structural behavior of a flexible pipe under axisymmetric and bending loads. (RAMOS JR, et al., 2003) updated the model by proposing an equation to estimate the equivalent bending stiffness of flexible risers and the bases behind its derivation. Besides this, a set of equations to estimate the slip of armor wires in a flexible pipe under constant curvature was also discussed.

(TAN, *et al.*, 2005) presented a theoretical model based on the minimum strain energy to study higher order effects in bent tensile armor wires. In short, the authors presented the results, showing that this model demonstrates the effect of the wire cross-

section size over its deflected configuration during bending. The analytical study was compared with a simplified FE approach in which just a supporting cylinder and two identical wires (with one complete pitch length) are modeled. Finally, the authors warn that their conclusions apply only to flexible pipe experiencing uniform bending and being away from the constraint effect of the end fitting.

(FERGESTAD & LØTVEIT, 2014) states that the wire path is somewhere between loxodromic and geodesic, and so the dynamic bending torsion and curvature in each wire is somewhere between both paths. Also, according to this reference, assuming harmonic helix motion and no end effects, an arbitrary cross-section of flexible pipe can be divided into two zones where one part of the cross-section will be in the slip domain (neutral line region), whereas the other will still be in the stick-domain (intrados and extrados region). Another important highlight is that flexible pipe's tension and external pressure vary along its length, hence the critical moment and friction moment will also change along its length.

(TANG, *et al.*, 2015), presented a comparison between seven previous models proposed to get in a standardized form the bending stress at the corner point of the armor wire section. These models were compared also with a simplified FE model under a constant curvature for an 8in flexible pipe. Despite improvements that may be necessary, it is important to note the extreme importance of consolidating studies of this type.

In this context, it is important to mention that the bending load induces three different stress components in the armor wires: axial stresses induced by friction between the layers, σ_t, normal bending stresses, σ_n, (bending along the axis of least moment of inertia of the wire, i.e. normal axis or x direction) and binormal bending stresses, σ_b, (bending along the axis of greatest moment of inertia of the wire, i.e. binormal axis or y direction) as presented in Figure 2.9.

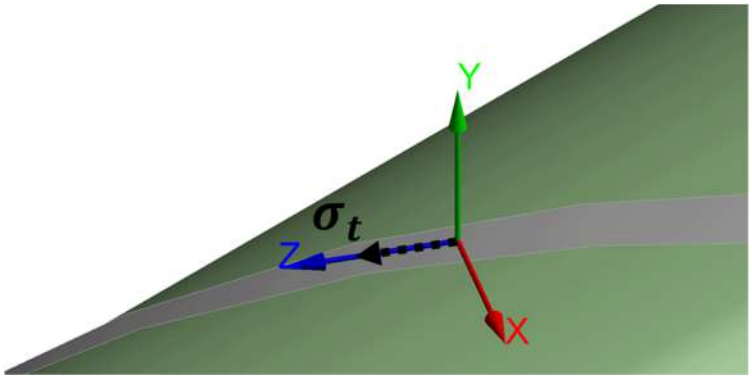

Figure 2.9. Armor Wire – Stress Components

In the present study, only few equations will be used and presented as an analytical reference purpose. The equations used to obtain the critical curvature and also the normal axial strain due to friction come from (ESTRIER, 1992).

Regarding FE models, several of them have been presented in the last decades to better understand the bending behavior of flexible pipes. It should be mentioned that the complexity and computational cost of these models have increased considerably with the processing capacity of computing. In order to simplify this complex analysis, some models represented only few armor wires.

(SÆVIK, 1993) proposes a FE model in which one tensile armor wire is modeled with three-dimensional beam elements. Initially, the wire could move both longitudinally (along its lay direction) and transversally. However, due to convergence issues, the transverse translation was restricted and, consequently, the wire follows a loxodromic of the supporting surface.

Over time, however, some models have been developed with the capacity to represent all the armor wires and flexible pipe layers. In this scenario, it is possible to highlight the already mentioned RISERTOOLS® initiative presented by (SOUSA, 2005) for ANSYS®, which was used by several bending studies as (SOUSA, 2005), (LONDOÑO, et *al.*, 2014), (LODOÑO, 2013) and (SOUSA, *et al.*, 2015).

More recently, some other FE models have been presented as (BAHTUI, *et al.*, 2009), (ALFANO, *et al.*, 2009), (LEROY, *et al.*, 2010), (PERDRIZET, *et al.*, 2011), (SANTOS, *et al.*, 2015), (XIQIA, *et al.*, 2015) and (TANG, *et al.*, 2015). All these models were developed in ABAQUS®.

(BAHTUI, *et al.*, 2009) and (ALFANO, *et al.*, 2009) presented FE models of six and seven-layered flexible pipes, respectively. Both models use an 8-noded linear brick finite element for the plastic sheaths and anti-wear layers and a 4-noded doubly curved thin shell element for the carcass. It is not clearly stated which elements are adopted for the armor layer, which is fully represented in this study. Contact is addressed by using the penalty contact method and Coulomb friction is also assumed. The explicit-dynamics solver of ABAQUS® was used due to the large number of contact surfaces.

The study of (PERDRIZET, *et al.*, 2011) presents a FE model of a five-layered flexible pipe with 7.0 m in length. This model adopts three-dimensional brick elements to all armor wires and shell elements for the anti-wear layer. For the internal and external

layers of the pipe, it was briefly described the adoption of two equivalent kernels. In addition to representing all the armor wires, this model can take into account non-uniform curvature distribution along the pipe and used both ABAQUS® solvers. It should be noted the use of IFPEN's supercomputer due to the large number of DOFs (up to 2.5 billions) involved in the analysis. In specific regions, ABAQUS® /Explicit results exhibit larger axial stresses than the test data and ABAQUS® /Implicit solver. These differences are the consequence of a dynamic effect of the ABAQUS®/Explicit simulation (short simulated time adopted). In short, the authors considered ABAQUS®/Standard model as a proper and an expert tool to be used to analyze specific configurations. (LEROY, *et al.*, 2010) also used and described the application of this FE model based on the explicit solver of ABAQUS® and can be used for reference purposes.

The work of (SANTOS, *et al.*, 2015) presents a FE model developed in ABAQUS® to investigate the effect of the external sheath viscoelastic behavior on the local bending response of flexible pipes, adding the effect of the time-dependent response of the polymeric material. In order to obtain reliable material properties, a linear viscoelastic model was calibrated for the HDPE (high-density polyethylene), using an experimental campaign from a flexible pipe. In addition, contact is addressed based on Coulomb friction model. The FE model uses a solid pipe with a bi-material helical construction for the armor layers, by taking an artificial and totally compressible material with almost null mechanical properties to fill the voids between wires. This strategy speeds up the numerical solution, as enable Abaqus to deal with surface-to-surface contact models. The authors emphasize the synergy between the effects of Coulomb friction between armor wires and the viscoelastic behavior of the polymer layers, in particular the outer sheath. The structural damping in bending, considering the combined effects, is superior to the simple sum of those from the separate effects.

(XIQIA, *et al.*, 2015) briefly presented a short FE model of a seven-layered flexible pipe with 1.8m in length, which is equivalent to 1.5 linear pitches of the outer armor wires, developed in ABAQUS® and using its explicit solver. All layers of the flexible pipe are modeled separately. The pressure sheath, anti-wear layer and tensile armor layers are modeled with an eight-noded linear brick element and the pressure armor is modeled with a four-noded doubly curved thin shell element using orthotropic properties following the study from (SOUSA, 2005). Contact is accounted for by using a penalty contact method and Coulomb friction model. In short, as expected, some analyses

show that axisymmetric loads, as axial load and internal and external pressures, are the main sources of the contact pressure, which changes the bending response of the studied flexible pipe.

Unlike (XIQIA, *et al.*, 2015), (TANG, *et al.*, 2015) made use of ABAQUS®/Standard, the implicit non-linear solver of ABAQUS®, to study the bending response of a flexible pipe. The carcass and pressure armor layer were modeled as orthotropic shells while the polymeric layers and anti-wear tapes were modeled as isotropic shells with linear elastic properties. In order to eliminate end effects, authors mention that the model should have three pitches of the helical tendons. In this work, just one single armor wire was considered in this FE model, thus characterizing a simplified model. As already mentioned, this simplified FE model represented an 8" flexible pipe submitted to a constant curvature and was compared to seven previous analytical models.

In addition to Finite Element Method, the studies from (SÆVIK, 2010) and (SÆVIK, 2011) presented two alternative numerical formulations to predict dynamic stresses in the tensile armors of flexible pipes. The local elastic bending stresses of the helically wound armors were treated by application of differential geometry, whereas shear interaction from the interlayer stick-slip behavior was treated in two alternative ways: MM (Moment Model) and SBM (Sandwich Beam Model). The MM formulation considers the cross-section resultant in terms of the friction moment and SBM considers the sandwich beam formulation for each individual tendon. These numerical studies were compared with experimental results from FBG (Fiber Bragg Grating) sensors embedded in the wires, enabling a stress comparison.

Besides this, it should be noted two numerical models based on the Finite Difference Method as (ZHOU & VAZ, 2017) and (LEROY & ESTRIER, 2001). (ZHOU & VAZ, 2017) investigated the behavior of two armor layers of a flexible pipe under bending. The numerical solution is determined by finite difference method. To ensure a unified process of calculation, all formulas are simplified to build up a system of quasi-linear partial differential equations. This bending study only includes the contribution from tensile armor layers and is not able to determine when the slip exactly occurs and the direction of these slips for both two armor layers.

Despite the numerical models for bending analysis mentioned above, it is important to highlight the low availability of full-scale tests for validation in the literature. Many of the FE studies properly consider true referenced structures, but without the

validation of bending tests. The main references with full scale bending tests and structure datasheet are: (WITZ, 1996), (LONDOÑO, *et al*., 2014) and (SOUSA, *et al*., 2015), respectively with a 2.5", 9.13” and 2.5” flexible pipe samples.

CHAPTER 3. PROPOSED NUMERICAL MODEL FOR THE FLEXIBLE PIPE

3.1 INTRODUCTION

Finite element based models typically avoid the restrictions and simplifications of analytical formulations, though increased accuracy generally coming with the cost of greater computational expense. The availability of reliable general-purpose commercial software, such as ANSYS® and ABAQUS®, has increased the possibilities for creating and analyzing complex unbonded flexible pipe models.

There are some studies, such as (LI, *et al.*, 2013), presenting FE models that consider all flexible pipe layers with a geometry quite close to the real flexible pipe structure. Despite the advances in the computational field of recent years, these approaches, however, are still costly regarding time and computer requirements. Therefore, an approach capable of reducing the number of degrees of freedom involved in the modelling of these structures and, at the same time, representing their response to mechanical loading would be valuable.

Generally, the main difficulties in constructing numerical models to the local mechanical analysis of flexible pipes are the:

- Representation of all layers of the pipe including the complex cross-sections of the inner carcass and the pressure armor.
- Adequate modeling of the interaction between layers (sliding with friction, possible gap formation etc).
- Suitable treatment of possible material nonlinearities.
- Frequent need to represent relatively long lengths of these structures to avoid the effect of boundary conditions.

In this work, a FE model in which all layers of the pipe are modeled with shell elements is proposed. Shell elements approximate a three-dimensional continuum with a surface and may be efficient to model bending and in-plane deformations. Moreover, they also have integration points throughout their thickness, which allows evaluating changes in stress along this direction. Altogether, these characteristics allow a reduction in the number of finite elements required to model the complex layers of the flexible pipe, such as the inner carcass and the pressure armor.

The FE model was constructed in ANSYS® Mechanical FE package and a general view is presented in Figure 3.1 and the definition of the global and local coordinate axes (X, Y, Z) employed in the development of the model is presented in Figure 3.2.

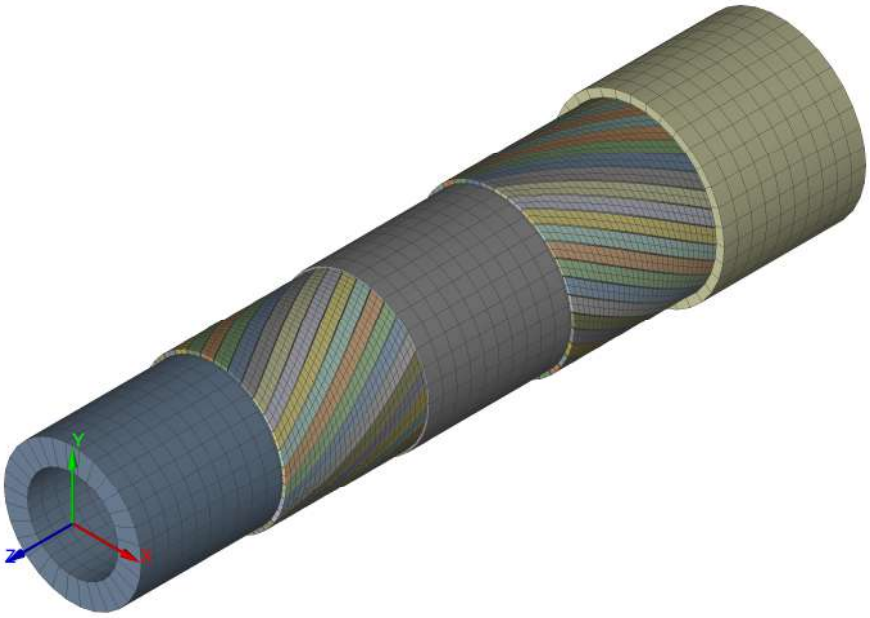

Figure 3.1. FE Mesh of all layers

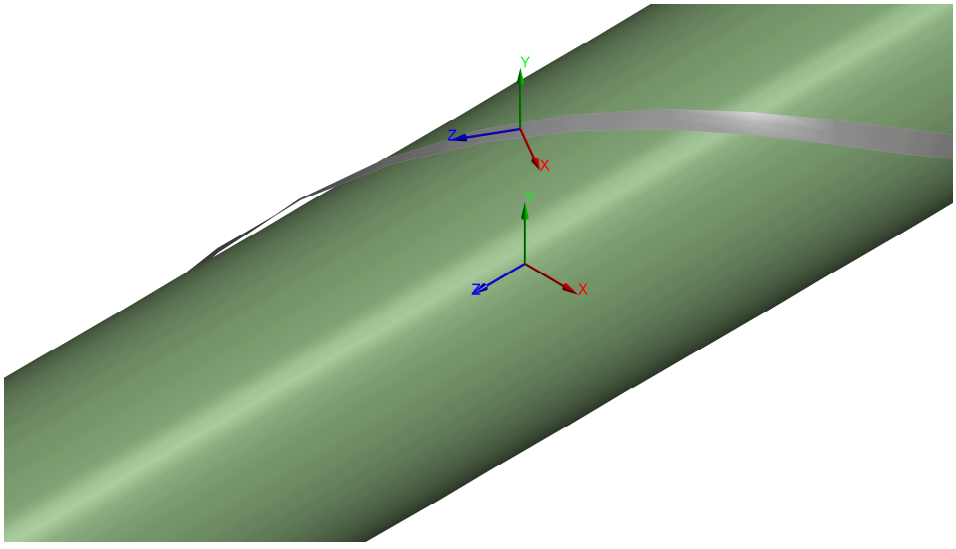

Figure 3.2. Local and Global Coordinate Systems

3.2 FE MODEL FOR THE CORE OF THE PIPE

The core of a typical flexible pipe consists of an inner carcass, an internal plastic sheath, a pressure armor and, possibly, an anti-wear tape, as shown in Figure 3.3.

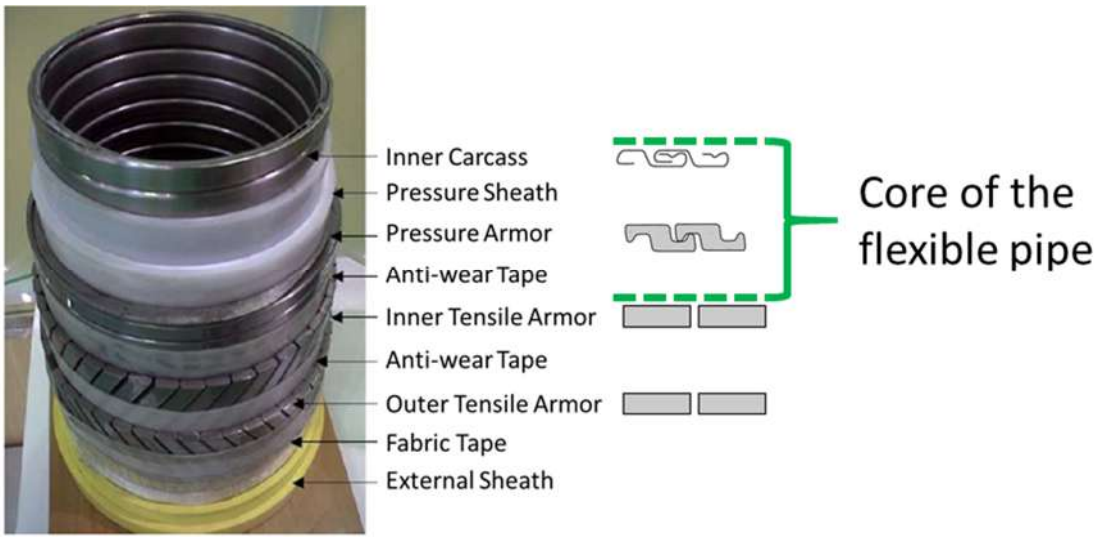

Figure 3.3. Core of the pipe

In the work of (SOUSA, 2005), the inner carcass and the pressure armor are modeled with shell elements by relying on an equivalence between the axial and bending stiffness of these elements and those from the actual layers. This equivalence is based on the analogy between orthotropic grids and shells presented by (TIMOSHENKO & WOINOWSKY-KRIEGER, 1959) and leads to equivalent thickness h_{shell} and longitudinal and transverse modulus, E_{shell} and G_{shell}, given by:

$$h_{shell} = \sqrt{12 \cdot \frac{K \cdot I_x}{A}} \tag{3.1}$$

$$E_{shell_z} = \left(\sqrt{12 \cdot \frac{n_t \cdot A}{L_p \cdot h_{shell}}} \right) \cdot E \tag{3.2}$$

$$G_{shell_{zx}} = \frac{3 \cdot n_t \cdot J_t}{L_p \cdot h_{shell}} \cdot G \tag{3.3}$$

where n_t is the number of tendons, L_p is pitch of the tendon, A is the cross-sectional area of the profile, E and G are the longitudinal and transverse shear modulus of the material, J_t is the torsional constant of the tendon; and K is the compacity factor given by:

$$K = 12 \cdot n_t \cdot \frac{I_x}{L_p} \cdot \frac{1 - \upsilon^2}{h^3} \tag{3.4}$$

where I_x is the minimum principal moment of inertia.

The lay angles of the inner carcass and the pressure armor are around 90° and, consequently, these layers practically do not withstand axial load. Therefore, the values adopted for the other components of E_{shell} and G_{shell} can be assumed small, avoiding null values that would lead to numerical difficulties.

According to (SOUSA, 2005), the equivalence between the stiffness of the helical tendon and the orthotropic shell does not lead to an equivalence between stresses. Thus, membrane, bending and shear stress correction factors are required for a proper stress analysis of these layers. These stress correction factors are given by:

$$f_{c_m}^{\sigma} = \frac{L_p \cdot h_{shell}}{n_t \cdot A} \qquad f_{c_b}^{\sigma} = \frac{L_p \cdot h}{n_t \cdot A} \qquad f_{c_s}^{\sigma} = \frac{L_p \cdot t \cdot h_{shell}^2}{n_t \cdot J \cdot 6} \tag{3.5}$$

Using the membrane and bending stresses calculated by the numerical model, $\sigma_{shell_z}^{m}$ and $\sigma_{shell_z}^{b}$, the extreme fiber stresses, $\sigma_{grid_z}^{m}$ and $\tau_{grid_{zx}}$, in the tendons of the inner carcass or the pressure armor are given by:

$$\sigma_{grid_z}^{m} = f_{c_m}^{\sigma} \cdot \sigma_{shell_z}^{m} \pm f_{c_b}^{\sigma} \cdot \sigma_{shell_z}^{b} \qquad \tau_{grid_{zx}} = f_{c_s}^{\sigma} \cdot \tau_{shell_{zx}} \tag{3.6}$$

The internal plastic sheath and the anti-wear tape are modeled in (SOUSA, 2005) with individual shell layers. The internal plastic sheath is extruded over the inner carcass and has its material properties equal in all directions and, consequently, this layer is modeled with isotropic shell elements. On the other hand, the anti-wear tape is wound around the pressure armor and is not continuous along the length of the pipe. This layer is thus modeled with orthotropic shell elements.

In the model proposed in this work, however, in order to reduce the computational cost, an equivalent shell layer for the core of the pipe is used. This equivalent layer is constructed using layered shell elements and considers the equivalent properties calculated for the inner carcass and the pressure armor and the geometrical and physical characteristics of the internal plastic sheath and the anti-wear tape.

It should be noted, however, that layered elements do not allow the existence of gaps between its layers and the equivalent thickness of the inner carcass and the pressure armor are lower than their actual thickness. Hence, aiming at overcoming this difficulty, “fake contact layers”, which employ materials with negligible stiffness, are used to fill the voids between the inner carcass and the pressure armor and the surrounding polymeric layers, as shown in Figure 3.4.

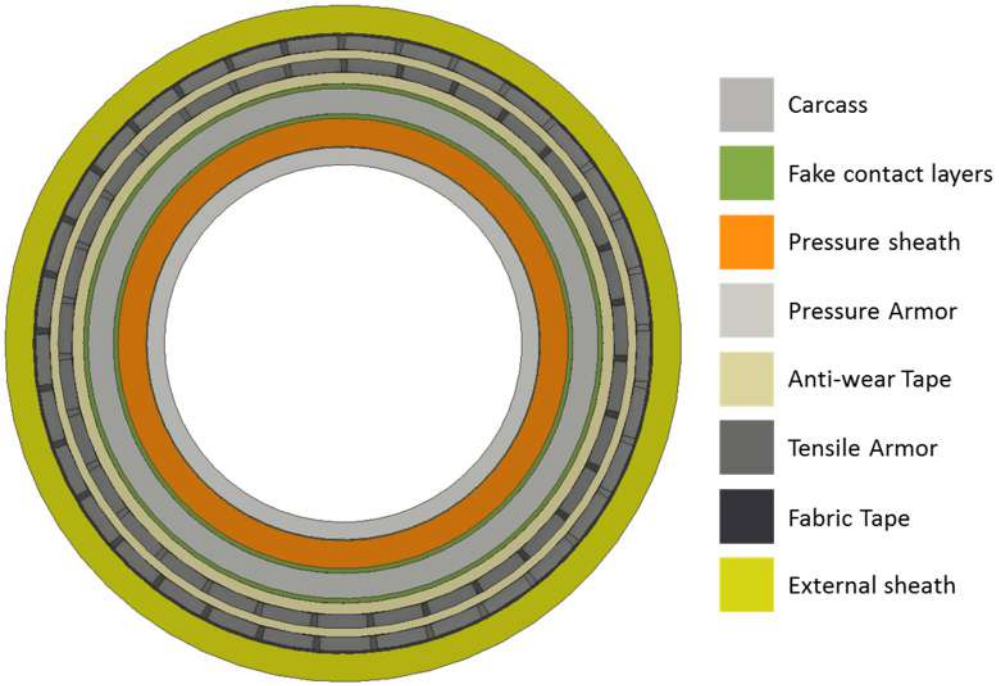

Figure 3.4. – Position of the “fake layers” added to the matrix of composite shell

3.3 FE MODEL FOR THE ARMOR WIRES AND ANTI-WEAR TAPES

In the FE model proposed in this work, the tensile armor wires are individually modeled with isotropic shell elements, as indicated in Figure 3.1, while the anti-wear tapes between them are modeled with orthotropic shell elements.

3.4 FE MODEL FOR THE OUTER LAYERS

As adopted for the core of the flexible pipe (section 3.2), the outer layers (Figure 3.5), *i. e.*, the fabric tape and the external sheath, are modeled as a single outer layer with layered shell elements. The tapes are modeled with orthotropic properties, as they are wound around the axis of the pipe. On the other hand, the external sheath is modeled with isotropic properties, as this layer is extruded over the fabric tape.

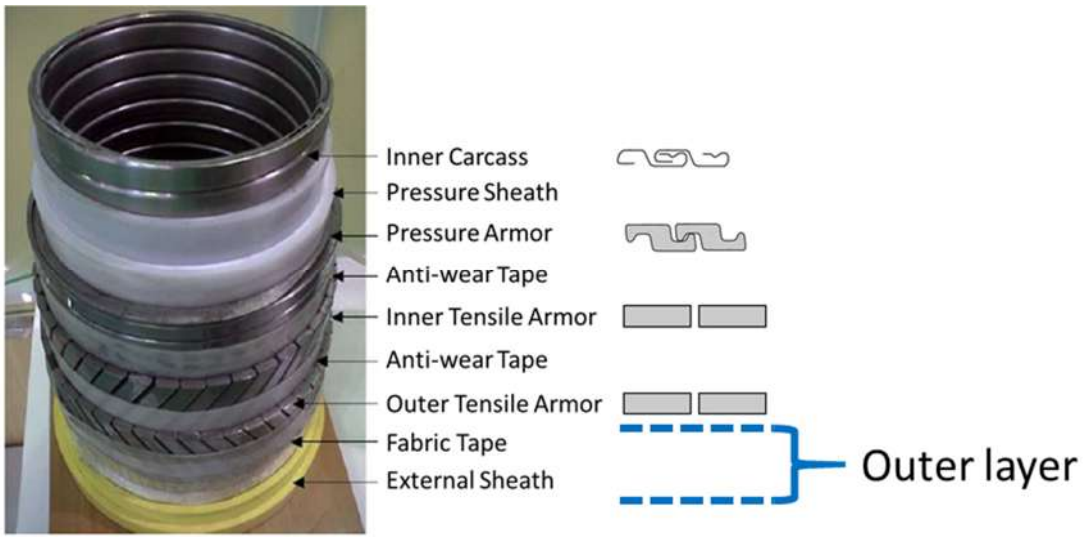

Figure 3.5. – Material Properties and FE model for the Outer Layers

3.5 MODELING THE CONTACT BETWEEN LAYERS

The layers that constitute the core of the pipe and the outer layers are assumed to be physically bonded. On the other hand, all contacts between the armor wires and the concentric layers are modeled with contact elements that allow relative sliding with friction between the surfaces in contact. These elements employ a contact detection algorithm based on the pinball technique (ANSYS, 2016) and contact forces are evaluated with the augmented Lagrangian method, which demands the use of a normal contact stiffness and an allowable penetration tolerance in each interface (ANSYS, 2016).

The first step in defining the contact between two layers is to assign the contact and target surfaces. In this work, all armor wires are set as contact surfaces and the surrounding layers are set as target surfaces. The reason for this choice is mainly based on the comparatively smaller area and better discretization of the armor wires.

Furthermore, the decision to use the armor wire as a contact surface enables the properly use of the contact post-processing tool focused on the armor wires.

The choice of the contact stiffness considers its impact on the convergence of the model. Higher stiffness values decrease the amount of penetration, but can lead to the ill-conditioning of the global stiffness matrix and, consequently, to convergence difficulties. On the other hand, lower stiffness values can lead to a certain amount of penetration and may produce an inaccurate solution. Ideally, the goal is to employ a contact stiffness high enough to enforce small penetration, but not as high to induce convergence difficulties. In this context, ANSYS® Mechanical calculates through its solver appropriate values for the normal contact stiffness and allowable penetration.

The value of this normal contact stiffness is a function of the layers' geometries, elements, meshes and materials. The contact stiffness proposed by the solver may be modified by multiplying the calculated value by a factor known as normal penalty stiffness factor, *FKN*. The impact of this factor and normal stiffness on the response of the pipe is studied in CHAPTER 4.

The impenetrability condition is satisfied if penetration is lower than the allowable penetration value, which is given by (ANSYS, 2016):

$$TOLN = FTOLN \cdot d_{ue} \tag{3.7}$$

where $FTOLN$ is the allowable penetration factor and d_{ue} is the depth of the underlying shell element. According (ANSYS, 2016), if the underlying elements are shell, the depth is four times the element thickness.

In this work, $FTOLN$ and FKN are respectively set as 0.1 and 1.0, according to the general guideline described in (ANSYS, 2016).

Friction is addressed with the Coulomb friction law, which is given by:

$$\tau_{max} = \tau_i + \mu \cdot \sigma_n \tag{3.8}$$

where τ_{max} is the limit shear stress, τ_i is the initial adhesion, μ is the friction coefficient and σ_n is the normal contact stress.

Just as for the normal stiffness, ANSYS® Mechanical calculates appropriate values for the tangential contact stiffness and allowable elastic slip, which are stated, respectively, as:

$$KT = FKT \cdot \frac{MU \cdot PRES}{TOLF} \tag{3.9}$$

$$TOLF = SLTO \cdot l_{ue} \tag{3.10}$$

where *PRES* is the contact normal pressure, *TOLF* is the allowable slip, *MU* is the interface coefficient of friction, FKT is a multiplying factor known as tangential contact stiffness factor that can be used to change the tangential contact stiffness proposed by the ANSYS® solver, *SLTO* is the allowable slip factor, and l_{ue} is the average underlying element length.

In this work, *SLTO* and *FKT* ae respectively set as 0.01 and 1, according to the general guideline presented in (ANSYS, 2016).

3.6 IMPLEMENTATION

The model is implemented in ANSYS® and uses shell elements for all layers, specifically SHELL181, a four-node element with six degrees of freedom at each node (translations in the x, y, and z directions, and rotations about the x, y, and z-axes). This element supports geometric and material nonlinearities and relies on the Reissner-Mindlin hypothesis. This element also includes a more accurate model of transverse shear deformation. The difference between typical Kirchoff-Love shell element and a typical Reissner-Midlin shell element like SHELL181 in ANSYS is that any shell element based on Kirchoff-Love shell theory does not account for transverse shear stresses. In short, the resulting deformations using SHELL163 with Kirchoff-Love assumption might be underestimated, especially in very thick shell structures (NELSON & WANG, 2004), which is not the case, presumably.

All contacts between the armor wires and the concentric layers (core, anti-wear and outer layer), in a total of 132 contact pairs, are modeled with contact elements

(CONTA 174/TARGE170) that allow relative sliding with friction between 3-D surfaces in contact based on Coulomb friction model.

All analyses are performed with ANSYS® implicit solver. This specific solver is suitable for problems in which time dependency of the solution is not an important factor.

CHAPTER 4. CASE STUDY

4.1 EXPERIMENTAL TESTS

In order to verify the model, its results are compared with a set of full-scale tests performed at Structures and Materials Laboratory (LABEST - *Laboratório de Estruturas e Materiais Fernando L. L. B. Carneiro*) of COPPE/UFRJ – Rio de Janeiro – Brazil. Figure 4.1 presents general view of the experimental apparatus.

Figure 4.1. Test overview with experimental apparatus (SOUSA, *et al.*, 2015)

The structure used in this test is a 2.5” flexible pipe sample with a free span of 5.82m, which is equivalent to approximately 10 linear pitches of the outer tensile armor wires. The main properties of its layers are presented in Table 4.1.

Table 4.1. Flexible Pipe Sample

Layer (Material)	Properties		
Interlocked Carcass	h = 3.5mm n_t = 1 α = +87.6°	*Interlocked profile* A = $19.6mm^2$ υ = 0.30	I = $23.1mm^4$ E = 192GPa
Pressure Sheath	h = 5.0mm	E = 330MPa	υ = 0.45
Pressure Armor	h = 6.2mm n_t = 2 α = +85.6°	*Z profile* A = $54.1mm^2$ υ = 0.30	I = $173.4mm^4$ w = 8.0mm E = 205GPa
Anti-Wear Tape	h = 2.0mm	E = 345MPa	υ = 0.45
Inner Tensile Armor	h = 2.5mm n_t = 32 α = -30°	*Rectangular profile* υ = 0.45	h= 2.5mm w = 8.0mm E = 205GPa
Anti-Wear Tape	h = 1.5mm	υ = 0.45	E = 345MPa
Outer Tensile Armor	h = 2.5mm n_t = 34 α = +30°	*Rectangular profile* υ = 0.45	h = 2.5mm w = 8.0mm E = 205GPa
Fabric Tape	h =0.5mm	υ = 0.45	E = 345MPa
External Sheath	h = 5.0mm	υ = 0.45	E = 215MPa

In this pipe, part of the outer plastic sheath was removed around its middle section thus exposing the outer tensile armor wires. Strain gages were then fixed to each of these wires in its longitudinal direction, as shown in Figure 4.2.

This lack of outer sheath certainly influences the bending response after the start of slip. In any case, this phase was not reached during the bench tests. Therefore, the FE model considered the outer layer intact, being able to properly represent the bending stiffness after the start of the slip.

Figure 4.3 presents a schematic of the experimental apparatus. In this apparatus, tensile loads are applied by a hydraulic actuator connected to one of the flexible pipe sample's ends. This actuator has a total load capacity of 1000kN. Bending loads were applied by a very stiff beam, which is linked to another hydraulic actuator (transverse

actuator) and supported by two shoes that rests on the flexible pipe body, as shown in Figure 4.3. The transverse actuator has a total load capacity of 250 kN and the maximum displacement of both actuators is 150 mm.

.

Figure 4.2. Strain gauges installed // outer tensile armors (SOUSA, *et al.*, 2015)

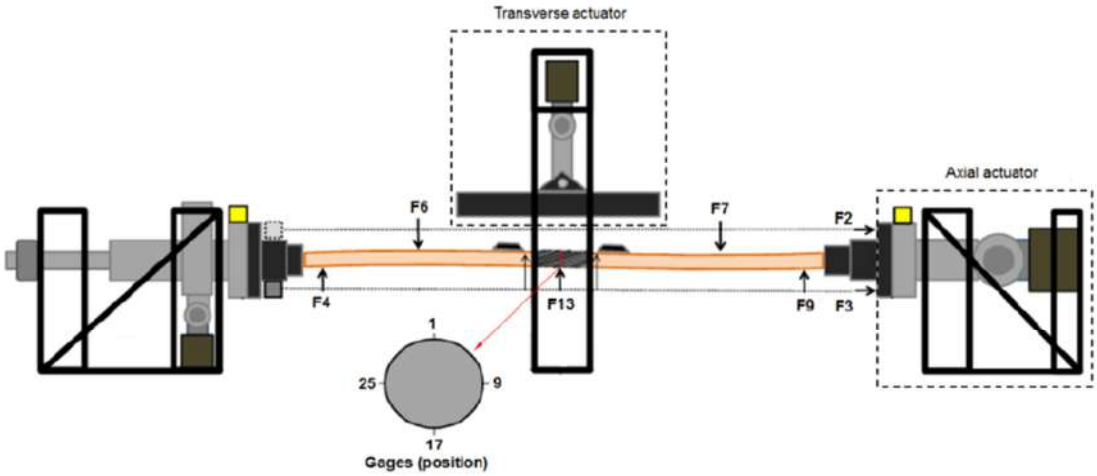

Figure 4.3. Test layout (SOUSA, *et al.*, 2015)

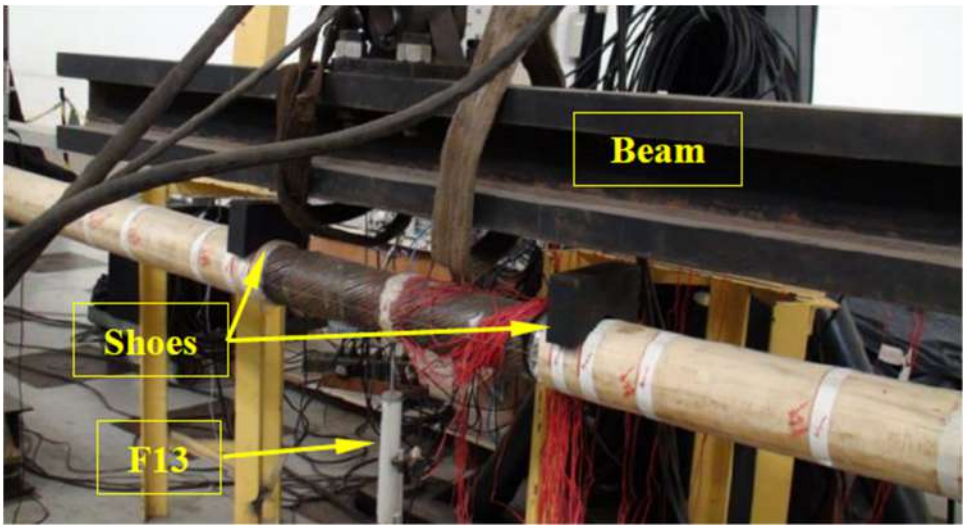

Figure 4.4. Transverse actuator with a transverse displacement transducer (SOUSA, *et al*., 2015)

In addition, there are several displacement transducers (F2, F3, F4, F6, F7, F9 and F13) as shown in Figure 4.3. Two of them (F2 and F3) are used to measure the axial displacements of the pipe and both are fixed to one of the end fittings of the flexible pipe. Transducer F13 is positioned at the middle section of the pipe to measure the central transverse displacement.

Two different load cases were tested with this apparatus, both subjected to displacement control:

- Case 1, pure tension: the flexible pipe sample is tensioned until a maximum load of 700kN. This load is approximately half of the estimated damaging pull of the pipe. After that, three load cycles with total amplitude of 250kN and mean value of 575kN are applied. In this case, the twist of the pipe is restrained at both ends.
- Case 2, tension combined with bending: a pre-tension of 700kN is firstly imposed on the pipe followed by a maximum transverse load of 25kN. Three load cycles from zero to maximum transverse load test are then applied.

4.2 FE MESH

After performing some FE mesh tests for the model representing the structure with its 5.82 m, the cylindrical and concentric layers of the 2.5” flexible pipe were discretized

with 45 finite elements along their circumference and 582 elements along their length. Each tensile armor was discretized with 2 finite elements along its width. Therefore, the resulting FE mesh has around 450,000 nodes, leading to a problem with around 2,700,000 degrees of freedom. Figure 4.5 presents a general view of this FE mesh.

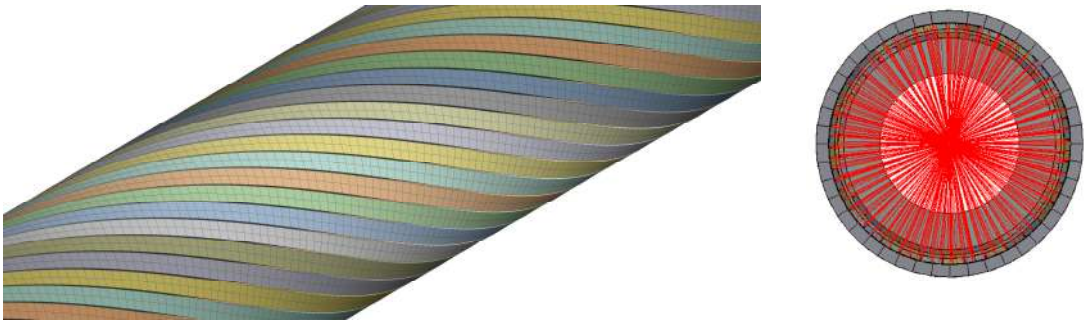

Figure 4.5. Typical FE Mesh for the armor wires

In this FE mesh, two nodes are positioned in the axis of the pipe at their extremities. These nodes are rigidly linked to the nodes in these cross-sections, as shown in Figure 4.5 and Figure 4.6, thus simulating the boundary conditions imposed on the experimental tests. In the pure tension analysis, one extremity is fixed and, in the opposite one, only the axial translation is allowed. At this extremity, an axial displacement is imposed to simulate the applied tensile load. In the bending combined with tension analysis, the pre-tension is applied as in the pure tension case. The transverse load is applied by modeling the shoes employed in the experimental tests, as shown in Figure 4.7.

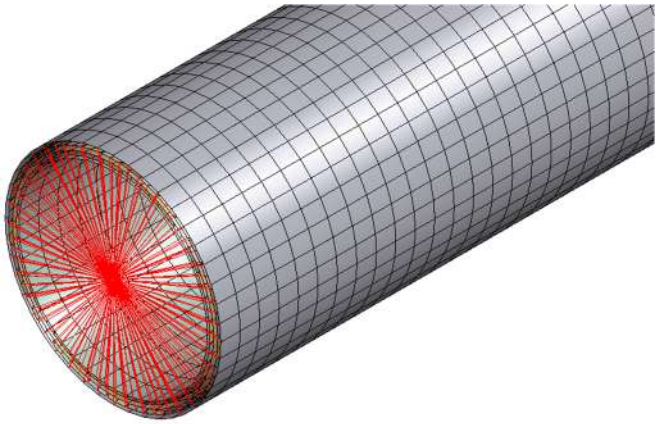

Figure 4.6. Boundary conditions with rigid behavior

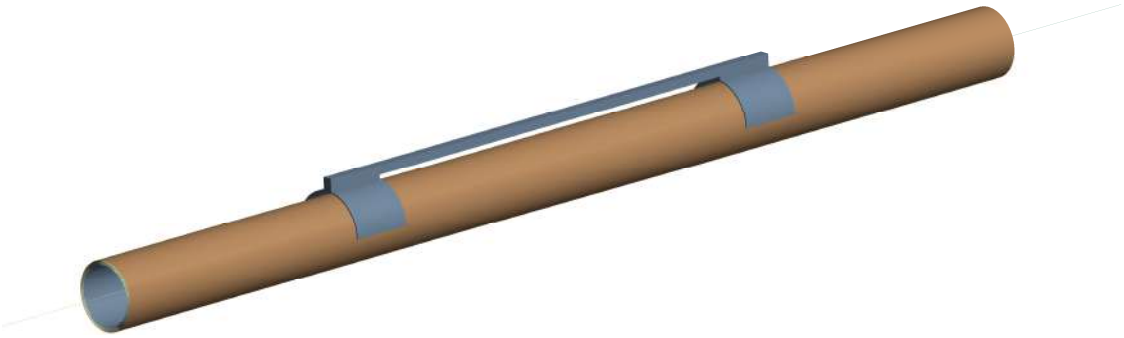

Figure 4.7. Shoes

These shoes are modeled as a single rigid body. It should be noted that in a FEM, certain relatively stiff parts can be represented by rigid bodies when stress distributions and wave propagation in such parts are not critical. An advantage of using rigid bodies rather than deformable finite elements is the computational efficiency. Elements that belong to the rigid body have no associated internal forces or stiffness and their movements are determined by the six degrees of freedom (DOFs) of a pilot node. The transverse force is applied by prescribing a transverse displacement (Y direction) at the pilot node and the interaction between the shoes and the pipe is ensured with contact elements that allow relative sliding with friction (Coulomb friction model).

Several studies, such as (BAHTUI, *et al.*, 2009), (SÆVIK & BERGE, 1995), (KEBADZE, 2000), (REN, *et al.*, 2014) and (XIQIA, *et al.*, 2015), mentioned the use of a friction coefficient between layers equal to 0.1. Based on this, initially, all analyses are performed using this value for the coefficient.

4.3 PURE TENSION ANALYSIS

Figure 4.8 presents the variation of the axial displacement at the extremity of the pipe with the imposed tensile load. Two different curves are presented: experimental and numerical (proposed FE model).

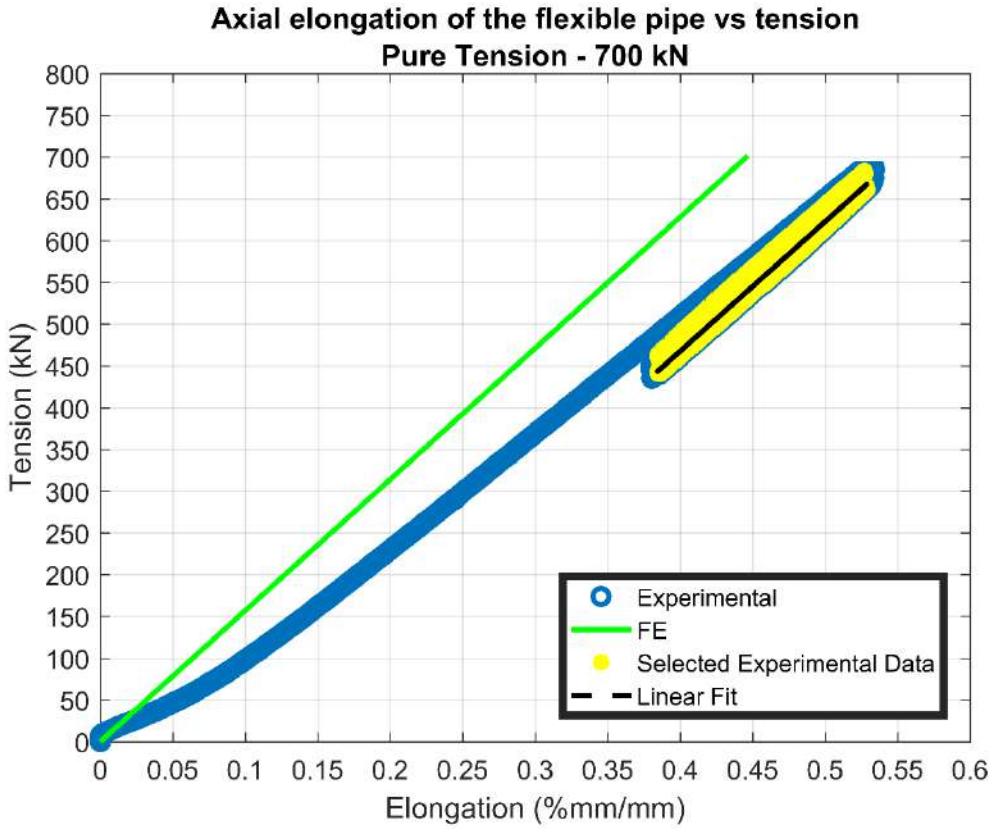

Figure 4.8. Experimental and Numerical Results - Pure Tension

The experimental tests indicate that, after accommodation, the response of the pipe is linear until reaching the cyclic load phase. The accommodation may be related to the anchoring conditions of the tensile armor wires inside the end fittings (SOUSA, *et al*., 2013a) and/or interlayer gaps (KEBADZE, 2000). During the cyclic loading, a small hysteretic loop is also observed, but, by fitting a linear regression curve to the experimental load cycles points, an axial stiffness of 155 MNmm/mm is obtained with a correlation factor of 0.984. This indicates that the experimental response of the flexible pipe sample to the tensile axial load can be assumed linear. This linear behavior is in accordance with the FE model, which also shows a linear response with axial stiffness of 157 MNmm/mm.

It should be noted that the FE model, unlike the analytical model, does not assume that the cross sections of the flexible pipe should remain in the same plan in the deformed structure. In other words, the armor layers may slide relative to each other, presenting, for example, different translations and axial rotations from one layer to another in the same cross section of the flexible pipe. Therefore, it is interesting to observe the evolution

of the contact conditions during the load application. Figure 4.9 shows the variation of the number of contact sticking points along a wire of the outer tensile armor. In the Coulomb friction model, two contacting surfaces can carry shear stresses up to a certain magnitude across their interface before they start sliding relative to each other. This state is known as sticking. In this context, the contact sticking points are the quantity of contact points not sliding. It should be noted that for sticking contact condition, the numerical model allows small amount of slip also known as allowable elastic slip. According Figure 4.9, there is a remarkable increase in the number of sticking points with low tensile loads, when some contact points change its status from open to closed. After a tensile load of about 150 kN, this number is approximately constant. This response evidences the effect of friction along the length of the wire.

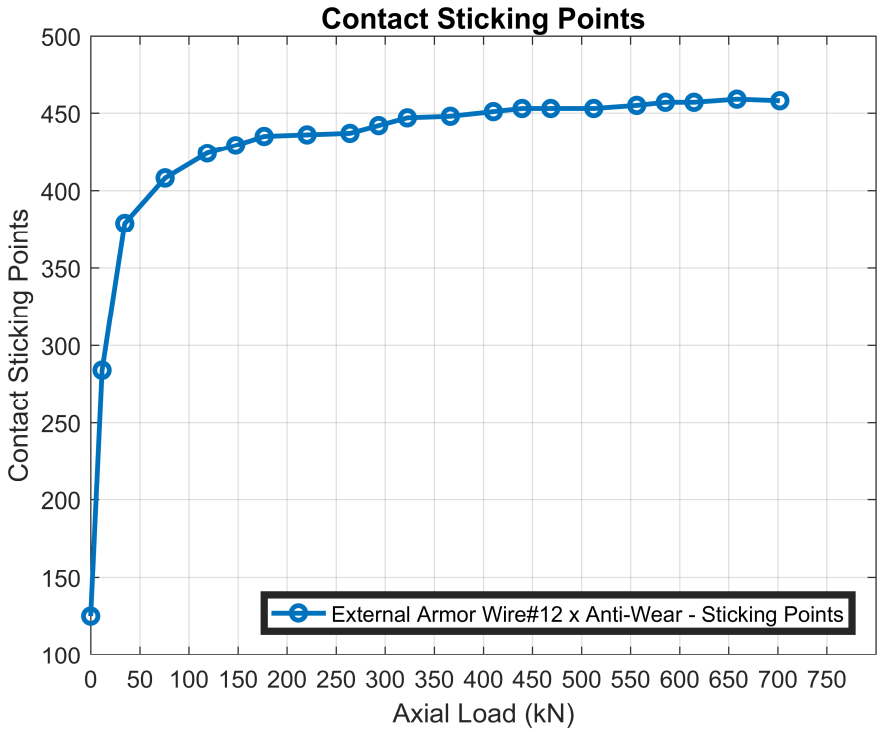

Figure 4.9. Contact Sticking Points

In addition, a sensitivity analysis on the effect of the friction coefficient influence was performed considering values of 0.10, 0.15 and 0.20. In these analyses, all axial stiffness remained almost constant and equal to 157MNmm/mm. Thus, the friction coefficient does not impact the axial stiffness of the pipe, which is well-known and indicated for example in (MERINO, *et al.*, 2016) and (GONZALEZ, *et al.*, 2015).

Another parameter that deserves attention is the normal contact stiffness factor, FKN, described in CHAPTER 3. This parameter plays a significant role on general contact behavior and its variation may modify the response of the FE model. Using a normal stiffness factor, FKN, equal to 1, the normal stiffness between the armor wires vary between 2000 and 2500 N/mm³.

Overestimating or underestimating this value can greatly increase or decrease the stiffness of the model, respectively. Thus, another sensitivity analysis was carried out by considering FKN values of 0.25, 1.00 (suggested by ANSYS®) and 4.00. Figure 4.10 shows the results obtained and indicates an increase of the axial stiffness with the increasing value of FKN. Factors of 0.25, 1.00 and 4.00 leads to axial stiffness of 125 MNmm/mm, 157 MNmm/mm and 170 MNmm/mm, respectively.

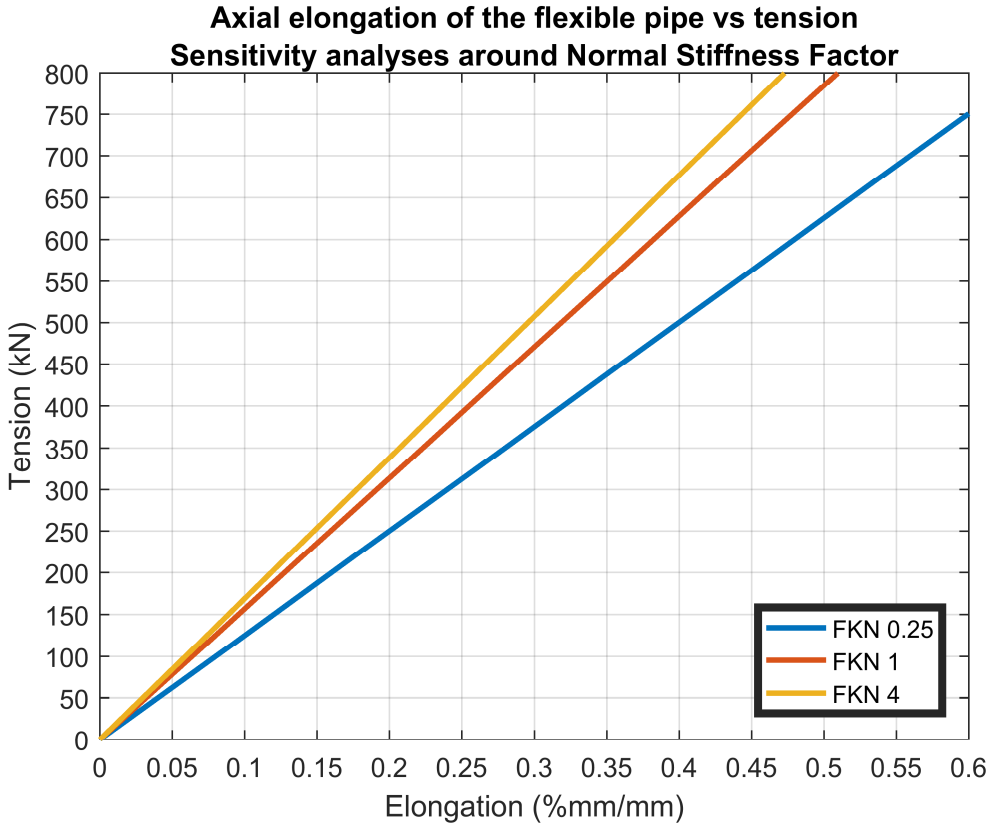

Figure 4.10. Tension vs axial elongation curves with different FKN values.

The model is thus dependent on the normal contact stiffness, but the value suggested by ANSYS® led to an axial stiffness quite close to the experimental value.

As a final check, it is possible to compare the strains measured with the strain gauges described in Figure 4.2 with the results from the FE model (considering the same positions of the strain gages). Figure 4.11 presents the FE strains and Figure 4.12 illustrates the normalized strains obtained in the experimental tests and the numerical model in each outer tensile armor wire. The normalized strain results are the strains divided by the maximum tension load, i.e., strains divided by 700kN.

As showed in this section the numerical results concerning the axial stiffness of the flexible pipe and axial strain of the external armor wires agreed well with the experimental results, indicating that the proposed FE model is suitable to be used for this kind of analysis.

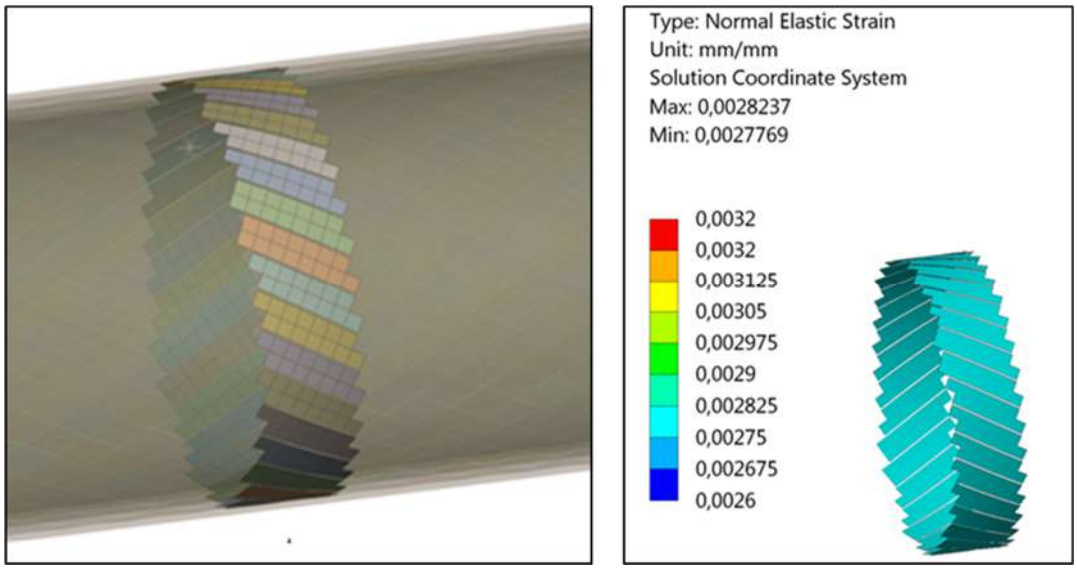

Figure 4.11. Strain of each outer tensile armors
(central region // Tension only / 700kN)

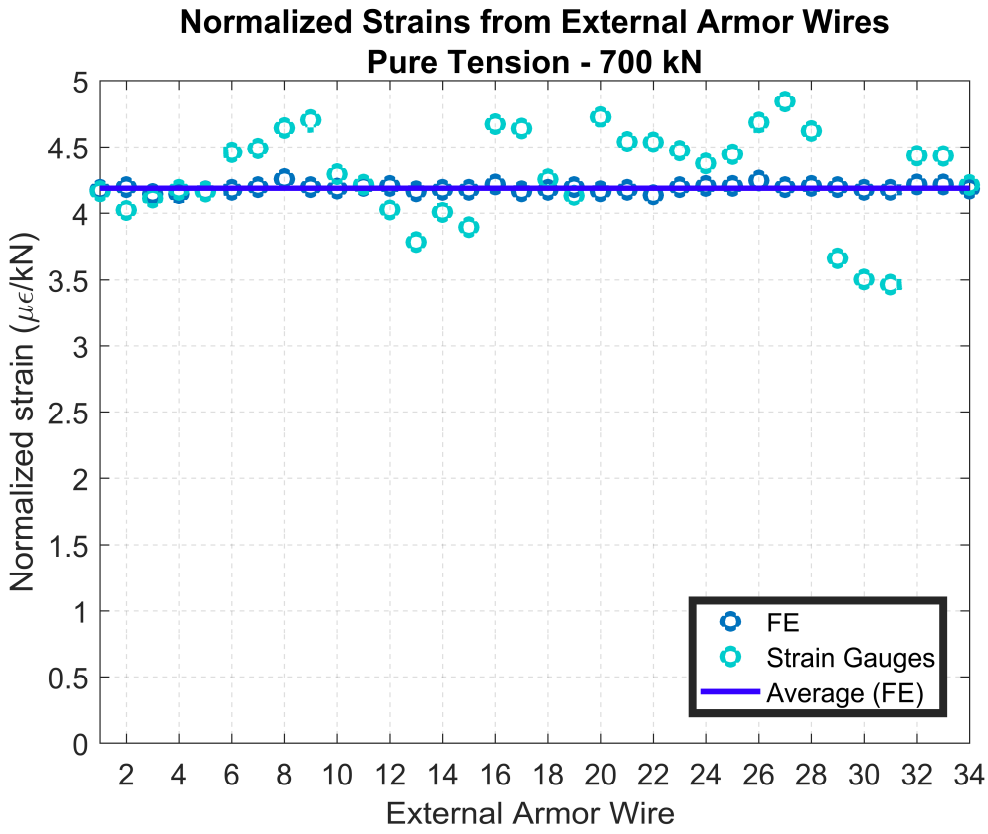

Figure 4.12. Normalized strains in the external wires

4.4 BENDING COMBINED WITH TENSION ANALYSIS

The imposition of the bending load in the tensioned pipe may induce the relative sliding between its layers and, aiming at properly accounting for this aspect, a fine FE mesh, such as the one described in section 4.2, is needed to avoid convergence problems. Moreover, this type of analysis requires more load steps than the pure tension case and two extra contact regions, i. e., the contact regions between the shoes and the pipe, as described in section 4.2, which demanded extra 134 contact pairs. Altogether, these characteristics led to a problem with very high computational cost and, initially, unfeasible. Therefore, an alternative FE mesh was employed to reduce the computational cost demanded by this analysis

In this alternative FE mesh, equivalent beams (BEAM188 in ANSYS®) replace part of the original FE model, as shown in Figure 4.13. These equivalent beams have the same axial and no-slip bending stiffness of the flexible pipe. The axial stiffness was evaluated in section 4.3, while the no-slip bending stiffness was evaluated with the

original FE model, as this analysis is linear and does not require many load steps to converge. This no-slip bending stiffness is presented in the next section. Furthermore, the equivalent beams are positioned in regions where no relative slip between the tensile armor wires will occur, i. e., the pipe has constant axial and bending stiffness (no-slip). These regions have a total length of 2m, which are connected to the shell FE model by employing rigid constraints at their extremities, representing 3 linear pitches of the outer tensile armor wires, as shown in Figure 4.13.

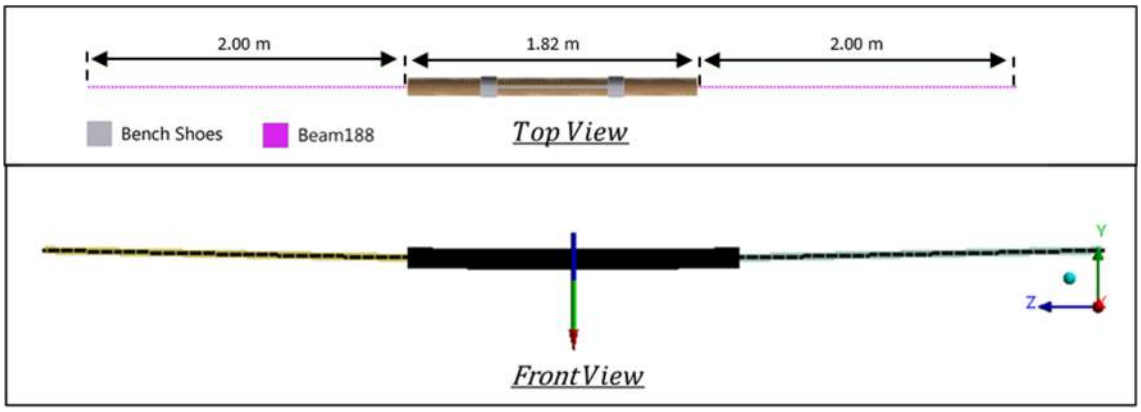

Figure 4.13. Model with Equivalent Beam

Another difficulty is to evaluate the curvature along the FE mesh, as a three-dimensional model is employed. This difficulty was overcome by adopting a central beam with negligible stiffness whose nodes are connected to the inner layer of the flexible pipe, as shown in Figure 4.14**.**

Finally, due to internal clearances in the experimental apparatus, the extremities of the FE model are considered pinned, *i. e.*, translations are restrained, but the rotation around the X axis (Figure 4.13) is allowed.

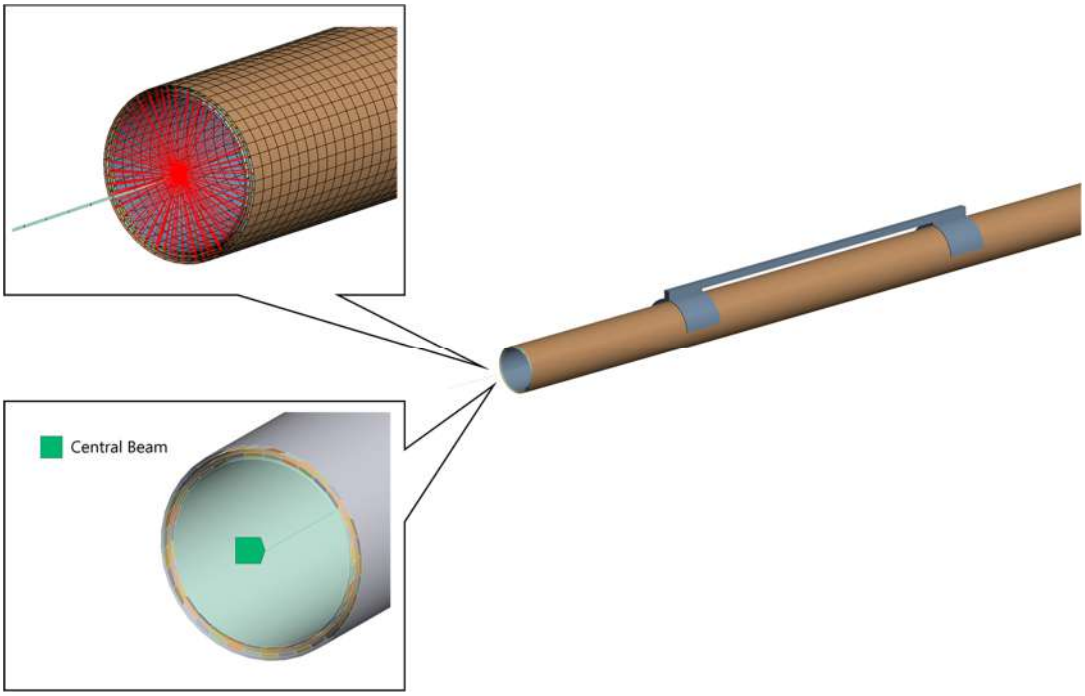

Figure 4.14. Locations of the beams in the model

BENDING STIFFNESSES

The transverse load *vs* transverse displacement experimental and numerical curves, considering a pretension of 700kN, are presented in Figure 4.15. The transverse displacements correspond to those from the mid-section of the pipe.

As mentioned in section 4.1, three load cycles are applied in the experimental tests and they are considered (yellow markers) for a linear regression, as indicated in Figure 4.15. The angular coefficient of the straight line, which means the ratio between the imposed transverse load and the transverse displacement, is 0.595 kN/mm with a correlation factor of 0.998. The numerical response is also linear and agrees quite well with the experimental data. The numerical ratio between the imposed transverse load and the transverse displacement, is 0.592 kN/mm.

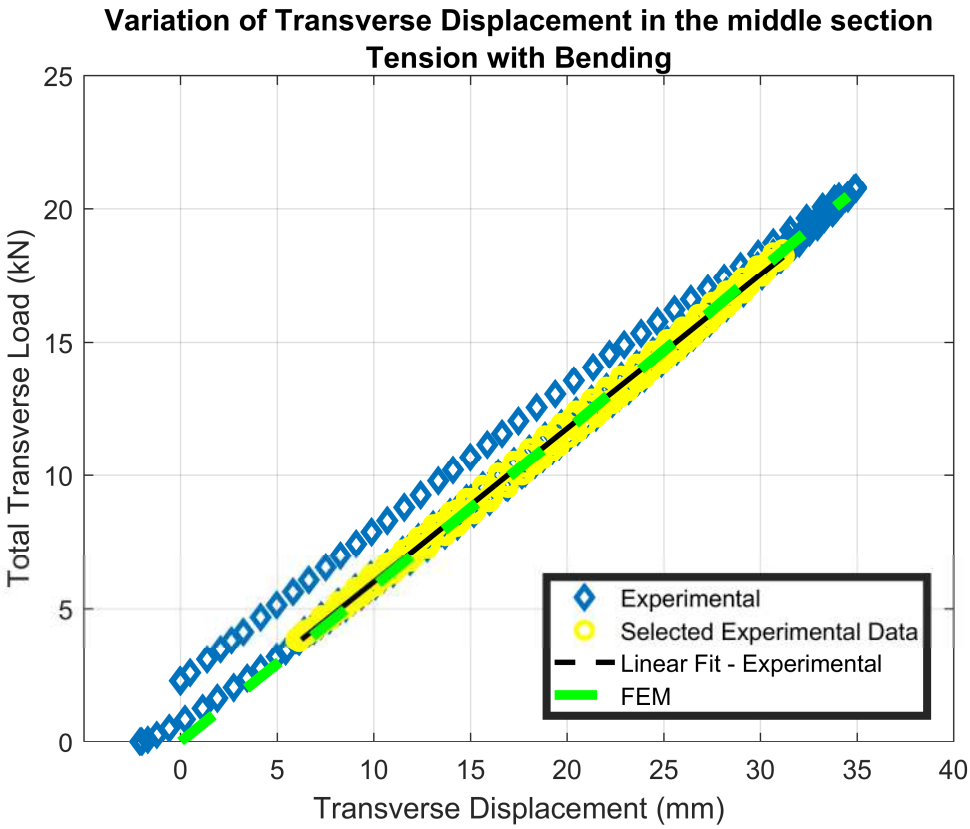

Figure 4.15. Transverse load vs transverse displacement: no-slip response.

(SOUSA, *et al*., 2015) idealized the experimental apparatus as a beam of total length l subjected to an axial load P and two concentrated loads Q/2 (total load is Q), as shown in Figure 4.16.

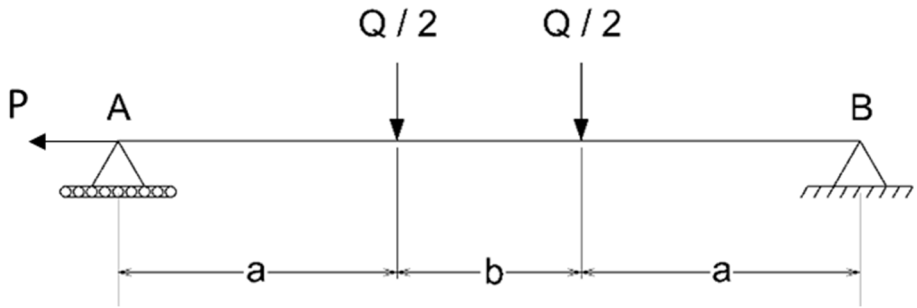

Figure 4.16. Transverse load vs transverse displacement: no-slip response.

The transverse displacement along the pipe is thus given by:

$$v(x)=\begin{cases} C_1\cdot\sinh(k\cdot x)+\dfrac{Q}{2\cdot P}\cdot x,\ 0\le x\le a \\ C_2\cdot\sinh(\mathrm{k}\cdot \mathrm{x})+C_3\cdot\cosh(k\cdot x)+\dfrac{Q}{2\cdot P}\cdot a,\ a\le x\le \dfrac{l}{2} \\ C_2\cdot\sinh[\mathrm{k}\cdot(\mathrm{l}-\mathrm{x})]+C_3\cdot\cosh[k\cdot(l-x)]+\dfrac{Q}{2\cdot P}\cdot a,\ \dfrac{l}{2}\le x\le l-a \\ C_1\cdot\sinh[\mathrm{k}\cdot(\mathrm{l}-\mathrm{x})]+\dfrac{Q}{2\cdot P}\cdot(l-x),\ l-a\le x\le l \end{cases} \tag{4.1}$$

where:

$$C_1=\frac{Q}{2\cdot k\cdot P}\cdot\left\{\frac{1}{\cosh(k\cdot a)}+\frac{\sinh\left[k\cdot\left(\frac{l}{2}-a\right)\right]}{\cosh\left(k\cdot\frac{l}{2}\right)}\cdot\tanh(k\cdot a)\right\} \tag{4.2}$$

$$C_2=\frac{Q}{2\cdot k\cdot P}\cdot\sinh(k\cdot a)\cdot\tanh\left(k\cdot\frac{l}{2}\right) \tag{4.3}$$

$$C_3=\frac{Q}{2\cdot k\cdot P}\cdot\sinh(\mathrm{k}\cdot\mathrm{a}) \tag{4.4}$$

$$k=\sqrt{\frac{P}{EI}} \tag{4.5}$$

By considering the ratios obtained from the curves presented in Figure 4.15 in Eqs. 4.1 to 4.5, experimental and numerical no-slip bending stiffness of 120 kN.m² are obtained. According (SOUSA, *et al.*, 2015), using the analytical model from (WITZ & TAN, 1992), it is possible to estimate the analytical no-slip bending stiffness as 200 kN.m². Figure 4.17 presents the transverse displacements obtained along the FE model

and Figure 4.18 compares these displacements to those obtained in the experimental tests as well as those calculated with Eqs. 4.1 to 4.5 considering a bending stiffness of 120 kN m^2. Figure 4.18 indicates that all results agree quite well.

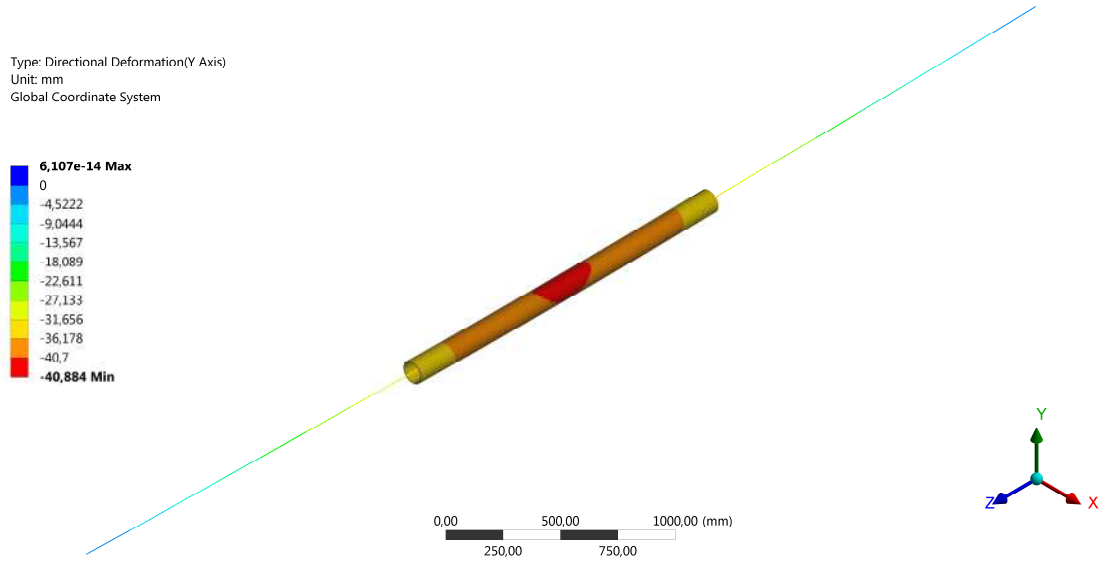

Figure 4.17. Transverse displacements, in mm, along the FE model.

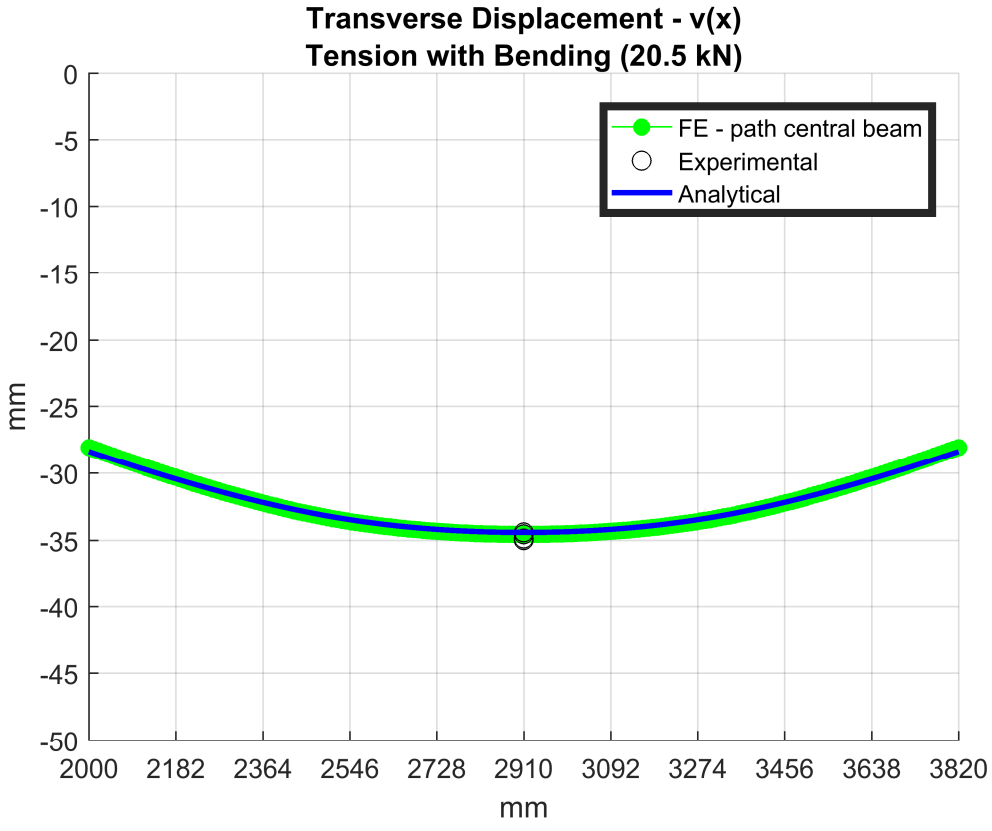

Figure 4.18. Transverse Displacement over the length of the Shell-Beam model.

The curvature variation $\kappa(x)$ along the beam idealized by (SOUSA, *et al.*, 2015) can be calculated as:

$$\kappa(x) = \frac{v''(x)}{[1 + (v'(x))^2]^{3/2}} \tag{4.6}$$

where v(x) is given by Eq. (4.1).

The curvatures along the FE model can be directly obtained at the nodes of the central beam and they are compared to those estimated with Eq. (4.6) in Figure 4.19.

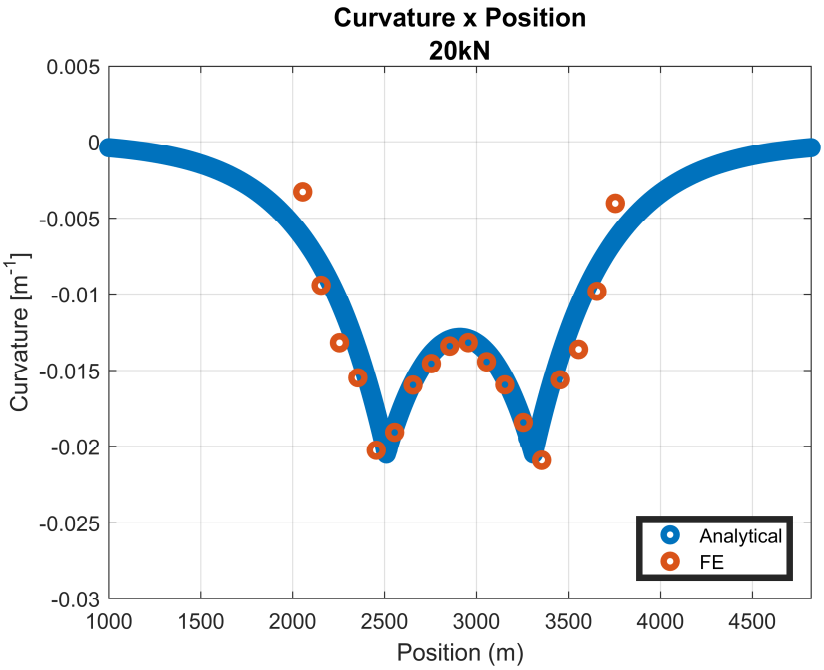

Figure 4.19. Curvature - Numerical and Analytical/Experimental Results

Figure 4.19. indicates that the numerical and analytical values for the curvature agree well. In short, the curvature vary between the shoes of the test bench and has its maximum values in the load application regions.

REACTION FORCES

It should be mentioned that the imposed transverse load elongates the flexible pipe sample. Thus, an increase in the axial load acting on the structure is expected, adding an extra axial load to the pre-tension load. This increase can be analytically estimate based on the formulation presented by (SOUSA *et al*, 2015):

$$\Delta P = \frac{EA}{l}\left[\int_0^l \sqrt{1+\theta(x)}\,dx - l\right] \tag{4.7}$$

where EA is the axial stiffness and $\theta(x)$ is the rotation of the points along the flexible pipe, which is given by:

$$\theta(x) = \begin{cases} k \cdot C_1 \cdot \sinh(\mathrm{k}\cdot \mathrm{x}) + \dfrac{Q}{2\cdot P},\ 0 \le x \le a \\ k \cdot \left[C_2 \cdot \sinh(k\cdot x) + C_3 \cdot \cosh(k\cdot x)\right],\ a \le x \le \dfrac{l}{2} \\ -k \cdot \left\{ \begin{matrix} C_2 \cdot \sinh\left[k\cdot(l-x)\right] + \cdots \\ \cdots + C_3 \cdot \cosh\left[k\cdot(l-x)\right] \end{matrix} \right\},\ \dfrac{l}{2} \le x \le l-a \\ -k \cdot C_1 \cdot \sinh\left[k\cdot(l-x)\right] - \dfrac{Q}{2\cdot P},\ l-a \le x \le l \end{cases} \tag{4.8}$$

Table 4.2 compares the axial reaction force predicted with Eqs. (4.7) and (4.8) and the force obtained in the numerical model considering a transverse load of 25 kN. The obtained results again agree quite well.

Table 4.2 – Analytical and Numerical - ΔP

Transverse load of 25kN		
model	ΔP [N]	Relative difference
Analytical	17770 N	3.4%
Numerical	18370 N	

STRAIN AND STRESS OF EXTERNAL ARMOR WIRES

Figure 4.20 presents the strains obtained with the numerical model along the outer armor wires for a transverse load of 20 kN. This figure shows that each wire has a different strain distribution.

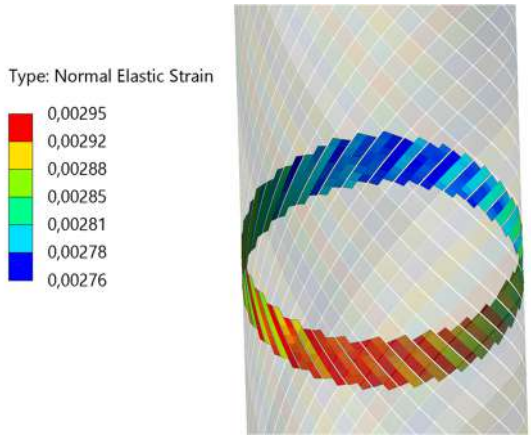

Figure 4.20. Normal Strain in all external armor wires in the central region

Figure 4.22 presents the numerical variation of the strains along two opposite wires (named EW-12 and EW-29) between the shoe pads as described in Figure 4.21. This figure indicates a strain variation between the shoes, due to the curvature variation indicated in Figure 4.20. Moreover, it is also noticed that the responses are out of phase, because the wires in the extrados of the pipe are tensioned and those in the intrados are compressed.

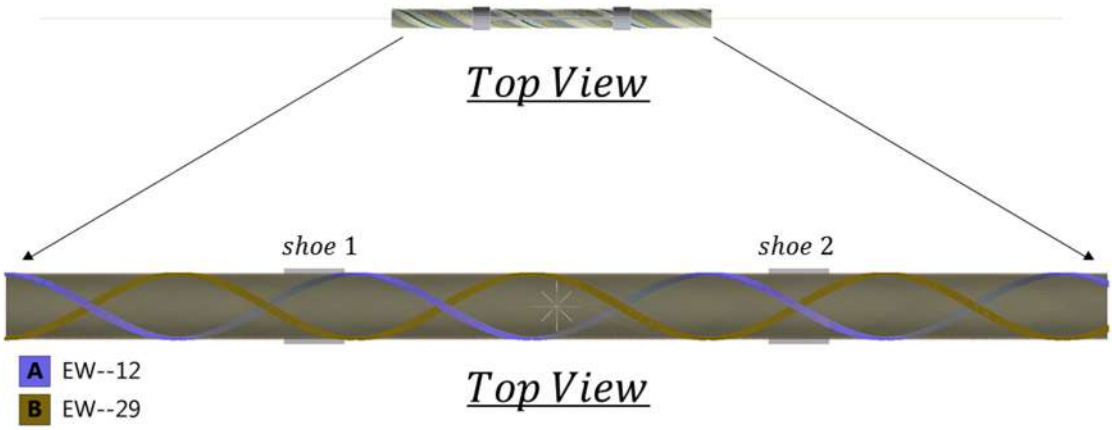

Figure 4.21. Position of external armor wire #12 and #29

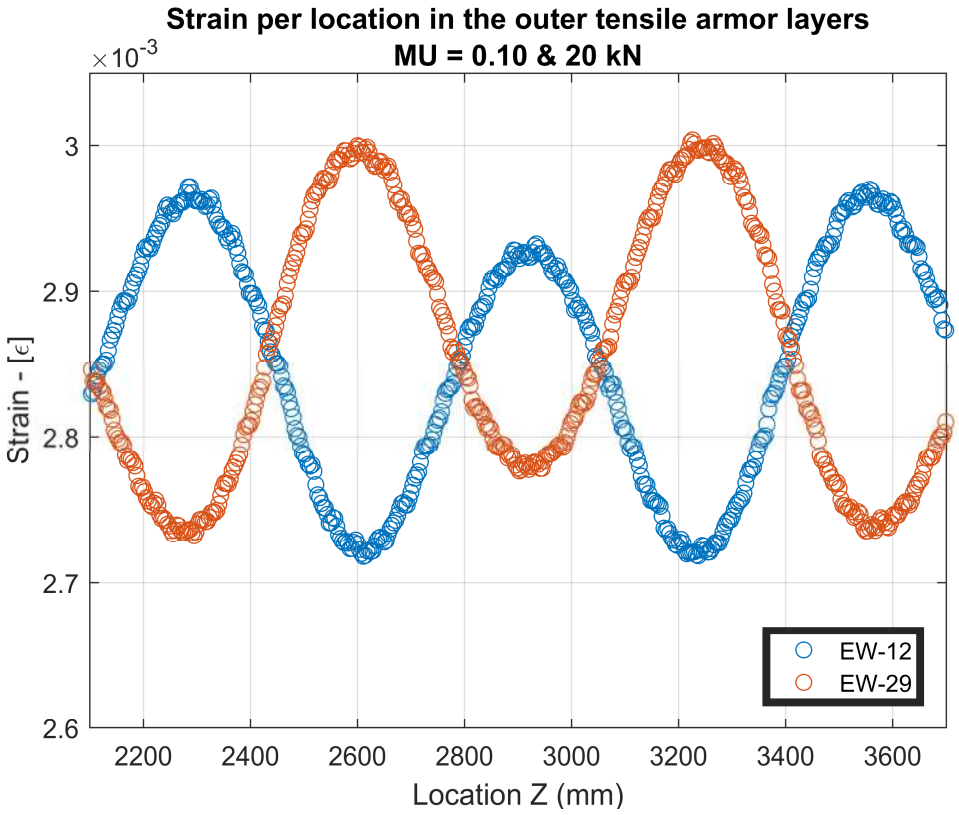

Figure 4.22. Normal Strain in two diametrically opposed external armor wires

Figure 4.23 presents the distribution of the strains along three different cross-sections obtained with the numerical model.

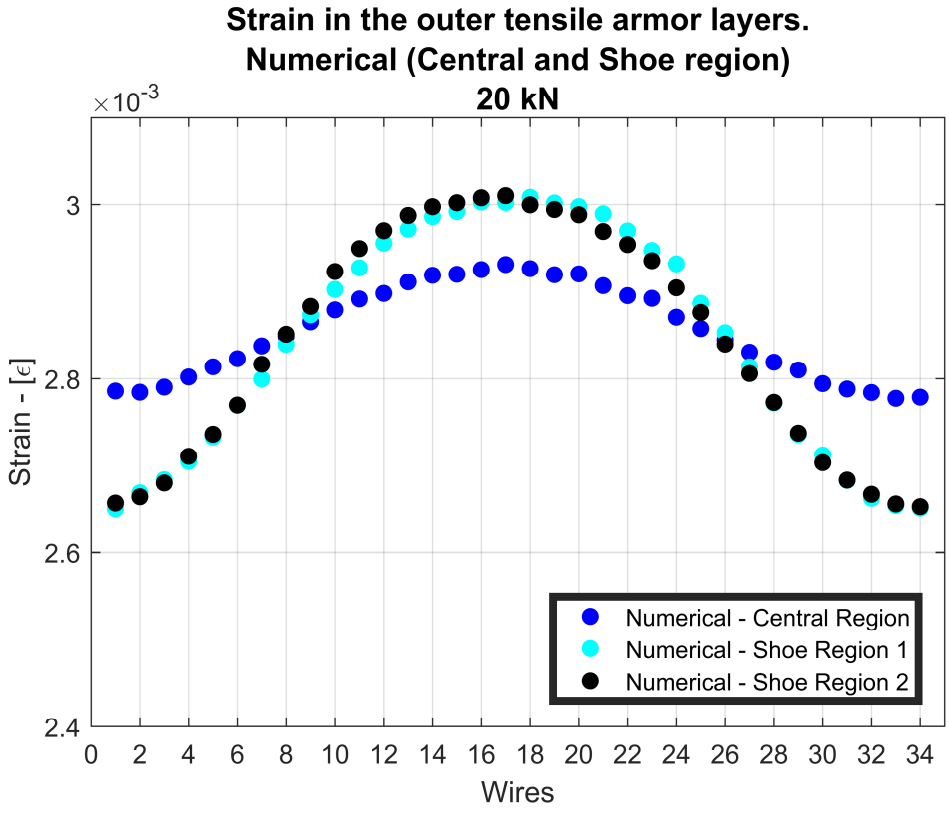

Figure 4.23. Normal Strain in three sections (bench shoes and central region)

In order to compare just the normal axial strain due to friction induced by the bending load, the normal strain induced by the axial tension (axial pre-tension and extra axial tension from the bending load) is removed from the numerical results presented in Figure 4.23. These numerical results are compared with the experimental and analytical model in Figure 4.24.

The analytical model adopted to estimate the normal strain is described by (ESTRIER, 1992). According this work, the strain caused by the friction increases with the contact pressure between the layers which constrains the sliding and induces residual stress of tension or compression which is called Normal Axial Stress due to Friction, $\sigma_t(P_c, \kappa_f, \theta)$.

In short, this stress is positive (tensile stress) in wires located in the extrados and negative (compressive stress) in wires located in the intrados of the flexible pipe. The value is also associated with the critical curvature as the slip reduces any further tension increase at the extrados and compression increase at the intrados of the bent pipe, and so slippage reduces further increases in the bending moment.

This stress component is given by (ESTRIER, 1992).

$$\sigma_t = \begin{cases} \dfrac{2 \cdot \pi \cdot a^2}{n} \dfrac{1}{A} \cdot \dfrac{1}{\tan(\alpha)} \sum (\mu \cdot P_C) \dfrac{\kappa}{\kappa_f} \cdot \sin(\theta), & \kappa < \kappa_f \\ \dfrac{2 \cdot \pi \cdot a^2}{n} \dfrac{1}{A} \cdot \dfrac{1}{\tan(\alpha)} \sum (\mu \cdot P_C) \cdot \sin(\theta), & \kappa \geq \kappa_f \end{cases} \tag{4.9}$$

where a is the average radius of the layer, A is cross sectional area of the tensile armor profile, θ is the circumferential angle of flexible pipe, P_c is the Contact pressure between layers, κ is the Curvature and κ_f is the Critical Curvature.

Figure 4.24 compares the numerical strains to those obtained from the analytical model and experimental tests. These values correspond to those measured in the mid-section of the pipe.

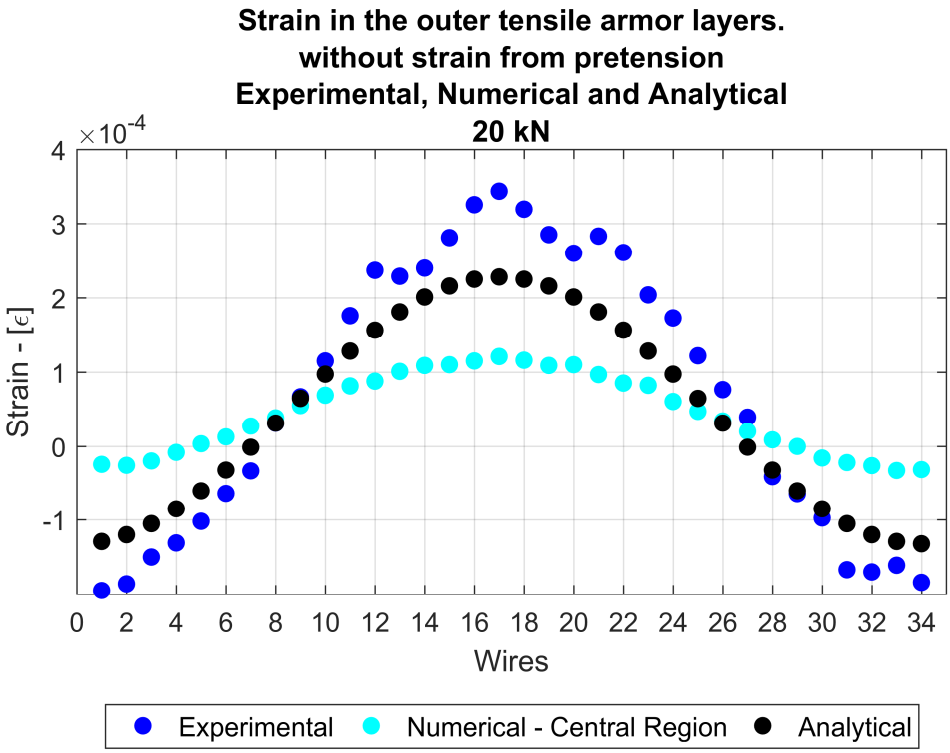

Figure 4.24. Numerical, Experimental and Analytical Normal Strain

The numerical and analytical results of the strains in the wires are smaller than the values measured experimentally. Among the main possible causes, we can suppose:

- decentralization of the region of strain gauges in relation to the bench shoes;
- non-uniformity and experimental uncertainty of strain measurement with strain gauges as noted in Figure 4.12.
- friction coefficient may play an important role for bending response of the numerical model (this parameter may also be influenced by the corrosion of the armor wires);
- elastic slip of 0.01, i.e. 1% of the underlying element, may still be too much for accuracy purpose;

In order to evaluate the effect of friction coefficient and elastic slip in strain response, two sensitivity studies are presented respectively in Figure 4.25, Figure 4.26, Figure 4.27 and Figure 4.28 where these parameters were varied.

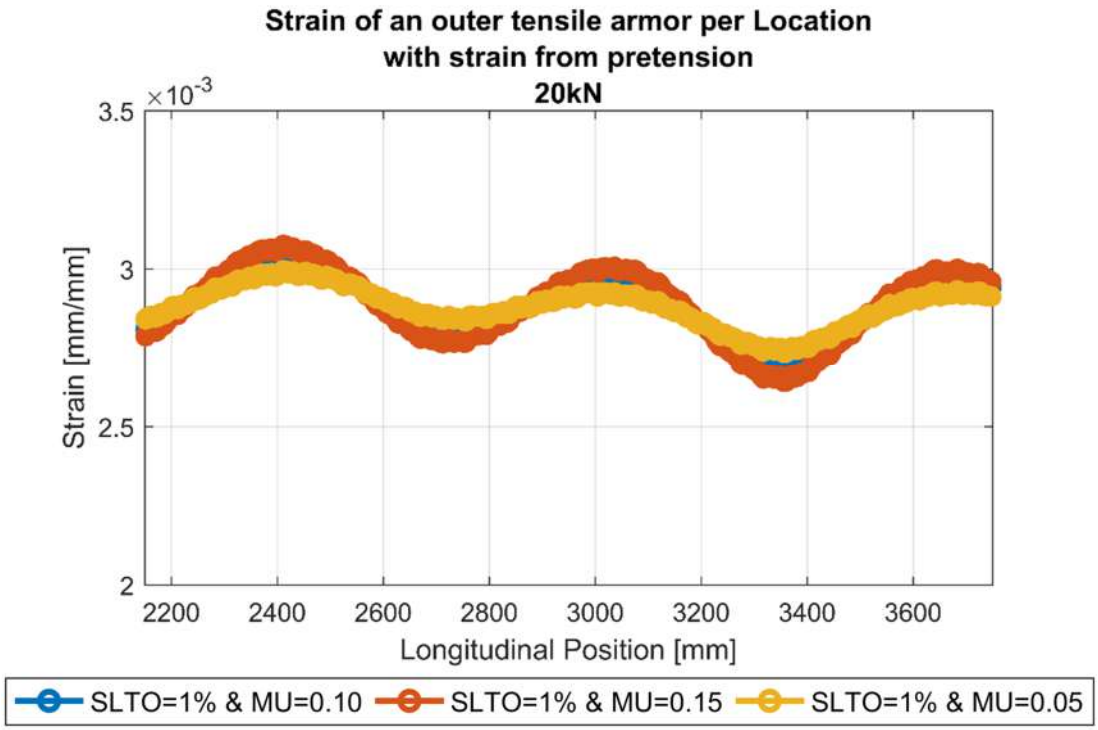

Figure 4.25. Normal Strain with pretension strain for different friction coef.

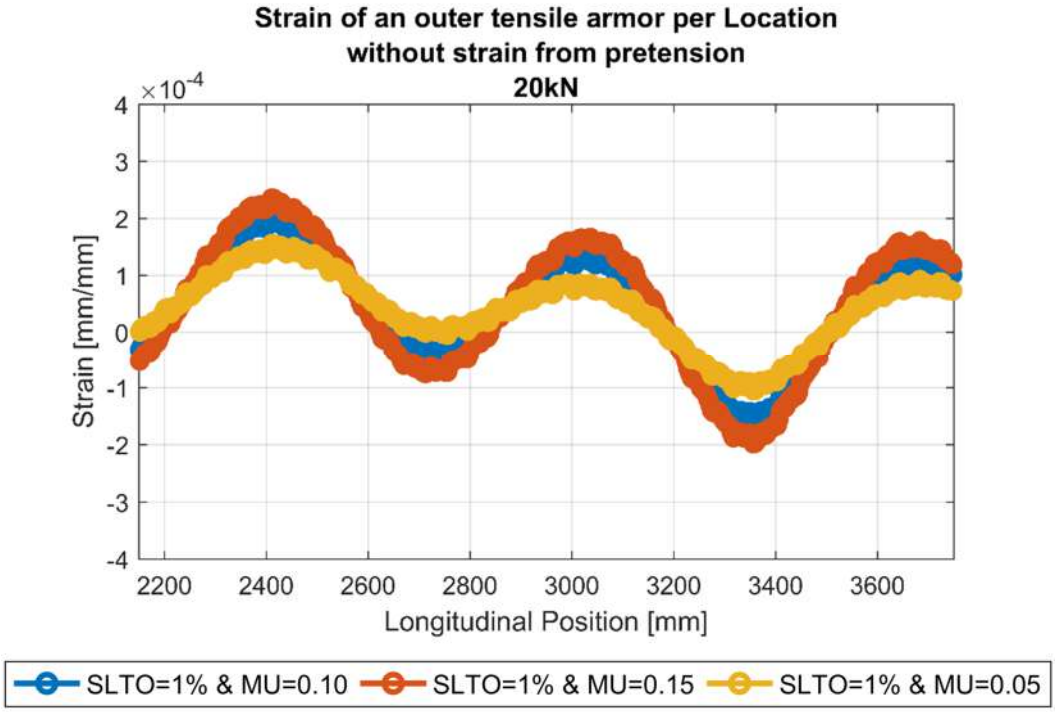

Figure 4.26. Normal Strain without pretension strain for different friction coef.

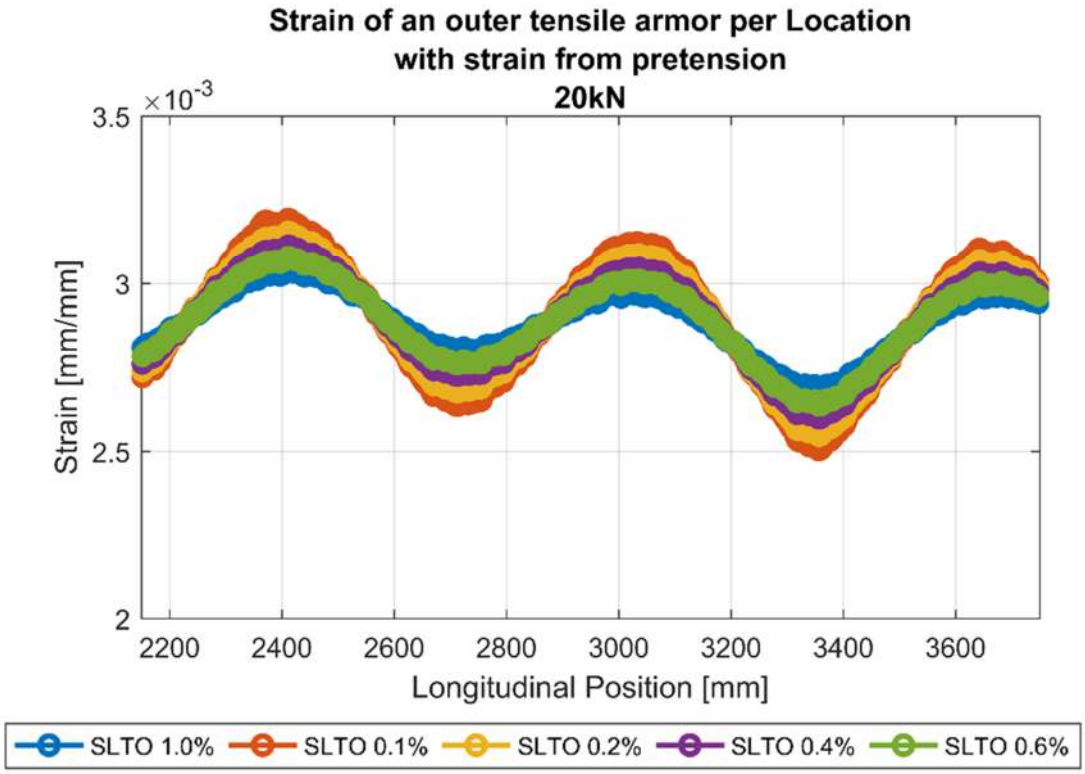

Figure 4.27. Normal Strain with pretension strain for different elastic slips.

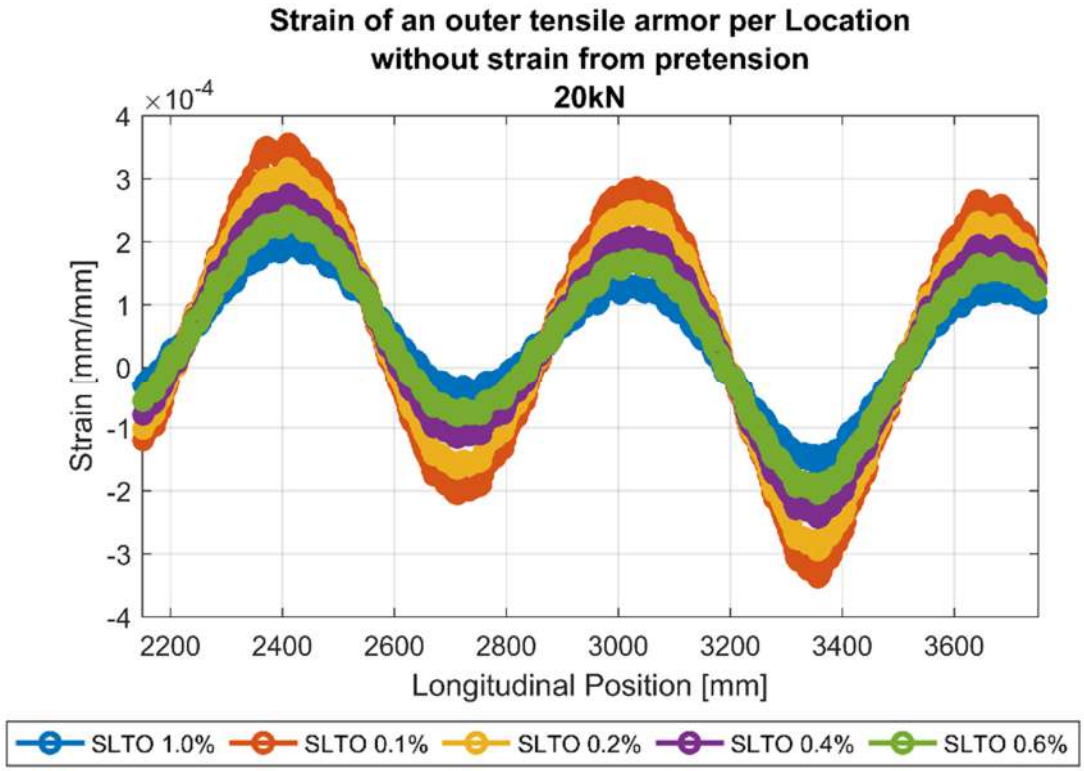

Figure 4.28. Normal Strain without pretension strain for different elastic slips.

Both the increase in the friction coefficient and the reduction of elastic slip, increase the difficulty of convergence and the time required for solution. Elastic slip has an even greater impact on convergence and solution time than the friction coefficient.

It is noteworthy that both parameters do not impact the pure tensile analysis and its induced strains.

As presented in Figure 4.26 and Figure 4.28, elastic slip is also the most important factor to impact the strain response.

Since the total normal strain in the armor wires are not too far from the experimental values and considering also the limitation of available computational capacity and the high computational cost for a cyclic analysis with slip, the FE analyzes for the cyclic part were run with the same parameters used before the sensitivity analysis, i.e. allowable slip factor and friction coefficient respectively 0.01 and 0.1.

Before the evaluation of slip and cyclic behavior, it is interesting to note in Figure 4.24 that there is a clear offset with respect to zero. This is caused by the extra tension induced by bending. The axial force increase, ΔP, Eq. (4.7), lead to an increase $\Delta\varepsilon$ in the strains acting in each tensile armor wire equal to:

$$\Delta\varepsilon = \Delta P \cdot f_{t,\varepsilon} \tag{4.10}$$

where ε_{bend} is the strain due to bending, and $f_{t,\varepsilon}$ is a coefficient that converts the tension load imposed on the pipe into normal strains in the considered layer.

Considering the increase in the axial tensile load from the numerical model, using its factor $f_{t,\varepsilon}$ and Eq.4.10, it is possible to achieve the results of the Figure 4.29. It can be noted that the normal strain induced by the bending is sinusoidal and symmetric with respect to zero.

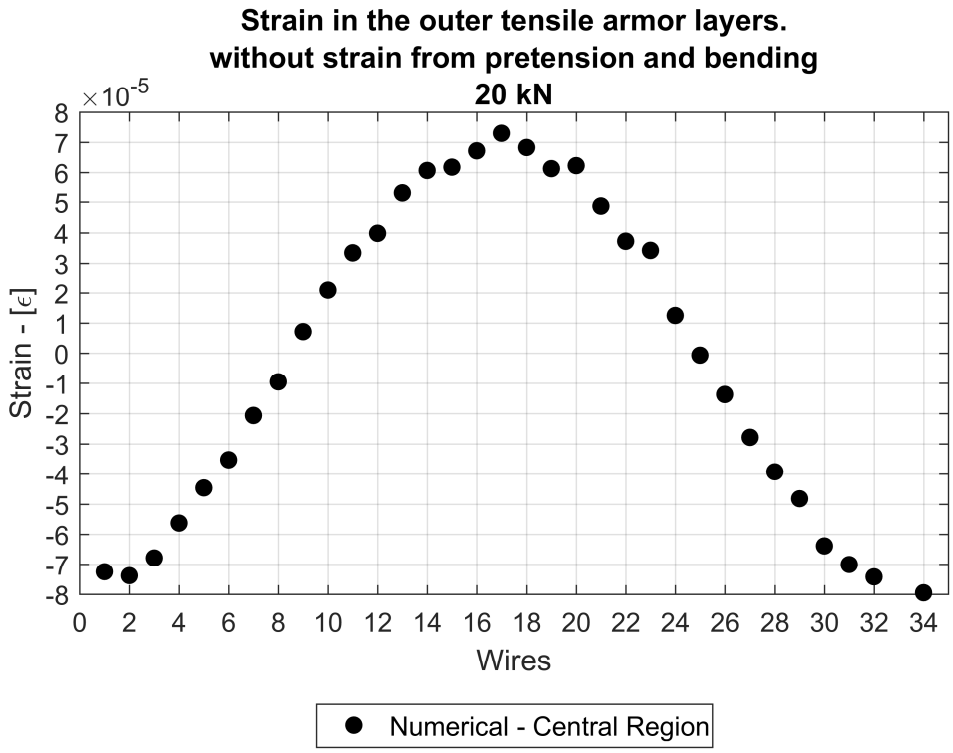

Figure 4.29. Normal Strain just from bending load

CYCLIC BENDING LOAD AND HYSTERETIC BEHAVIOR

As described in section 2.2, the critical curvature is the curvature that initiate the relative slipping of the armor wires. If this curvature is exceeded, the bending moment *vs* curvature relationship becomes nonlinear. (ESTRIER, 1992) states that the critical curvature can be estimated with the expression:

$$\kappa_f = \frac{\pi^2}{4} \frac{\sum \tau_{max}}{E \cdot h \cdot cos^2(\alpha) \cdot \sin(\alpha)} \tag{4.11}$$

$$\tau_{max} = \mu \cdot P_c \tag{4.12}$$

where τ_{max} is the limit shear stress in the contact interface; μ is the friction coefficient; h is the height (thickness) of the wire; α is the lay angle; P_c the contact pressure between layers; and the $\sum$ corresponds to the sum of the friction stresses in the outer and the inner surfaces of the wire.

By considering the interlayer contact pressures estimated numerically with a pre-tension load of 700 kN, a critical curvature of 0.025m^{-1} is calculated with Eqs. (4.11) and (4.12). The total transverse load associated with this curvature can be calculated with Eqs. (4.1) to (4.6), which indicates a value of 25.5kN and a maximum transverse displacement, Eq. (4.1), of 42mm. The curvature and transverse displacement curves obtained with Eqs. (4.6) and (4.1), respectively, are presented in Figure 4.30. Note that the maximum curvatures occur in the load application sections, while the maximum displacement occurs in the mid-section of the pipe.

It is worth remarking that a total transverse displacement of 42mm cannot be imposed by the transverse hydraulic actuator and, therefore, the cyclic bending response of the pipe can only be estimated numerically. Hence, the transverse load was increased to 51.5 kN and the bending moment vs curvature curve presented in Figure 4.31was obtained.

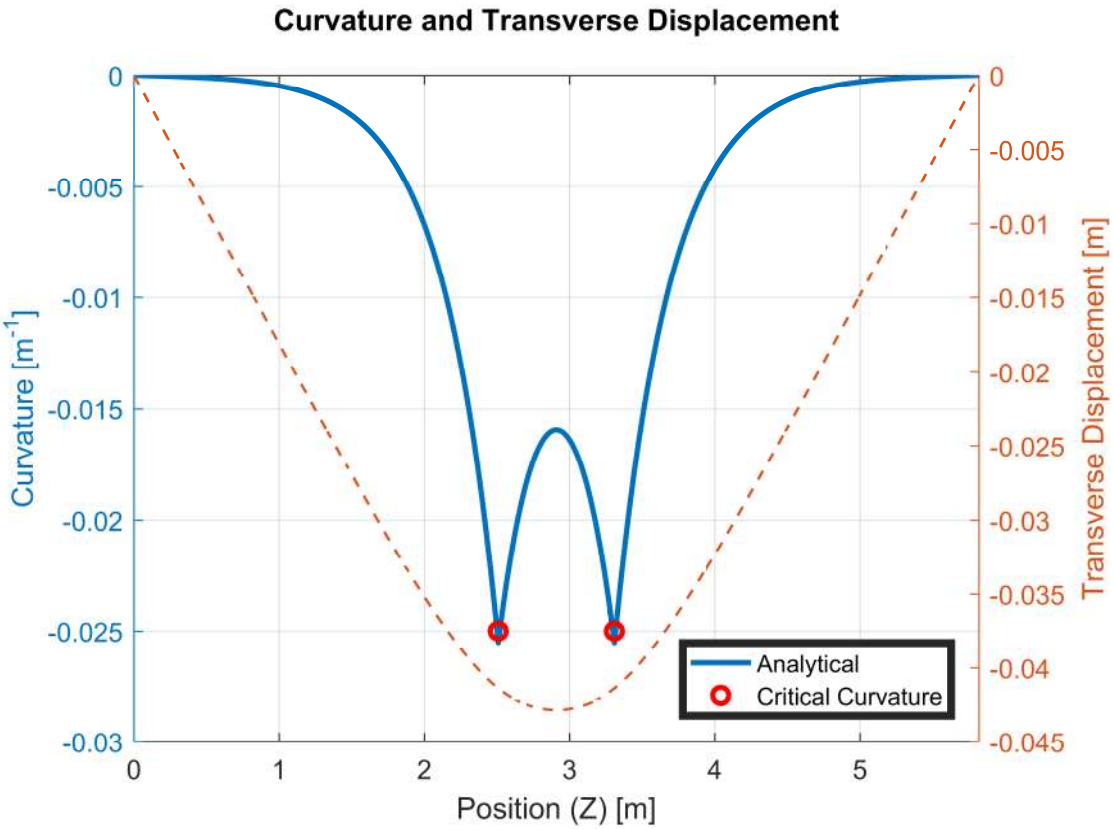

Figure 4.30. Critical Curvature (Transverse Load = 25.5 kN)

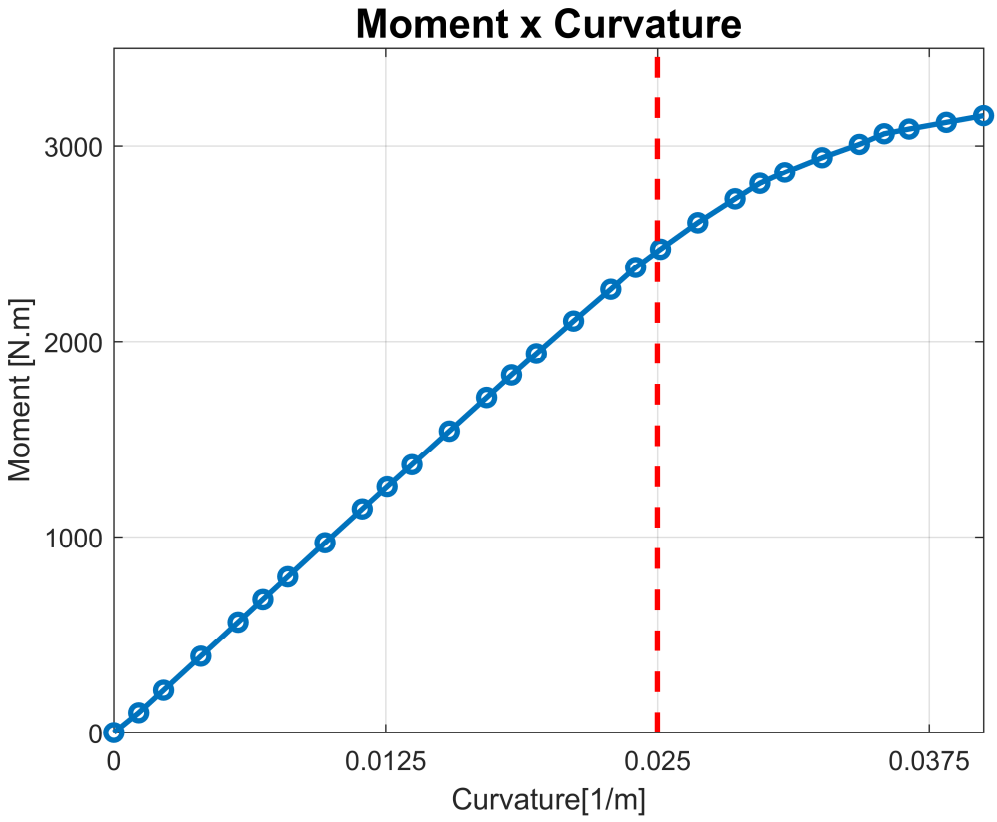

Figure 4.31. Moment vs. Curvature - monotonic

Figure 4.31indicates that, after a curvature of about 0.025m^{-1}, the curve presents a nonlinear response with decreasing bending stiffness, which suggests that the outer tensile armor wires started to slide relatively to the surrounding layers. This is corroborated by Figure 4.32, which presents the variation in the number of sticking points with the imposed transverse displacement. If no relative sliding is occurring, the number of sticking points should have remained constant (or almost constant) along the analysis, but this figure indicates that, for transverse displacements higher than 42 mm, the number of sticking points decrease significantly. Therefore, relative sliding starts at a curvature of about 0.025m^{-1}.

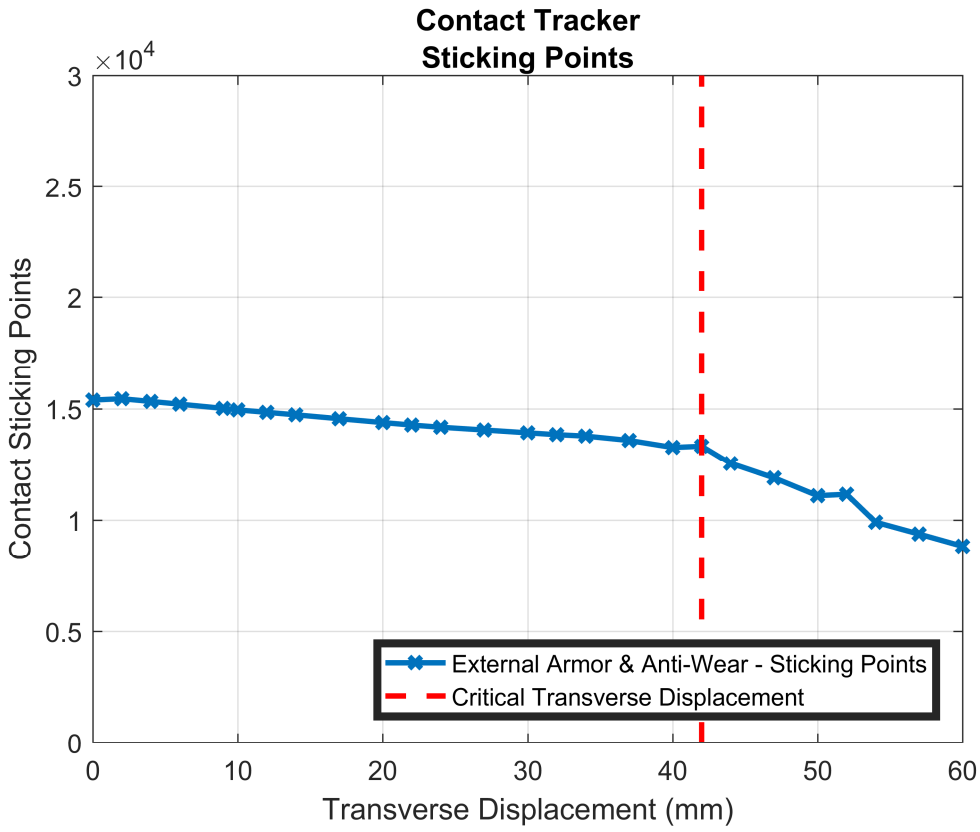

Figure 4.32. Sticking Points // External Armor Wires (42mm)

After reaching the maximum transverse load, this load is reversed and the bending moment vs curvature curve presented in Figure 4.33 was obtained. Initially, the pipe presents a bending stiffness equal to the one of the no-slip region of the monotonic loading phase. The wires start to slide after imposing a bending moment equivalent to two times the one applied in the monotonic phase. If the load is again reversed, an analogous

response is observed and, moreover, a residual curvature is noted when no bending moment is acting on the pipe and vice versa.

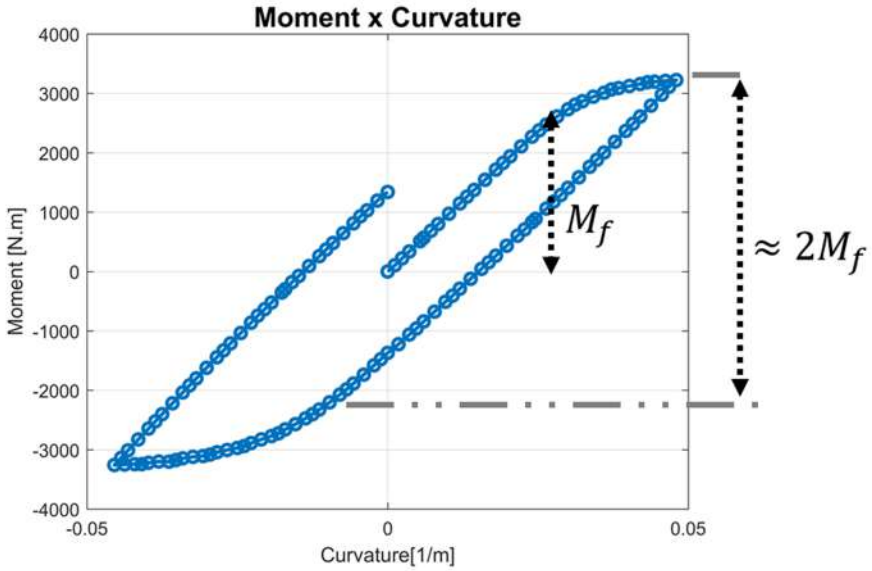

Figure 4.33. Moment vs. Curvature – cyclic

After performing a linear fit in the points referring to the full-slip regime, a stiffness of 1.007 kN.m2 is reached. This value is very close to the analytical value calculated in (SOUSA, *et al.*, 2015) which is 1.09 kN.m².

This response is also consistent with the hysteretic mechanism described in CHAPTER2 and the graph agree with the estimate that the full slip regime is achieved with twice the friction moment in case of curvature reversal.

Regarding the slip regime, it is important to note the asymmetry of the bench shoes with respect to each armor wire, i.e. the same armor wire may have a tendency to slip close to one shoe and not in the same manner close to the other shoe depending on the angular position that is encountered when passing close to the shoe.

Using Figure 4.21, it is noteworthy that the external armor wire 12 passes by shoe1 with its path close to neutral line and passes by shoe2 with its path close to intrados (top region). It is possible to note the nonlinear shape and hysteretic behavior in normal strains presented in Figure 4.34. In this graph, the right axis is included, allowing to know if it is in the neutral line or not, the Xmax and Xmin locations correspond to the neutral line.

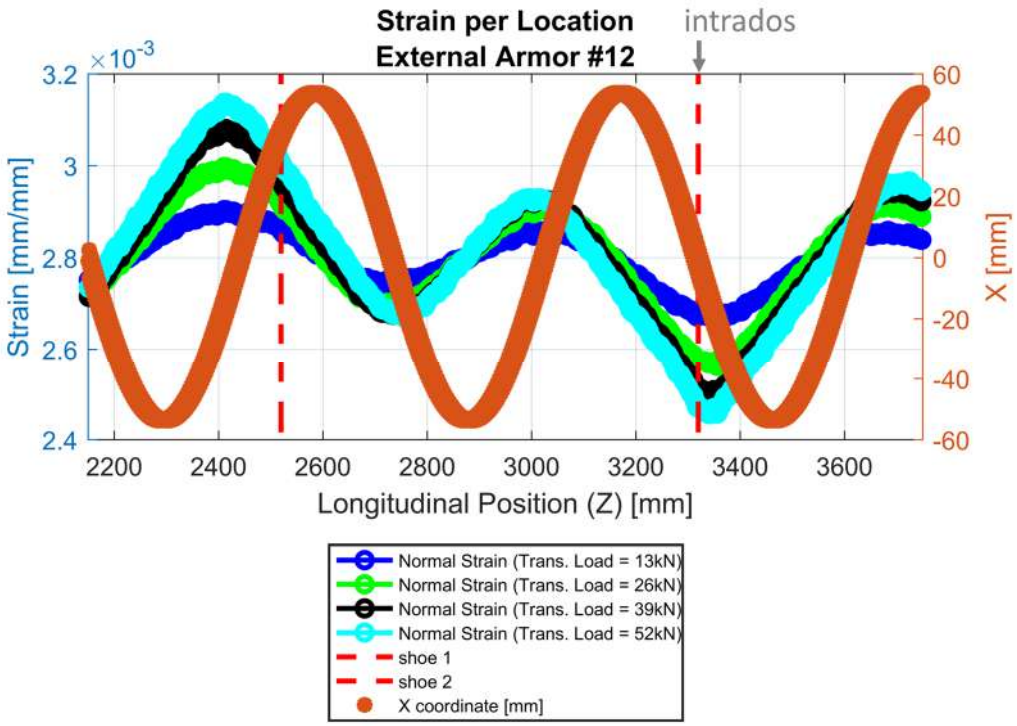

Figure 4.34. Strain during slip-regime – EW-12

Selecting a node of external armor wire 12 close to the bench shoe2, it is possible to present the hysteretic strain in Figure 4.35.

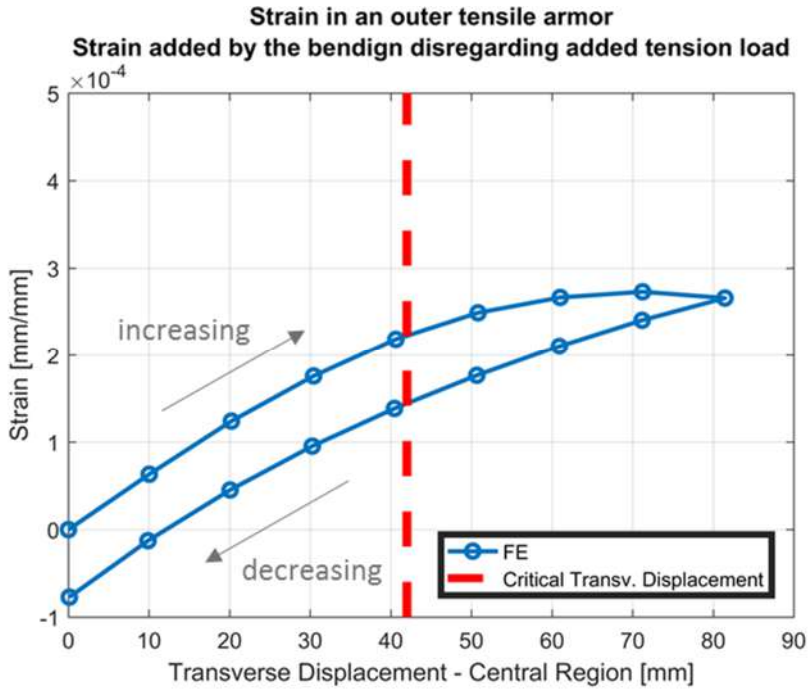

Figure 4.35. Armor Wire – Hysteretic Strain

Once presented these facts about the normal strain, it is important to evaluate the wire path configuration.

This is performed by making an evaluation of the relative displacement of three selected nodes of the external armor wire #12 using its local coordinate system as presented in Figure 4.36.

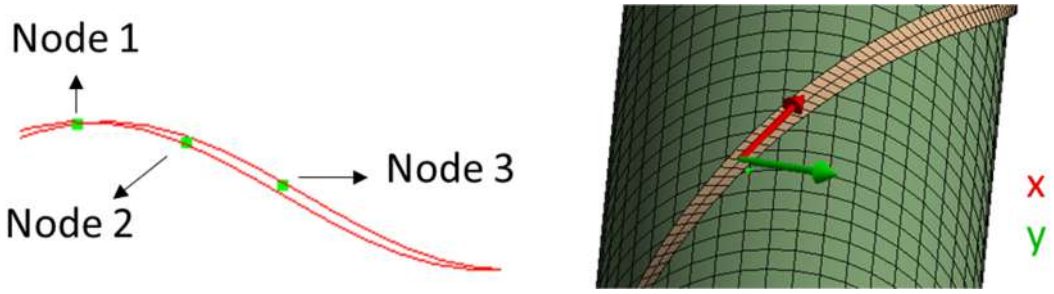

Nodal Location ***Local Coordinate System***

Figure 4.36. Selected nodes and its Coordinate System

The displacement results from these nodes are presented in Figure 4.38, Figure 4.39 and Figure 4.40. The angular reference included in these graphs are according Figure 4.37.

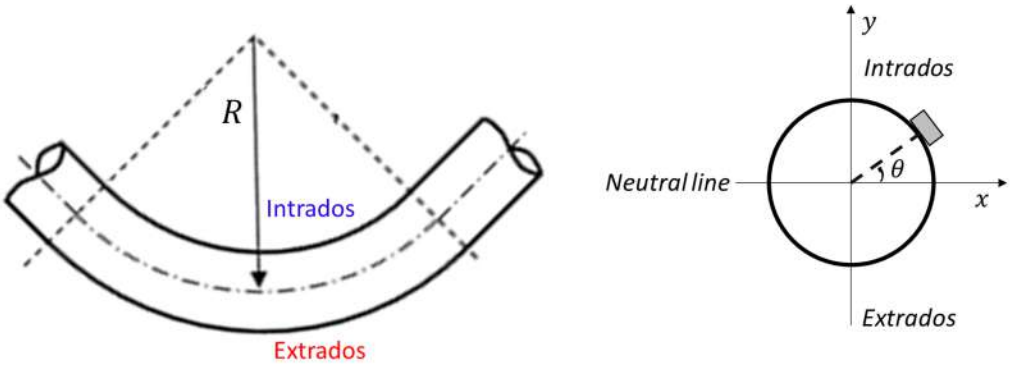

Figure 4.37. Intrados and Extrados

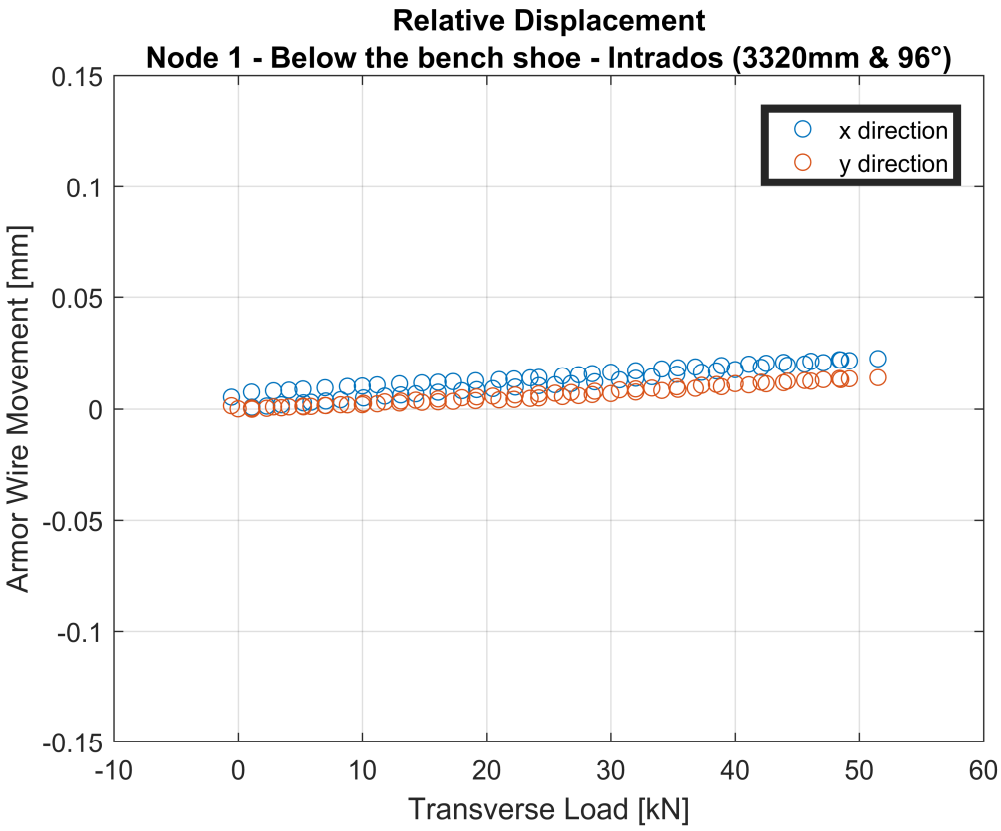

Figure 4.38. Armor Wire Movement – Node 1

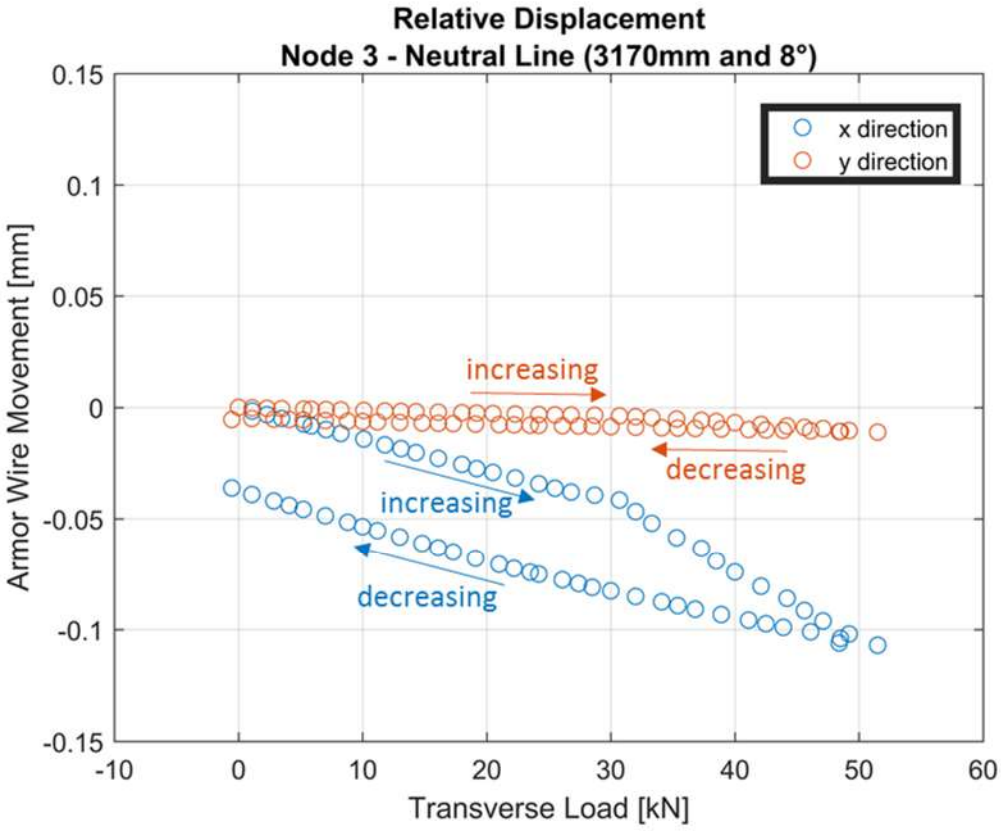

Figure 4.39. Armor Wire Movement – Node 2

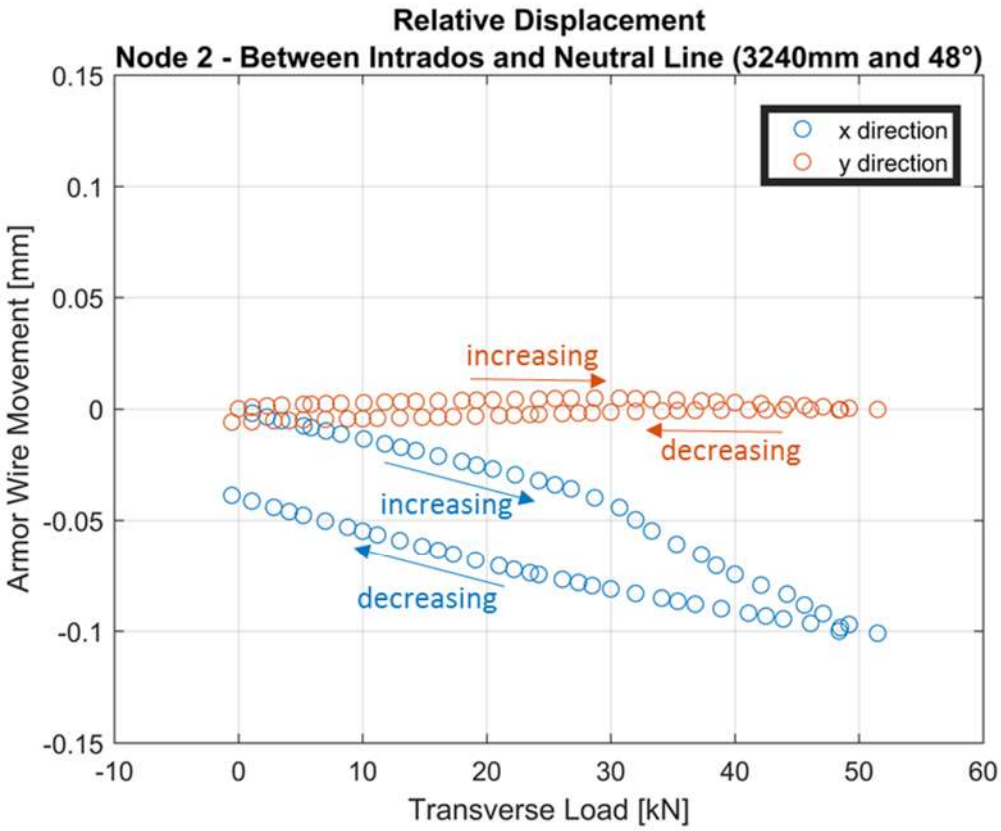

Figure 4.40. Armor Wire Movement – Node 3

Based on Figure 4.38, Figure 4.39 and Figure 4.40, it is possible to note that the armor wire displacements presented a displacement almost exclusively in the tangential direction of the wire. In short, the wire keeps its displacement following its lay angle and this characteristic is basically the loxodromic path, as described in Chapter 2.

In addition to the finding that the transverse displacement is negligible, a change in the longitudinal displacement rate for nodes 2 and 3 is remarkable.

This change occurs between 30kN and 20kN, which is close to 25.5 kN relative to the load for the critical curvature.

Thus, it is possible to suppose that the slip behavior of the wires can also be approximated by a bilinear curve.

In order to have a better overview about the slip phenomenon covering all the wires of the external armor, it is valuable to present another contact tracker, the sliding distance of the contact pairs. The total sliding distance is defined as the amplitude of total accumulated slip increments (a geometrical measurement) when the contact status is sticking or sliding. It should be mentioned that this value contains contributions from the elastic slip and the frictional slip.

It is possible to evaluate the slip distance with its respective location in the numerical model. In Figure 4.41, it is presented the result for the external armor wire in the tension only condition.

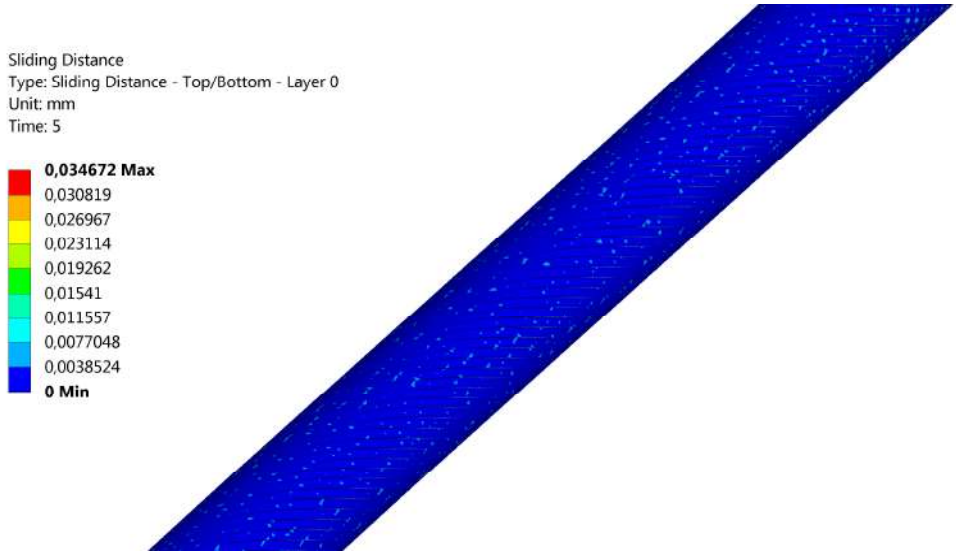

Figure 4.41. Sliding Distance Plot (700kN/Tension only)

It is possible to see in Figure 4.41 that there is no tendency of armor wire slip over a specific location of the armor wire path when the pipe is under pure tension.

On the other hand, when under bending, as presented in Figure 4.42, it is noteworthy the slip starting over the armor wires near the neutral line, and the opposite, i.e. no slip, happening in Extrados and Intrados location. This is in accordance with the analysis performed for the three nodes of armor wire 12 in Figure 4.38, Figure 4.39 and Figure 4.40.

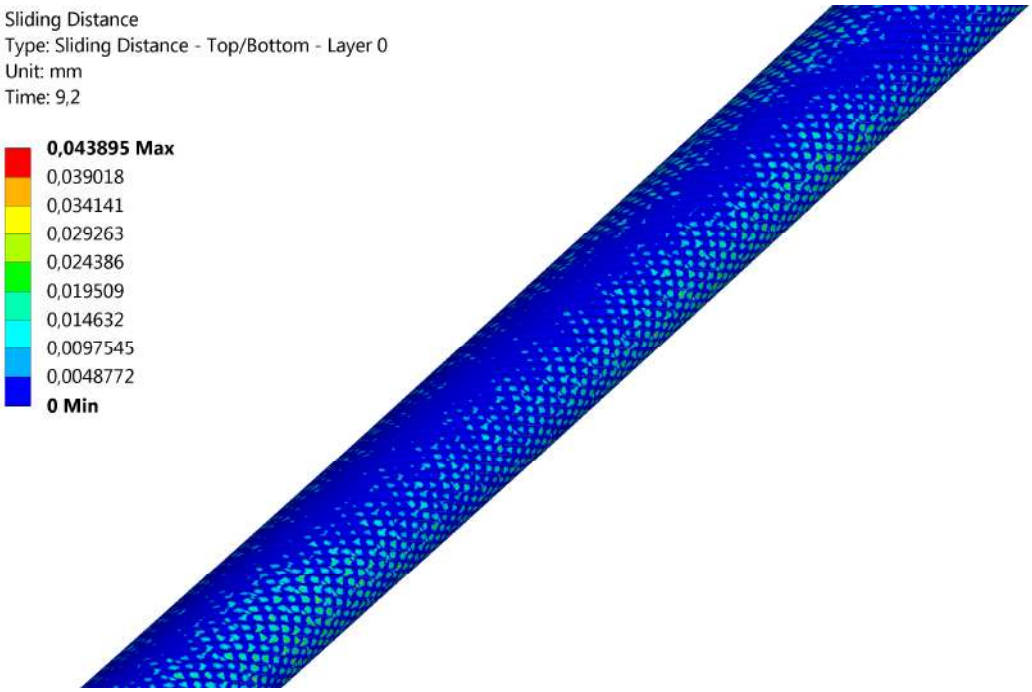

Figure 4.42. Sliding Distance Plot (25kN)

The armor wire path behavior is according with the study of (BERGE, *et al*., 1992) with indicated that the geodesic hypothesis does not provide adequate results and proposed, therefore, that the deformed configuration of these wires follows loxodromic curves. Anyway, it should be noted that for great curvatures the expected tendency is that the slip begins to behave like a geodesic.

In addition to this visual analysis of tendency and location of armor wire slip, it is valuable to post-process the numerical results of this contact tracker in order to evaluate relationship between the angular position of the wire, the curvature and the slip value.

For this, all external armor wires nodes below both shoe regions were selected to be further evaluated as described in Figure 4.43.

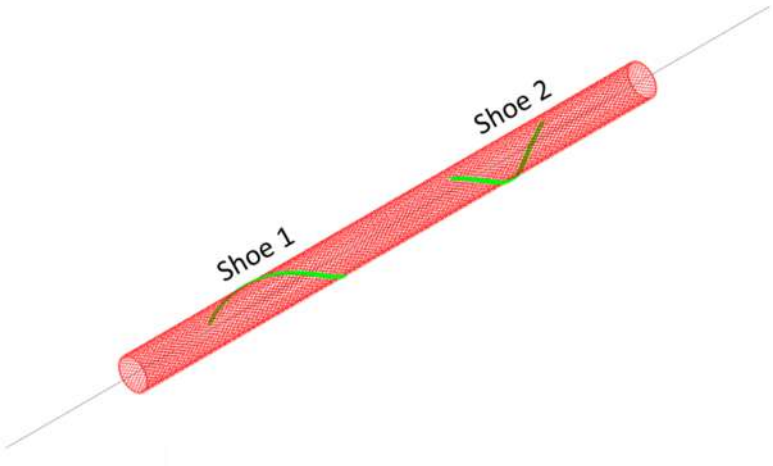

Figure 4.43. Shoe regions

The contact tracker is therefore defined according the angular position presented in Figure 4.37.

The first analysis is focused on the location called bench shoe#1 and it is presented in Figure 4.44.

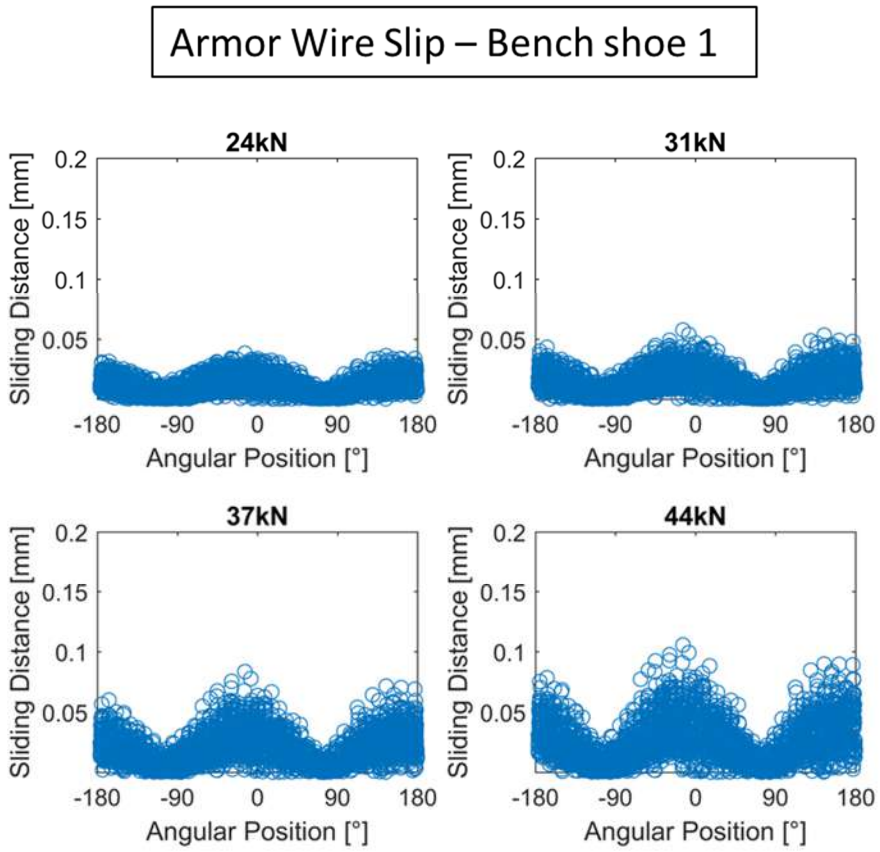

Figure 4.44. Sliding Distance (total) – Bench shoe 1

As expected, it is remarkable one more time the peak of slip close to the neutral line (-180°, 0° and 180°). Besides this, there is a clear sinusoidal response of the slip.

The results of bench shoe#1 is very close to the result present in Figure 4.45 for bench shoe 2.

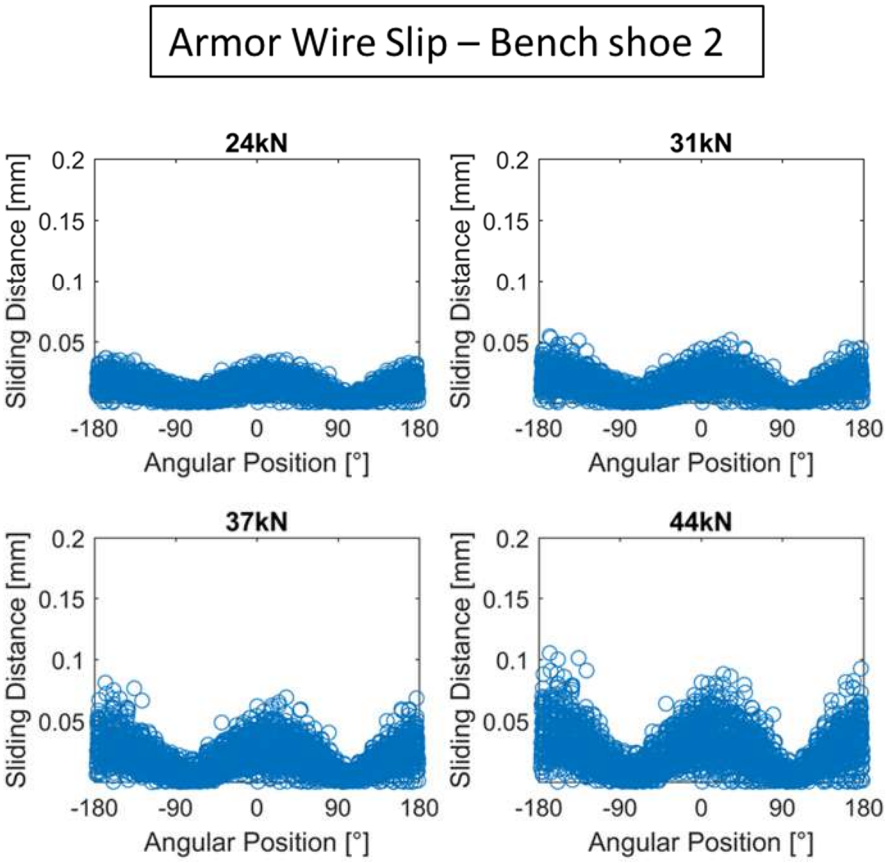

Figure 4.45. Sliding Distance (total) – Bench shoe 2

In addition, it is possible to evaluate the peak results of slip from Figure 4.44 and Figure 4.45 to evaluate in 2D graph and check the influence of curvature. This result is presented in Figure 4.46.

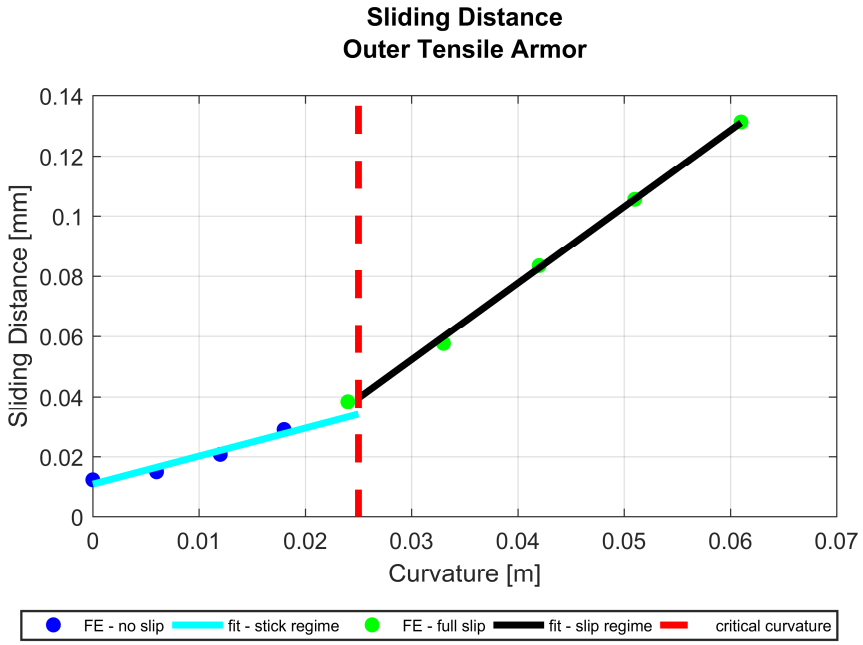

Figure 4.46. Sliding Distance – Outer Tensile Armor – Tension and Bending

In Figure 4.46, it is noteworthy the increase of the slip rate after the critical curvature.

Knowing that before the critical curvature, the flexible pipe presents a constant bending stiffness and knowing that elastic slip parameter has influence on the strain behavior of the numerical model as presented in Figure 4.27 and Figure 4.28, it is possible to assume that the negligible slip rate before the critical curvature can be attributed to the sliding tolerance (elastic slip) in the stick regime as defined in CHAPTER 3.

Thus, the numerical model must deal with a small and unavoidable pre-slip depending on the numerical method adopted. This behavior of the numerical model is presented in Figure 4.47. It is possible to foresee a linear or bilinear formulation, taking into account the critical curvature and the circumferential angle of flexible pipe, θ.

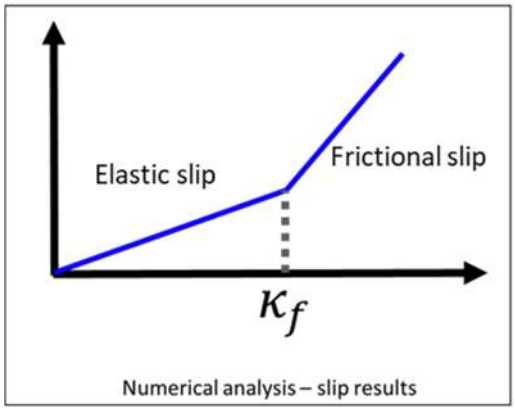

Figure 4.47. Numerical and Analytical Slip

A fitted curve from the results of the present study is presented in Figure 4.48.

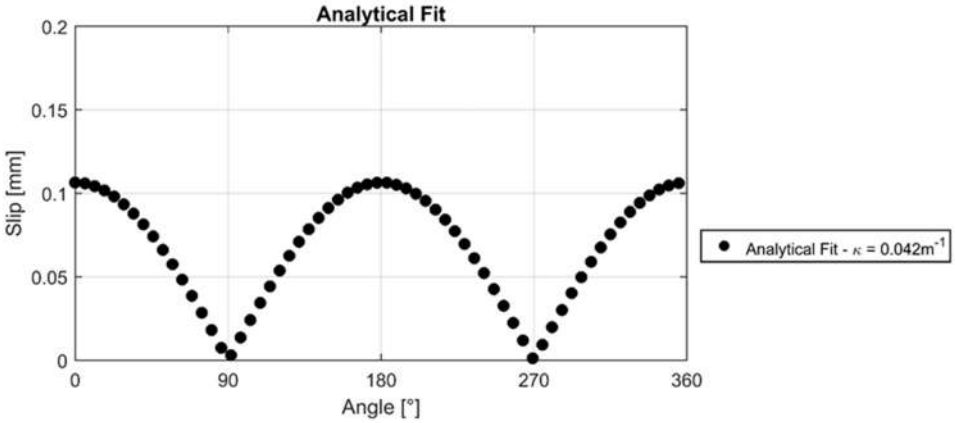

Figure 4.48. Slip – Analytical Fit (absolute value from the resultant)

The main formulation available in literature is from the work of (FERET & BOURNAZEL, 1986), which assumes the geodesic path, and states the following equation for the slip in tangential direction.

$$\Delta_a = \kappa a^2 \frac{cos^2(\alpha)}{\sin(\alpha)} \cos(\theta) \tag{4.13}$$

It is important to highlight, however, that according the authors that used Eq.4.13 as (FERET & BOURNAZEL, 1986) and (FERET & BOURNAZEL, 1987), the derivation of all these equations is valid for a flexible of great length and bent with a constant curvature. As this is not the case of the studied full-scale test, the formulation is not suitable for comparison purposes.

In the same way, the parameters that may affect the slip rate are not explored in the literature. There is only brief evaluation, which is presented in (TAN, *et al.*, 2005), that states that the slip would have a relation with the cross-section area of the armor wire.

Although extremely promising, a more comprehensive study on the armor wire slip and bending are necessary and some further works are proposed in CHAPTER 5.

.

CHAPTER 5. FINAL COMMENTS AND FUTURE WORK

This chapter presents some final comments and some suggestions for future work.

FINAL COMMENTS

The first part of the analysis describes the axial tension analysis using the shell based model. In this model, the tensile armor wires were individually modeled while the neighboring layers were modeled with composite shells in order to reduce the computational cost.

The model considers geometrical and contact nonlinearities, with friction considered using the Coulomb friction law. After a set of analyses, the model is validated through a comparison with a full-scale test used as case study for this work.

In short, the good agreement presented between the numerical and experimental results highlighted an adequate set-up of the model regarding material model, elements, normal stiffness, friction coefficient and FE mesh, qualifying this model as suitable for application in pure tension analysis.

The material model considering orthotropic properties using the analogy between grids and orthotropic shells successfully established an equivalence of the stiffness, agreeing with the studies that have already used this formulation.

The application of Shell 181 elements for all the layers demonstrated not only the consistency in terms of strain and stress, but also enabled the application of an equivalent layer, combining for example four internal layers into a single layer.

The spatial discretization of the tensile armor presented good results adopting two elements per armor wire.

The model presented a high dependency on the normal contact stiffness and as expected, due to the quantity of contact pairs, if they were not well defined, this parameter can generate a model with a poor physical correspondence.

Regarding the friction, as noted, its coefficient presented no important role when it comes to flexible pipe’s axial stiffness.

For the second part, the bending load, the requirement for refinement greatly increases the computational time, which was attenuated by the adoption of beams for the sections of small curvature and therefore linear and constant stiffness.

The transverse response presented excellent agreement. Besides this, the strain results from the model agree well with the analytical model and also experimental behavior, being able to model the relative slip of armor wires and full-slip bending stiffness. Some relative differences may be due to some uncertainties inherent with the experimental test and also the numerical model as described.

Some events that were not treated in other models were herein incorporated thus improving the capability of analysis over armor wire slip.

Regarding the slip behavior, the conclusion from this model is more similar to the theory proposed by (BERGE, *et al*., 1992) which states that the deformed configuration of the armor wires follows loxodromic curves.

Finally, it should be emphasized that all conclusions should still be explored in other configurations of bending loads and full scale tests.

FUTURE WORKS

The results from the present study are very encouraging to perform further investigations and validations on the topic. Some topics for future works are proposed as follows:

1) Perform full-scale tests with pure bending and bending combined with tensile load with different structures, leading them to the critical curvature. It would be interesting to perform these tests with non-uniform curvatures and also constant curvatures. If the tests are performed with curvatures higher than critical curvature, the external sheath should not be partially removed as it will influence the full slip bending stiffness. Besides this, the curvature could be directly measured with an optical tracking system, as used in (PESCE, *et al*., 2011).
2) Conduct further parametric studies on the influence of the friction coefficient and elastic slip parameter to the bending response. Check if the twist restraint can change this behavior.
3) Evaluate how the corrosion state of the armor wires can influence the coefficient of friction and consequently the critical curvature and the hysteretic behavior of the structure.

4) Compare the analyses with explicit and implicit solvers. Although (PERDRIZET, *et al*., 2011) briefly mention the application of both for bending analysis, this comparison should be further explored. Explicit dynamics solvers are particularly well-suited to solving some typical types of highly-nonlinear analyses as complex and changing contact interfaces with significant sliding, and models with nonlinear material properties. In this context, commercial explicit dynamics solvers such as LS-Dyna include robust contact algorithms and material models that can handle such problems without numerical difficulties, leading to an ease of convergence with much less solver settings changes (pre-processing phase). Despite these advantages, to have an accurate solution, it is important to avoid dynamic effects, checking, for example, the kinetic energy and added system damping. In a general way, while implicit solvers are still the first choice for statics problems, explicit solvers with appropriate transient time and damping settings can be used to provide robust solutions to problems like the one of the present work.

5) Compare the adoption of static friction models and dynamic friction models. The only study with this kind of comparison is (SÆVIK, *et al*., 2017), were a numerical model with reduced quantity of armor wires is performed and there is no experimental validation.

6) Integrate local analysis with global analysis, even though some studies already exist as (TAN, *et al*., 2007), (TAN, *et al*., 2009), (SMITH, *et al*., 2007) and (LIU, 2014). It would also be interesting to evaluate the possibility of coupling local analysis with global analysis through the ANSYS® Workbench and ANSYS® AQUA.

7) Evaluate the viscoelastic behavior from polymeric layers as external sheath. The only study with this kind of approach is (SANTOS, *et al*., 2015), which considers a set of small-scale tests of HDPE to calibrate a linear viscoelastic model and be used in FEM developed in ABAQUS®.

8) Evaluate the effect of creep of the polymers in bending behavior as briefly highlighted by (LØTVEIT, *et al.*, 1994).

REFERENCES

ALFANO, G., BAHTUI, A., BAHAI, H., 2009, "Numerical derivation of constitutive models for unbonded flexible risers.", *International Journal of Mechanical Sciences*, v. 51, pp. 295–304.

AMERICAN PETROLEUM INDUSTRY, *Recommended Pratice for Flexible Pipe*, 17B, 5th ed., USA, 2014.

AMERICAN PETROLEUM INDUSTRY, *Specification for Unbonded Flexible Pipe*, 17J, 4th ed., USA, 2014.

ANSYS, 2016, *Reference Manual (version 17.2)*, ANSYS Inc.

BAHTUI, A., BAHAI, H., ALFANO, G., 2008, "A Finite Element Analysis for Unbonded Flexible Risers Under Axial Tension.", *27th International Conference on Ocean, Offshore and Artic Engineering*, 57627, Estoril, Portugal, 15-20 June 2008.

BAHTUI, A., BAHAI, H., ALFANO, G., 2009, "Numerical and Analytical Modeling of Unbonded Flexible Risers.", *Journal of Offshore Mechanics and Arctic Engineering*, v. 131, i. 2, pp. 021401-1 - 021401-13.

BATISTA, R. C., BOGARIN, J. A. G., EBECKEN, N. F. F., 1989, "Local Mechanical Behaviour of Multilayered Flexible Risers." In: *Proceeding of 7th International Symposium on Offshore Engineering*, pp. 494-510, Rio de Janeiro, August.

BERGE, S., LEIRA, B. J., NYGAARD, I.; M., LARSENC; OLUFSEN, A.; FYLLING, I.; ENGSETH, A., 1992, *Flexible Risers and Pipes: Handbook of design and operation of flexible pipes.* 1ed. Trondheim, SINTEF.

BRAESTRUP, M., ANDERSEN, J.B., ANDERSEN, L.W., BRYNDUM, M.B., 2009, *Design and Installation of Marine Pipelines.* 1ed. Noida, Wiley-Blackwell.

BREUNLE, M., 2015, *Structural mechanic FE-analysis of the nonlinear behavior of multilayer cables.* Undergraduate Project, Friedrich-Alexander University Erlangen-Nürnberg (FAU), Erlangen and Nuremberg, Bavaria, Germany.

CAIRE, M., "Flexible Riser Bending Hysteresis Influence on Bend Stiffener Response". *33rd International Conference on Ocean, Offshore and Artic Engineering*, 23151, San Francisco, USA, 08-13 June 2014.

CRUZ, F. L. T., 1996, *Análise Estrutural de Linhas Flexíveis pelo Método de Elementos Finitos*. M.Sc. thesis, Escola Politécnica da Universidade Federal de São Paulo, São Paulo, SP, Brazil.

CUSTÓDIO, A., VAZ, M., 2002, "A nonlinear formulation for the axisymmetric response of umbilical cables and flexible pipes", *Journal of Applied Ocean Research*, v. 24, pp. 21-29.

EIA - THE U.S. ENERGY INFORMATION ADMINISTRATION, *Short-term Energy Outlook*, 2016. Available in: https://www.eia.gov/forecasts/steo/data.cfm?type=figures. Accessed in: 11 August 2016.

EDMANS, B.; ALFANO, G.; BAHAI, H.; ANDRONICOU, L.; BAHTUI, A., "Local Stress Assessment of Flexible Unbonded Pipes Using FEA". *31st International Conference on Ocean, Offshore and Artic Engineering*, 84248, Rio de Janeiro, Brazil, 1-6 July 2012.

ELOSTA, H., GAVOUYERE, T. & GARNIER, P., "Flexible Risers Lifetime Extension: Riser In-Service Monitoring And Advanced Analysis Techniques.". *36th International Conference on Ocean, Offshore and Artic Engineering*, 62700, Trondheim, Norway, 25-30 June 2017.

ESTRIER, P., "Updated Method for the Determination of the Service Life of Flexible Risers.". *1st European Conference on Flexible Pipes, Umbilicals and Marine Cables (Marinflex 92)*, London, England, United Kingdom, 10-11 November 1992.

FACHINI, E. “O Uso Offshore de Dutos Flexíveis no Brasil”. In: Curso de Extensão (COPPE/UFRJ) - Dutos Flexíveis e Umbilicais, Rio de Janeiro, August 2014.

FERET, J. J. & BOURNAZEL, C. L., 1987, “Calculation of Stresses and Slip in Structural Layers of Unbonded Flexible Pipes”, *Journal of Offshore Mechanics and Artic Engineering*, v. 109, pp. 263-269.

FERET, J. J. & MOMPLOT, G., 1991, *CAFLEX - A program for Capacity Analysis of Flexible Pipes - Theory Manual.* Trondheim, SINTEF Structural Engineering & IFP.

FERGESTAD, D., LØTVEIT, S. A., 2014, *Handbook on Design and Operation of Flexible Pipes*. 2ed. Trondheim, Marintek, NTNU & 4Subsea.

GERFLEX, 1995, *Manual do Programa para geração automática de modelo tridimensional de tubos flexíveis para análise estrutural pelo Método dos Elementos Finitos.* São Paulo, Escola Politécnica de São Paulo.

GONZALEZ, G., SOUSA, J. & SAGRILO, L., “An Unbonded Flexible Pipe Finite Element Model.”. *XXXVI Ibero-Latin American Congress on Computational Methods in Engineering - CILAMCE 2015*, Rio de Janeiro, Brazil, 22-25 November 2015.

KEBADZE, E., 2000, *Theoretical modelling of unbonded flexible pipe cross-sections*. Ph. D. thesis, South Bank University, London, England, United Kingdom.

KEBADZE, E., KRAINCANIC, I., 2000, “Slip initiation and progression in helical armouring layers of unbonded flexible pipes and its effect on pipe bending behaviour”, *Journal of Strain Analysis*, v. 36, n. 3, pp. 265-275.

KOPITS, S., *Artic and Deepwater trends*, 1st ed., USA, 2012.

LEROY, J.M., ESTRIER, P., 2001, “Calculation of stresses and slips in helical layers of dynamically bent flexible pipes.”, *Oil & Gas Science and Technology*, v. 56, n. 6, pp. 545-554.

LEROY, J.M.; PERDRIZET, T.; LE CORRE, V.; ESTRIER, P., “Stress assessment in armour layers of flexible risers”. *29th International Conference on Ocean, Offshore and Artic Engineering*, 20932, Shanghai, China, 06-11 June 2010.

LI, J., WANG, H., ZHANG, K., “FEM Model and Mechanical Behavior of Flexible Risers.” *9th International Conference on Fracture & Strength of Solids*, Jeju,, South Korea, 9-13 June 2013.

LIU, X., J, 2014, *Dynamic Response of Flexible Pipes Considering Different Damping Models.*, M.Sc. thesis, Norwegian University of Science and Technology, Trondheim, Norway.

LODOÑO, T., 2013, *Análise Teórica-Experimental de Dutos Flexíveis.*, M.Sc. thesis, COPPE /UFRJ, Rio de Janeiro, RJ, Brazil.

LONDOÑO, T., ROITMAN, N., MAGLUTA, C. & SOUSA, J. R. M., “A Theoretical and Experimental Analysis of the Bending Behavior of Unbonded Flexible Pipes.”. *33rd International Conference on Ocean, Offshore and Artic Engineering*, 24247, San Francisco, California, USA, 8-13 June 2014.

LØTVEIT, S.A.; BRYN, P.; HJERMAN, B.K., 1994, “Upheaval Buckling of Flexible Pipes Method Selected at the Troll Olje field”, *Advances in Subsea Pipeline Engineering and Technology by Society for Underwater Technology (SUT)*, v. 33, pp. 77–110.

MATOSO, F., “Vision of Petrobras: Technologies and Challenges.”. *FRIM 2016 - Flowlines Risers Integrity Management.*, São Paulo, Brazil, 23 August 2016.

MERINO, H., SOUSA, J., MAGLUTA, C. & ROITMAN, N., “On the Coupled Extensional-Torsional Response of Flexible Pipes.”. *28th International Conference*

on Ocean, Offshore and Artic Engineering, 79468, Honolulu, USA, 31 May-5 June 2009.

MERINO, H., SOUSA, J., MAGLUTA, C. & ROITMAN, N., "Numerical and Experimental Response of a Flexible Pipe under Torsion.". *29th International Conference on Ocean, Offshore and Artic Engineering*, 20902, Shangai, China, 6-11 June 2010.

MERINO, H., SOUSA, J., MAGLUTA, C. & ROITMAN, N., 2016, "Improvements on the Numerical Analysis of the Coupled Extensional–Torsional Response of a Flexible Pipe", *Journal of Offshore Mechanics and Arctic Engineering*, v. 138, pp. 011701-1- 011701-13.

MIYAZAKI, M. N. R., 2015, *Stress Analysis of a Flexible Pipe Tensile Armor Wire During and After the End-Fitting Mounting.*, M.Sc. thesis, COPPE /UFRJ, Rio de Janeiro, RJ, Brazil.

NELSON, T., WANG, E., "Reliable FE-Modeling with ANSYS.", *International ANSYS Conference 2004*, Pittsburgh, USA, 24-26 May 2004.

OFFSHORE MAGAZINE, *Past Issues*, 2016. Available in: http://www.offshore-mag.com/past-issues.html. Accessed in: 30 May 2016.

PERDRIZET, T.; LEROY, J.M.; BARBIN, N.; LE-CORRE, V.; CHARLIAC, D.; ESTRIER, P., "Stresses in armour layers of flexible pipes: comparison of Abaqus models." *2011 SIMULIA Customer Conference.*, Barcelona, Spain, 16-19 May 2011.

PÉRONNE, S.; IZARN, C.; ESTRIER, P.; CARO, O.; LEROY, J.; CHARLIAC, D., "Flexible Pipe Hysteretic Bending Behavior: Comparison With Experimental Characterization and Finite Element Method". *34th International Conference on Ocean, Offshore and Artic Engineering*, 41281, St. John's, Canada, 31 May – 5 June 2015.

PESCE, C. P., TANAKA, R. L., GONÇALVES, R. T., FERREIRA, T. B., ROSETTI, G. F., FUJARRA, A. L., GODINHO, C., "Minimum Bending Radius (MBR) Tests of Flexible Pipes: An Experimental Approach Via Optical Motion Capture and Image Processing.". *Offshore Technology Conference*, 22690, Rio de Janeiro, Brazil, 4-6 October 2011.

RAMOS JR, R., 2001, *Modelos analíticos no estudo do comportamento estrutural de tubos flexíveis e cabos umbilicais*. D.Sc. thesis, Poli/USP, São Paulo, SP, Brazil.

RAMOS JR., R., PESCE, C. P., "A Consistent Analytical Model to Predict the Structural Behaviour of Flexible Risers Subjected to Combined Loads". *21st International Conference on Ocean, Offshore and Artic Engineering*, 28081, Oslo, Norway, 23-28 June 2002.

RAMOS JR, R., PESCE, C. P., ARRUDA, C., "A New Analytical Expression to Estimate the Bending Stiffness of Flexible Risers". *22nd International Conference on Ocean, Offshore and Artic Engineering*, 37320, Cancun, Mexico, 8-13 June 2003.

RAMOS JR, R. & PESCE, C., 2004, "A Consistent Analytical Model to Predict the Structural Behavior of Flexible Risers Subjected to Combined Loads.", *Journal of Offshore and Mechanic Arctic Engineering*, v. 126, pp. 141-146.

RAMOS JR., R., MARTINS, C., PESCE, C. & ROVERI, F., "A Case Study on the Axial-Torsional Behavior of Flexible Risers.". *27th International Conference on Ocean, Offshore and Artic Engineering*, 57514, Estoril, Portugal, 15-20 June 2008.

RAMOS JR., R., PESCE, C., ROVERI, F. E., 2014, "Some Further Studies on the Axial–Torsional Behavior of Flexible Risers.", *Journal of Offshore and Mechanic Arctic Engineering*, v. 136, pp. 011701-1-011701-11.

REN, S., TANG, W., GUO, J., 2014, "Behavior of unbonded flexible risers subject to axial tension.", *China Ocean Engineering*, v. 28, pp. 249-258.

SANTOS, C. C. P., PESCE, C. P., RABELO, M. A., RAMOS JR., R., "An Assessment of HDPE Viscoelastic Behavior Effects on the Bending of Offshore Flexible Pipes.". *23rd ABCM International Congress of Mechanical Engineering*, 1469, Rio de Janeiro, Brazil, 6-11 December 2015.

SÆVIK, S., 1993, "A finite element model for predicting stresses and slip in flexible pipe armouring tendons", *Computers & structures*, v. 46, n. 2, pp. 219-230.

SÆVIK, S. & BERGE, S., 1995, "Fatigue testing and theoretical studies of two 4 in flexible pipes.", *Engineering Structures*, v. 17, pp. 276-292.

SÆVIK, S., "Comparison Between Theoretical and Experimental Flexible Pipe Bending Stresses". *29th International Conference on Ocean, Offshore and Artic Engineering*, 20352, Shanghai, China, 06-11 June 2010.

SÆVIK, S., 2011, "Theoretical and experimental studies of stresses in flexible pipes", *Computers & structures*, v. 89, pp. 2273-2291.

SÆVIK, S., DAI, T. & YE, N., 2017, "Friction models for evaluating dynamic stresses in non-bonded flexible risers.", *Marine Structures*, v. 55, pp. 137-161.

SHI, Y., 2014, *Comparison of the stress distribution in the metallic layers of flexible pipes using two alternative Bflex formulations.* M.Sc. thesis., Norwegian University of Science and Technology, Trondheim, Norway.

SMITH, R., CARR, T. & LANE, M., "Computational Tool for the Dynamic Analysis of Flexible Risers Incorporating Bending Hysteresis.". *26th International Conference on Ocean, Offshore and Artic Engineering*, 29025, San Diego, USA, 10-15 June 2007.

SOUSA, J. R. M., 1999, *Análise Numérica de Risers Flexíveis.*, M.Sc. thesis, COPPE /UFRJ, Rio de Janeiro, RJ, Brazil.

SOUSA, J. R. M., 2005, *Análise Local de Linhas Flexíveis pelo Método dos Elementos Finitos*. D.Sc. thesis, COPPE /UFRJ, Rio de Janeiro, RJ, Brazil.

SOUSA, J. R. M., SOUSA, F. J. M., SIQUEIRA, M. Q. DE, SAGRILO, L. V. S., LEMOS, C. A. D., 2012, "A Theoretical Approach to Predict the Fatigue Life of Flexible Pipes", *Journal of Applied Mathematics*, v. 2012, ID 983819.

SOUSA, J., CAMPELLO, G., BERTONI, F. & ELLWANGER, G., "A FE Model to Predict the Stress Concentration Factors in the Tensile Armor Wires of Flexible Pipes Inside End Fittings". *32nd International Conference on Ocean, Offshore and Artic Engineering*, 10995, Nantes, France, 09-14 June 2013.

SOUSA, J.R.M., MAGLUTA, C., CAMPELLO, ROITMAN, N., LONDOÑO, T. V., "A Study on the Response of a Flexible Pipe to Combined Axisymmetric Loads". *32nd International Conference on Ocean, Offshore and Artic Engineering*, 11384, Nantes, France, 09-14 June 2013.

SOUSA, J., MAGLUTA, C., ROITMAN, N. & CAMPELLO, G., "Bending Analysis of a Flexible Pipe With Broken Tensile Armor Wires". *34th International Conference on Ocean, Offshore and Artic Engineering*, 41436, St. John's, Canada, 31 May – 5 June 2015.

SUBSEA WORLD NEWS, *subseaworldnews web site*, 2017. Available in: http://subseaworldnews.com/2014/01/23/ Accessed in: 30 November 2016.

TAN, Z., CASE, M. & SHELDRAKE, T., "Higher order effects on bending of helical armour wire inside an unbonded flexible pipe". *24th International Conference on Ocean, Offshore and Artic Engineering*, 67106, Halkidiki, Greece, 12-17 June 2005.

TAN, Z., QUIGGIN, P. & SHELDRAKE, T., "Time Domain Simulation of the 3D Bending Hysteresis Behaviour of an Unbonded Flexible Riser.". *26th International Conference on Ocean, Offshore and Artic Engineering*, 29025, San Diego, USA, 10-15 June 2007.

TAN, Z., QUIGGIN, P., SHELDRAKE, T., 2009, “Time Domain Simulation of the 3D Bending Hysteresis Behavior of an Unbonded Flexible Riser”, *Journal of Offshore Mechanics and Arctic Engineering*, v. 131, pp. 031301-1–031301-8.

TANG, M., YANG, C., YAN, J. & YUE, Q., 2015, “Validity and limitation of analytical models for the bending stress of a helical wire in unbonded flexible pipes”, *Applied Ocean Research*, v. 50, pp. 58-68.

TIMOSHENKO, S., 1956, *Strength of Materials,Part 2: Advanced Theory and Problems*. 3ed. Princeton, D. Van Nostrand Co., Inc.

TIMOSHENKO, S.; WOINOWSKY-KRIEGER, S., 1959, *Theory of Plates and Shells.*1ed. New York, McGraw-Hill.

WITZ, J. & TAN, Z., 1992, “On the axial-torsional structural behaviour of flexible pipes, umbilicals and marine cables.”, *Marine Structures*, v. 5, i. 2-3, pp. 205-227.

WITZ, J. A., 1996, “A Case Study in the Cross-Section Analysis of Flexible Risers.”, *Marine Structures*, v. 9, pp. 885-904.

XIQIA, C., SHIXIAO, F., YUN, G. & XIAYING, D., 2015, “A finite element analysis for unbonded flexible risers under bending loads”, *Ocean Systems Engineering*, v. 5, n. 2, pp. 77-89.

ZHANG, Y. & QIU, L., “Numerical Model to Simulate Tensile Wire Behavior in Unbonded Flexible Pipe during Bending.”. *26th International Conference on Ocean, Offshore and Artic Engineering*, 29025, San Diego, USA, 10-15 June 2007.

ZHOU, Y., VAZ, M. A., 2017, “A quasi-linear method for frictional model in helical layers of bent flexible risers”, *Marine Structures*, v. 51, pp. 152-173.